Contribution to modeling the dynamic behavior of an elastomeric device

Nidhal Jridi

N° d'ordre NNT: 2017LYSEC32

University of Lyon **University of Tunis Manar**

Central School of Lyon

in international partnership with

National Engineering School of Tunis

PhD Thesis

defended by

Nidhal Jridi

Contribution to modeling the dynamic behavior of an elastomeric device

---

Mechanical Engineering

20 September 2017

Front of the jury :

President	**Pr. Sylvie Ronel**	(Univ. Claude Bernard Lyon 1)
Reviewer	**Pr. Walid Larbi**	(CNAM)
Reviewer	**Pr. Noureddine Benseddiq**	(Univ. Sci. Techno. Lille)
Examiner	**Dr. Makrem Arfaoui**	(ENIT)
Examiner	**Dr. Olivier Bareille**	(ECL)
Examiner	**Dr. Adel Hamdi**	(ENIT)
Examiner	**Dr. Michelle Salvia**	(ECL)
Advisor	**Pr. Mohamed Ichchou**	(ECL)
Advisor	**Pr. Jalel Ben Abdallah**	(ENIT)

This thesis is part of the project "Elastomeric Devices"
ENIT/ECL/AIRBUS SAFRAN LAUNCHERS

This thesis were carried out within the laboratories

Laboratoire de Mécanique Appliquée et Ingénierie

of Ecole Nationale d'Ingénieurs de Tunis
LR-11-ES19 (LRMAI)
BP 37 Le Belvedère 1002 Tunis
Tunisie

Laboratoire de Tribologie et Dynamique des Systèmes

of Ecole Centrale de Lyon
CNRS UMR 5513 (LTDS)
36 Avenue Guy de Collongues, 69130 Ecully
France

Contribution à la modélisation du comportement dynamique d'un dispositif élastomérique

Abstract

This work is conducted as international collaboration with " **Airbus Safran Launchers** ", " **Ecole Centrale de Lyon** " and " **National Engineering School of Tunis** ".

Elastomeric compounds are widely used in industry for their high deformability and damping capabilities. Subjected to complex combinations of manufacturing and service loadings, elastomers show the fact to undergo severe loading conditions and the load case of large static predeformation superimposed by small amplitude dynamic excitation is commonly encountred for industrial applications e.g tires, shock-absorbing bushes, construction industry, aerospace applications... To design such industrial compounds efficiently, it is of major importance to predict the response of the products through simple modeling processes which have multiplied analysis methods: experimental, theoretical and numerical. Within this context, the present work focuses on design and analysis of dynamic properties of an elastomeric device at a predeformed configuration.

To this end, three rubber mixtures have been experimentally investigated: Natural Rubber (NR), Bromobutyl (BIIR) and a mixture of both (NR/BIIR). A discussion is made with concern to experimental set-up as well as the used procedures for an efficient specimens testings. Within these findings, we made judgement on the predictive capabilities, in time and frequency domains, of some single integral based hyper-visco-elastic models under time-strain seperability assumption. The considered models are widely used for engineering applications and focus have been made on the Simo model implemented in finite element commercial software Abaqus. This work is followed by an application on an industrial component. In the framework of this thesis, the finite element calculation code ABAQUS 6.14 was used to investigate the dynamic properties of such structure. An analysis methodology have been presented to carefully identify the set of parameters with the objective of satisfaction of some industrial requirements mainly mass, stiffness and damping capabilities.

Keywords:

rubber, experimental characterization, finite strain viscoelasticity, time-strain separability, frequency dependence, finite element analysis, structure dynamics

Résumé

Ce travail s'inscrit dans le cadre d'un partenariat international **Airbus Safran Launchers** ", " **Ecole Centrale de Lyon** " et " **Ecole Nationale d'Ingénieurs de Tunis** ".

Les composés élastomériques sont largement utilisés dans l'industrie pour leurs déformabilité et leurs capacités d'amortissement. Soumis aux combinaisons complexes de fabrication et de charges de service, les élastomères montrent la capacité de subir des conditions de chargement sévères et le cas de pré-déformation statique superposée par une excitation dynamique de petite amplitude est couramment utilisé pour des applications industrielles, par exemple des pneus, des amortisseurs, applications aérospatiales ... Pour concevoir efficacement ces composés industriels, il est primordial de prédire la réponse des produits à travers des processus de modélisation simples qui ont multiplié les méthodes d'analyse: expérimentale, théorique et numérique. Dans ce contexte, le présent travail se concentre sur la conception et l'analyse des propriétés dynamiques d'un dispositif élastomère autour d'une configuration préformée. À cette fin, trois mélanges de caoutchouc ont été expérimentés: Caoutchouc naturel (NR), Bromobutyl (BIIR) et un mélange des deux (NR / BIIR). Une discussion est faite avec préoccupation pour la mise en place expérimentale ainsi que les procédures utilisées pour des essais expérimentaux efficaces. Avec ces conclusions, nous avons fait un jugement sur les capacités de prévision, dans les domaines temporels et fréquentiels, de certains modèles hyper-visco-élastique à base d'intégrale unique sous l'hypothèse de séparabilité des effets temps-déformation. Les modèles considérés sont largement utilisés pour les applications d'ingénierie. Ce travail est suivi d'une application sur un composant industriel. Dans le cadre de cette thèse, le code de calcul d'éléments finis ABAQUS 6.14 a été utilisé pour étudier les propriétés dynamiques de cette structure. Une méthodologie d'analyse a été présentée pour identifier soigneusement l'ensemble des paramètres dans le but de satisfaire certaines exigences industrielles, principalement des capacités de masse, de rigidité et d'amortissement.

Mots clés:

Caoutchouc, caractérisation expérimentale, viscoélasticité en grande déformation, séparabilité temps-déformation, dépendance en fréquence, analyse par éléments finis, dynamique des structures

Aknowledgements

I would like to express my appreciation and thanks to my advisors Professor Mohamed Ichchou and Professor Jalel Ben Abdallah. My special appreciation goes to my advisors Dr. Makrem Arfaoui, you have been a tremendous mentor for me. I would like to thank you for encouraging my research and for allowing me to grow as a research scientist. Your advice on both research as well as on my career have been priceless. Very special thanks goes out to Professor Michelle Salvia with a special mention to Dr. Adel Hamdi and Dr. Olivier Bareille for all the special discussions and conversations we had.

I would also like to thank my committee members, Professor Sylvie Ronel, Professor Walid Larbi, Professor Noureddine Benseddiq for serving as my committee members even at hardship. I also want to thank you for letting my defense be an enjoyable moment, and for your brilliant comments and suggestions, thanks to you.

I am also grateful to Professor Bernard Troclet and M. Stéphane Muller from Airbus Safran Launchers for helping and providing the funding for the work.

And finally, last but by no means least, also to everyone in the laboratories E6 and D4 of Central School of Lyon and LRMAI of National Engineering School of Tunis... it was great sharing laboratory with all of you during last four years.

Thanks for all your encouragement!

Dedication

To you, dad and mom, Said and Malika
Words cannot express how grateful I am for all of the sacrifices that you've made on my behalf. Your prayers for me were what sustained me thus far.

To you sister and your little family,
with all my best wishes for your genius boy Mohamed Zayd

To you darling,
I would like express appreciation to my beloved fiancee Khaoula who spent sleepless nights with and was always my support in the moments when there was no one to answer my queries.

And finally,
last but by no means least,
I would also like to thank all of my friends who supported me in writing, and incited me to strive towards my goal:
You have been fabulous guys

Contents

List of Figures

List of Tables

General Introduction

Context

This work is part of an international partnership involving the Tribology and System Dynamics Laboratory LTDS of "Ecole Centrale de Lyon", Laboratory of Applied Mechanics and Engineering LMAI of "Ecole Nationale d'Ingénieurs de Tunis", as academics, and the industrial "Airbus Safran Launchers". The objective of the thesis is modeling the rubber compound to be used in a launcher configurations and whose main role is to ensure a good filtering in order to attenuate the vibrations of the system induced by the boosters and the solid rocket motor. By virtue of their use, these elements are thus caused to undergo small dynamic displacements around a large static preload or predeformation.

Nowadays, the design of industrial structures such as those found in the automotive, aeronautical or space industries uses a very complex architecture and is in the form of an assembly of different components having different geometric dimensions and different mechanical properties. The study of dynamic behavior of industrial structures becomes a primary feature in the design phase of industrial structures. Indeed, a high level of vibration can lead to destruction, to fatigue phenomena or to disrupt the functioning of certain systems. One of the most used solutions to attenuate vibrations is the addition of rubber-metal laminates or elastomeric devices located at the interface between two components of an industrial structure for transmission of static and dynamic stresses as well as damping. The geometrical dimensions of these elastomeric devices are generally small compared to those of the industrial structure. The analysis of the influence of these compounds (choice of material and geometry) on the vibratory behavior of industrial structures still requires heavy and expensive test campaigns. This is why the industrial players put forward the numerical simulations by finite elements in the design process in order to optimize the choice of the material and the geometry of these modules.

Problematics and objectives

Paradoxically, the design and dimensioning of elastomeric structures still poses many problems both from the characterization and modeling of the mechanical behavior of the material in its environment, as well as the associated numerical simulations. The design of this type of devices, which remain closely linked to safety, requires a great level of control and guarantees of reliability that are increasingly exigent. These goals are as critical as the use conditions of these elastomeric parts which are often very severe, subject to static, dynamic and thermal stresses.

To simulate the response of these parts, the complexity of the mechanical behavior of the elastomers must be taken into account. In fact, elastomers exhibit mechanical properties making them special materials: high deformability and damping capacity. Indeed, this behavior is highly nonlinear and the response of the part will depend on the predeformation, the frequency and the excitation amplitude, the temperature, among other parameters. These non-linearities are intervening at static level as well as dynamic one:

- In a quasi-static state, these materials can undergo very large deformations and then return to their initial configuration without any permanent deformation. Predeformation rates of several tens of percent can therefore be imposed. To model the behavior of the part under quasi-static stress, hyperelastic models are used. The nonlinearities involved are then both geometric (the material undergoes a great deformation) and behavioral (the models used make it possible to write a nonlinear relation between the stress tensor and the deformations tensor).

- In dynamic, these materials also have damping properties that allow them to dissipate energy. They exhibit frequency stiffening under harmonic excitation: viscoelastic behavior laws are used to represent these phenomena. It should be noted, however, that linear viscoelasticity is insufficient to fully understand the behavior of these parts: it does not take into account, on the one hand, the large deformation aspect and on the other hand the nonlinear characteristics of the material. The behavior is thus dissipative nonlinear: if we impose deformations sufficiently small around a predeformed configuration so that the hyperelastic model can be linearized, the frequency response obtained will be non-linear. The dynamic modulus strongly depends on the predeformation level, even at low levels.

It is thus necessary to control the phenomena to be taken into account for the simulation of the mechanical behavior of these elastomeric connecting elements.

However, to this difficulty is added the fact that the finite element model of an industrial structure can reach millions of degrees of freedom because of the difference in scale of the geometric dimensions between the elastomeric devices and the rest of the components. Moreover, this finite element model must take into account the different nonlinear behavior laws and the transient dynamic nature of the simulation. Thus, the use of finite element modeling and its implementation on the scale of a complete industrial structure leads to problems with a high number of degrees of freedom whose resolution requires huge means of calculation. Similarly, this finite elements model of very large size must be sufficiently handy for a parametric use although its recalibration with experimental measurements on the materials is very delicate.

The general framework of the work of this thesis concerns on one hand the experimental characterization at the scale of the material of some rubber mixtures and the analysis of hyperviscoelastic models developed on this subject and on the other hand the implementation of a finite elements structure model of a geometrical configuration of the launcher's inter-stage elastomeric device in order to allow the choice of the damping material as well as the geometrical parameters to be retained.

Methodology

In order to accurately define the structural behavior of the elastomeric device, the following methodology was followed:

- Experimental characterization and physical analysis of elastomers behavior: An experimental database was constructed to characterize the behavior of different materials. Indeed, three materials have been tested for their damping capacity: Natural Rubber (NR), Bromobutyl (BIIR) and a mixture of the two previous ones (NR / BIIR). A mechanical characterization of the long - term behavior (equilibrium) at high deformation was carried out through monotonic tests at different loading speeds taking into account different loading modes: uniaxial tensile and simple shear. The dynamic tests were carried out on DMA (Dynamic Mechanical Analysis) and allowed access to the vibratory response of the materials at different frequencies, temperatures and static preload levels.

These tests were supplemented by thermal characterization on DSC (Differential Scanning Calorimetry) to assess the thermal stability of materials as the service environment covers a wide range of temperatures. The characterization of the various elastomeric mixtures chosen made it possible to select the material for the elastomeric device to be retained.

- Analysis of hypervicoelastic models suitable to describe rubber-like materials behavior: The behavior laws governing elastomers response are highly nonlinear and several models have been proposed in the literature. An analytical analysis of the different models proposed for the study of Hyper-Visco-Elastic materials was carried out. This study focused on separable models (i.e time-strain separability, an experimental observation which afford a large modeling simplificity) based on a hereditary integral describing the effect of loading history. Well known models such as Christensen, Fosdick & Yu and a variant of the BKZ were considered as well as other more recent models. The Simo model, implemented in the ABAQUS finite element software, has been analyzed with the greatest interest, for the few identification parameters it requires, its ease of implementation and its ability to reproduce the sample tests with some acceptable fidelity.

- Development of a modeling methodology for the structure for a geometric launcher configuration of one of the elastomeric devices: A geometry proposal of the elastomeric device has been made, taking into account the geometric constraints. A configuration of the launcher type has led us to seek a suitable solution for integrating the elastomeric device. The previous steps of this thesis allowed us the construction of the finite element model which allowed the prediction of the dynamic behavior of the structure based on observable variables relevant for dynamic vibratory study. This structure modeling methodology is sufficiently handy for a parametric analysis and allowed to validate the choice of a geometry as well as a damping mixture from those previously tested.

Outline

This manuscript is subdivised to four chapters, organized as follows. The first chapter is devoted to a reminder of the mechanical properties of elastomers. It is a phenomenological study of rubber materials, allowing to review the specificities of

the behavior of this material. Moreover this chapter establishes a state of the art, not exhaustive, of the modeling of this behavior. This chapter focuses on three main points. First, we recall some elements of the continuum mechanics in large deformations, and then we review the main research work on models of both hyperelastic and viscoelastic behaviors. The second chapter is dedicated to the experimental investigation conducted to identify the materials parameter, the experimental set-up as well as the used procedures for an efficient specimens testings. This experimental database aims to draw conclusions and a comparison concerning the materials properties, with consideration to industrial applications. In the following chapter, a short review of the different modeling frameworks is made as well as a classification of models according to two criterions: integral-based or internal variables-based models, and time-strain separable or not criterion. This objective of this chapter is analysis of the predictive capabilities of some integral-based finite strain viscoelastic models under separability assumption, in time and frequency domains. Finally, the fourth chapter is dedicated to the concretization of the work on a geometrical launcher configuration, describing the modeling methodology adopted in the finite element code Abaqus 6.14 for the study of structures with viscoelastic materials inserts. The compromised solution found to lead to the satisfaction of all technical requirements is presented within this chapter, as well as numerical simulation results.

Chapter 1

Elastomers: physical aspects and continuum mechanics

Contents

1.1 Introduction

This introductive chapter aims to analyse the behavior of elastomers within a phenomenogical approach. The advent of rubber-like materials is the plethora of properties available for a vast range of engineering applications such as tires, shock-absorbing bushes, construction industry, and especially the construction of modern aerospace structures [1][2]. They are capable of sustaining large deformations, of about some hundreds of percents, and quickly and forcibly retract to their original dimensions. Rubbers are resilient and yet exhibit internal damping. Due to their complex nature, and in particular the presence of carbon chains, this class of materials is of highly non-linear behaviors [3][4][5][6][7]. This introductive chapter is mainly subdivised in two parts: the first is dedicated to the phenomenology of rubber materials and their physical aspects while within the second part we recall the main elements of the theory of finite elasticity for the description of elastic and viscoelastic phenomenon.

1.2 Phenomenology of elastomers

1.2.1 Generalities

Natural rubber and its synthetic counterparts, elastomers, are widely used in the field of industry. The multiplicity of uses of elastomers comes from very interesting mechanical characteristics:

- Ability to undergo large deformations
- Ability to dissipate energy, making possible to obtain vibratory and acoustic isolators

This makes elastomeric compounds widely used in industry for damping applications, from seals and bushes to motor support, launchers softeners and others [8][9][10][11]... Rubber-like materials are often used interchangeably with the term elastomers. The term “elasto” recalls the great potential of elastic deformation, and the “mer” evokes nature of polymers and thus their macromolecular constitution. Natural rubber (also called caoutchouc and which appearance date early 20^{th} century) as initially produced, consists of polymers of the organic compound isoprene, and is harvested mainly in the form of the latex from the rubber tree "*hevea*" or

others. Nevertheless, the latex is a sticky, milky colloid drawn off by making incisions in the bark and collecting the fluid in vessels in a process called "*tapping*". Hence, rubber at the raw state have no interesting properties. To obtain a reversible elastic material, it must be created between the different macromolecules bridges that form a three-dimensional network. This process, called vulcanization, was accidentally discovered by Goodyear in 1839 and is still at the base of the rubber manufacturing industry. During the vulcanization, the long chain molecules of the rubber are chemically united to adjacent chains forming crosslinks. From a chemical point of view, natural rubber is a product of polymerization of isoprene chemical formula $(C_5H_8)_n$, n having a value of about 10 000. The manufacture of synthetic rubbers is based on the same principle. To obtain an efficient industrial material, elastomers are often a mixture of a lot of components: processing agents as sulfur, metallic oxides or other additives prime for "curing", catalysts to accelerate the process mainly mercaptobenzothiazole (MBT/MBTS) and ethylene thiourea (ETU), activators like zinc oxide and stearic acid, dyes for colored elastomers, antidegradants... Elastomers which contain only processing agents and chemicals for protection, coloring and vulcanization are referred to as pure gum. The majority of elastomers used for mechanical applications contain a filler, hence referred to as filled rubbers: the fillers can improve the elasticity of the final product without increasing its hardness (based on calcium carbonate or barium sulface) or improve its resistance (carbon black, zinc oxide, magnesium carbonate...). The carbon black, which remains the main reinforcing filler of the rubber, is in the form of small carbon particles mixed with the natural gum before vulcanization. The obtained material then constitutes a continuous network and the fillers form an agglomerate inside the network. Elastomers are then diphasic materials composed of components with completely different mechanical properties.

1.2.2 High deformability

Rubbers behavior can be primarily described as hyperelastic materials under static or quasi-static loadings [12] where dissipative effects are negligible. There have been numerous experimental studies addressing the response of rubbers under quasi-static loading conditions, including uniaxial tension/compression, shear, equibiaxial tension... Under all these experimental conditions, the resulting constitutive responses are strongly nonlinear, as shown in fig. 1.1. Moreover, the incompressibility of rubbers has been confirmed by a number of different researchers over the years [3][13].

Experiments show a limited volume variation (V/V0=0.01) at large strain (500% of deformation), as shows fig. 1.2, corroborating the incompressibility constraint introduced in many constitutive equations.

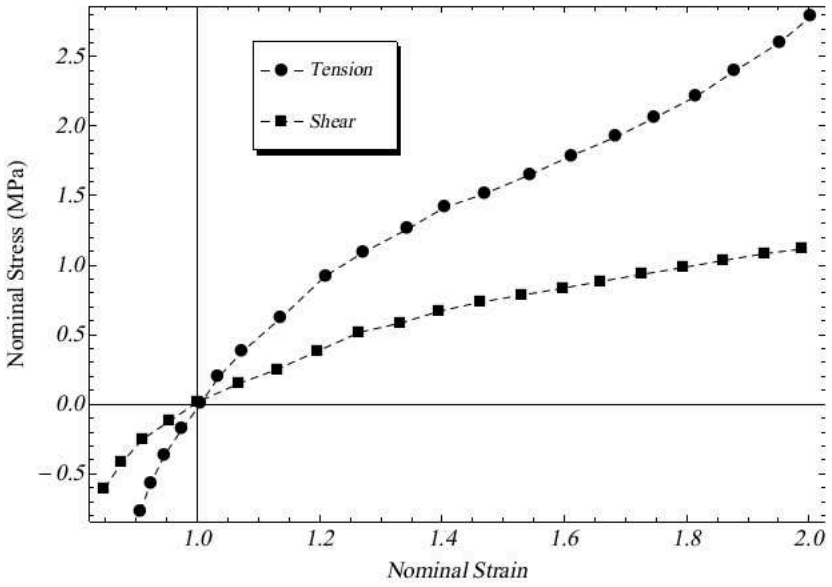

Figure 1.1: Nominal stress vs strain for quasi-static loadings [14]

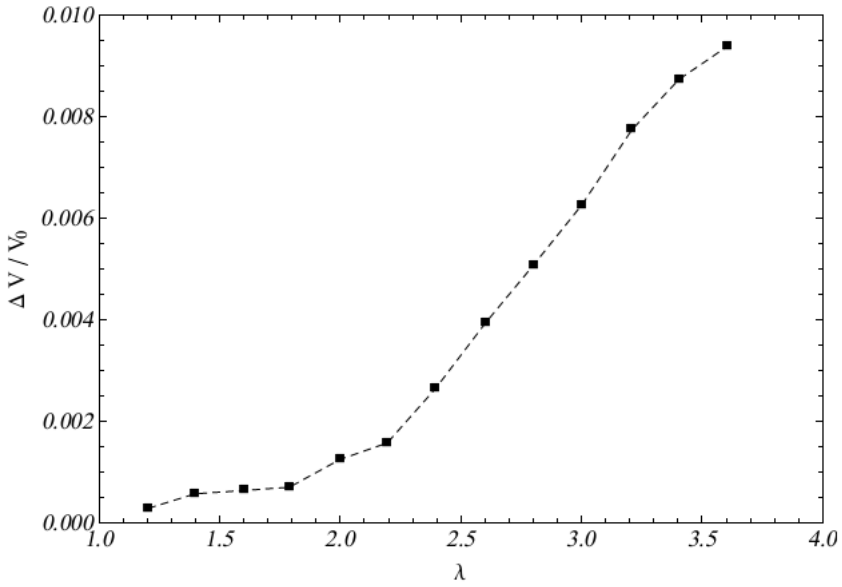

Figure 1.2: Volume change of filled rubber materials [15]

1.2.3 Dissipative properties

1.2.3.1 Relaxation and Creep phenomenon

The material behavior above-described refers to the quasi-static response. However, elastomers subjected to real world loading conditions possess fluid-like characteristics typical of a viscoelastic material [16]. When loaded by means of a stepwise strain, they stress-relax as shows fig. 1.3. The reaction force resulting from the application of an initial peak falls to an asymptotic value, which is theoretically reached after an infinite time. Moreover, if an external force is suddenly applied, creep is observed and the strain begins to change slowly towards a limiting value. This behavior provides evidences of the fading memory property of the material. Therefore, the entire strain history must affect the constitutive behavior of elastomers [17]. While the strain-rate sensitivity and the failure time dependency are recognized and well documented in the case of other materials such metals, the incorporation of history-dependent properties of elastomers requires further clarification.

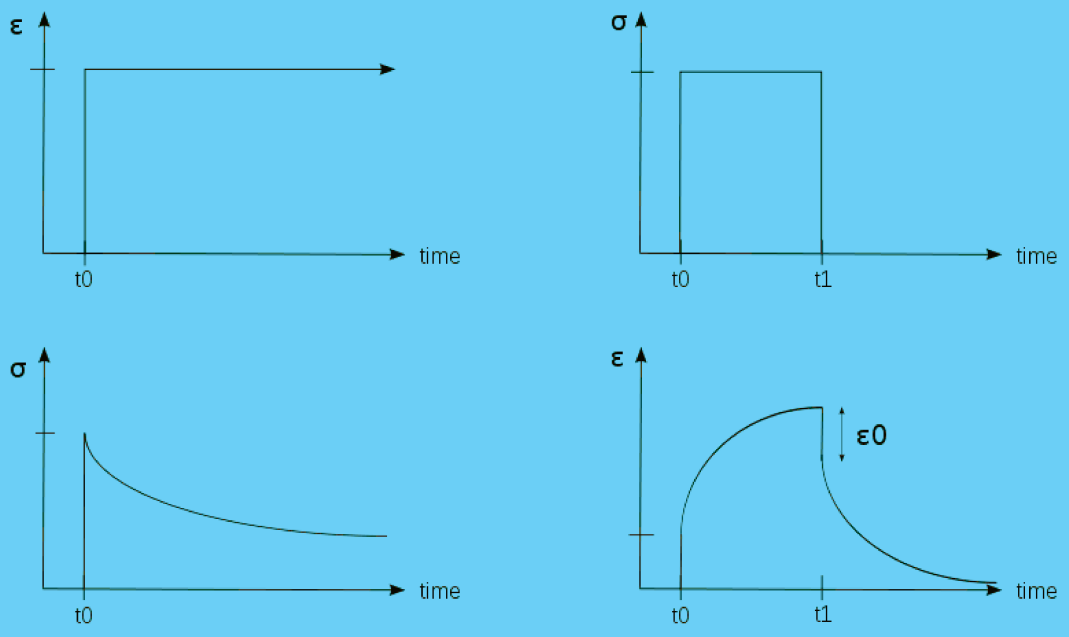

(a) Relaxation (b) Creep/Recovery

Figure 1.3: Relaxation and Creep/Recovery experiments

1.2.3.2 Dynamic response

A frequently employed characterization of elastomers is achieved through sinusoidal strain histories of frequency ω. Under the action of dynamic loadings, the deformation of rubbers, like other viscoelastic solids, occurs with a certain delay owing to viscous friction inside the material as shows fig. 1.4. Under harmonic deformations, this delay manifests itself by a phase shift between the applied displacement and the load. This shift is proportional to the viscous losses. Nevertheless, the properties measured on a rubber are dependent on the desired operating point.

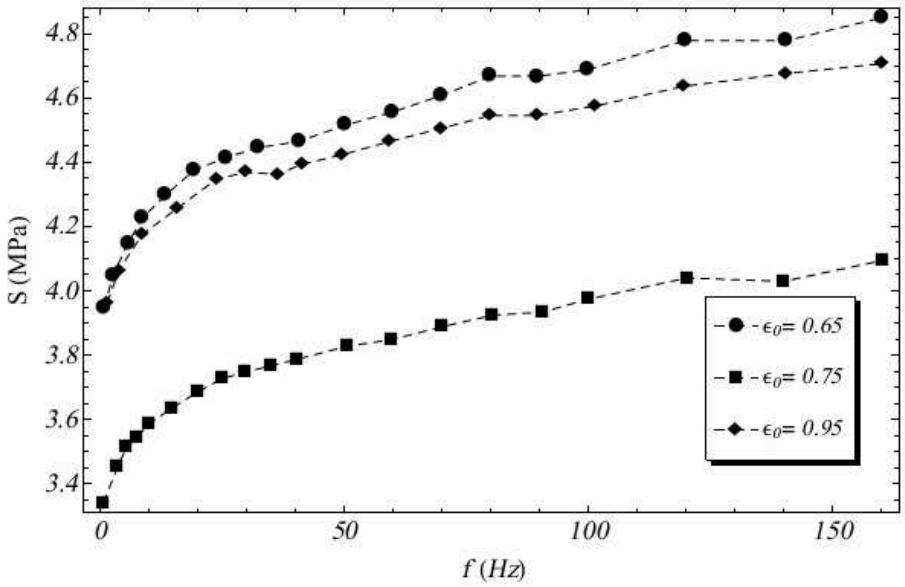

Figure 1.4: Dynamic response of rubber-like materials [18]

1.2.4 Thermal response

The variation of dynamic mechanical properties (storage modulus and loss factor) with temperature provide fundamental knowledge for understanding the filled rubber characteristics [19]. Figure 1.5 shows that at low temperature, the shear storage modulus is at its maximum, and the loss factor at its minimum. This area of behavior is the hard or brittle state of the material. Increasing the temperature, the storage modulus decreases suddenly and the loss factor see its maximum. For higher frequencies, the behavior is stable and not too dependent of temperature compared to the previous areas. This domain is called the "rubbery plateau" [9].

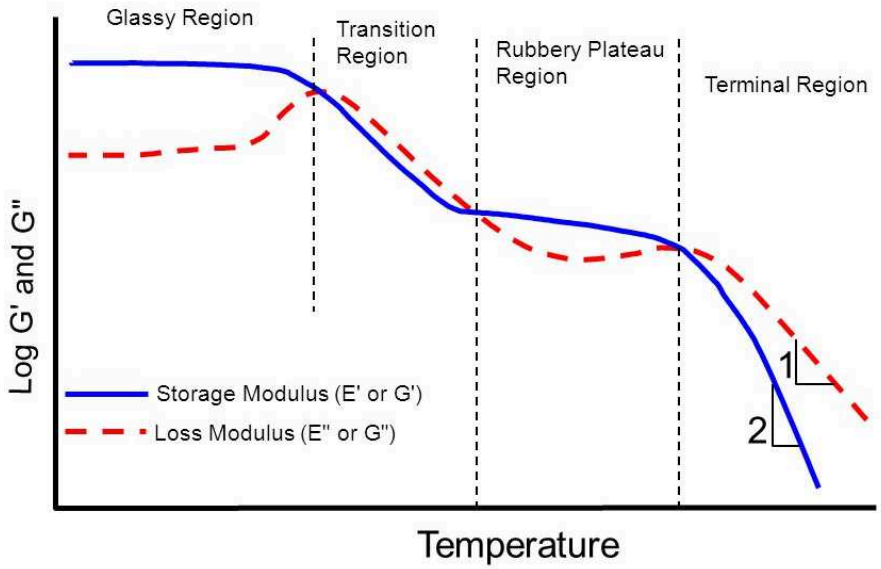

Figure 1.5: Evolution of the dynamic properties as function of temperature [20]

1.2.5 Some other non-linearities

1.2.5.1 Mullins effect

The Mullins effect is a strain induced softening phenomenon, which is mainly associated with a significant reduction in the stress at a given level of strain during the unloading path as compared with the stress on initial loading in stress-strain cyclic tests [21][22][23]. A typical cyclic loading path where Mullins effect is evident is represented in fig. 1.6 in terms of stress-strain curves. In fact, on the initial loading (abb') the virgin material exhibits a relatively stiff response. When the material is subsequently unloaded, then reloaded, the stress-strain curve follows a significantly softer path (aBb') until the point of max deformation previous applied (b') is reached for the second time. Continuing to increase further on the stretch, the stress-strain curve will return to follow the primary path until next unload is performed (b'cc').

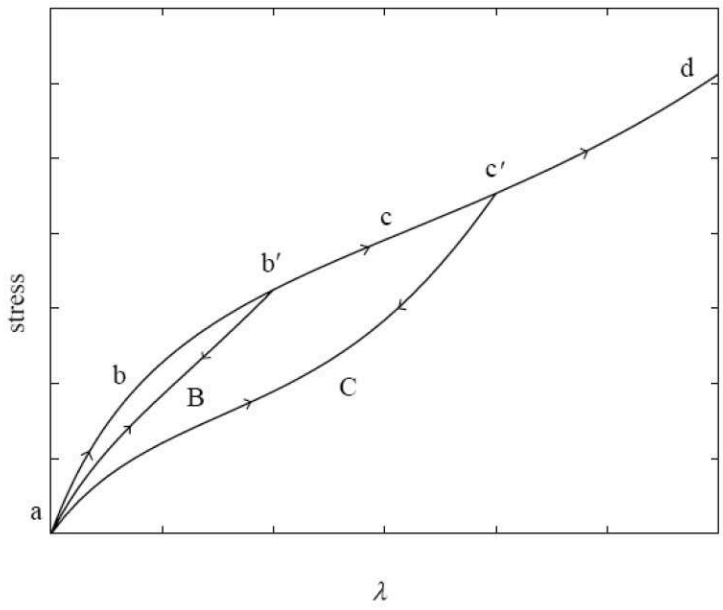

Figure 1.6: Cyclic loading with evident Mullins effect [24]

1.2.5.2 Payne Effect

Another softening phenomenon which shows the dependency of the stress upon the entire history of deformation is the so-called Payne effect [25][26]. Like the Mullins effect, this is a softening phenomena but it concerns the behavior of rubbers subjected to oscillatory displacement. Indeed, the dynamic part of the stress response presents rather strong non-linear amplitude dependency, which is actually the Payne effect shown in fig. 1.7. The Payne effect is essential for the frequency and amplitude-dependent dynamic stiffness and damping behavior of rubbers bushings, automotive tires and other products...

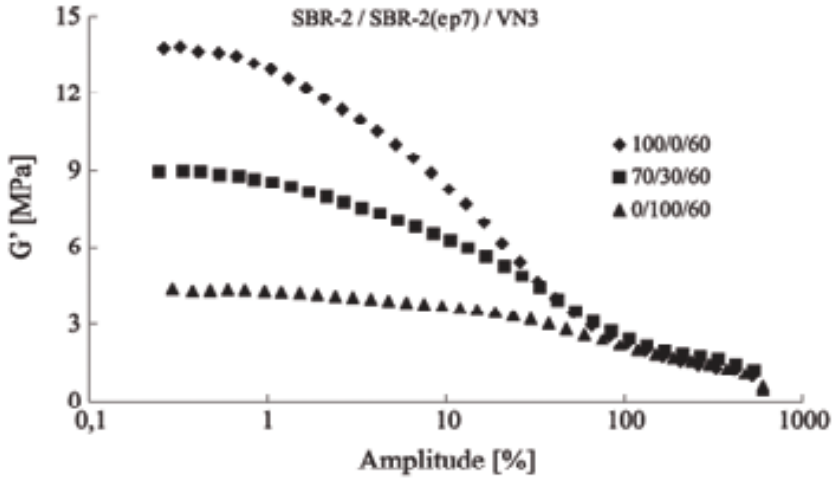

(a) Shear storage modulus

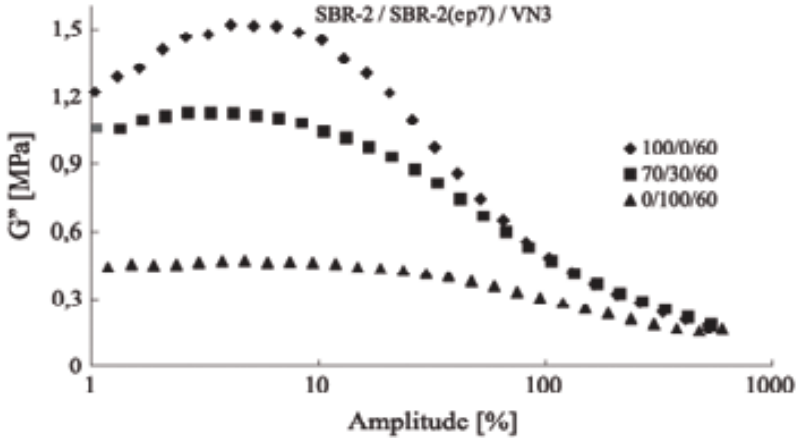

(b) Shear loss Modulus

Figure 1.7: Payne effect on dynamic properties [27]

1.3 Elements of the theory of finite elasticity: Kinematics

In the previous section, we have highlighted some physical aspects of elastomeric materials [4][28], that in addition to undergo large deformations, own a dissipative component on behalf of their viscoelastic nature [16]. In this section, we recall some basic concepts of the general framework of finite elasticity [29]. A non-exhaustive list of hyperelastic models, then viscoelastic models will be presented.

1.3.1 Material and Spatial Representation

We consider a three-dimensional Euclidean space. We denote C_0 the reference configuration, where the solid S occupies Ω_0. The set of material particules P defines the deformable solid position in the actual configuration C_t, of a volume Ω at time t, as shows fig. 1.8. In the reference configuration, the point P is defined by the vector $\boldsymbol{X}$ while it is defined by $\boldsymbol{x}$ in the current time t. Deformation state is the defined by χ:

$$\chi : \begin{cases} C_0 \to C_t \\ \boldsymbol{X} \to \boldsymbol{x} = \chi(\boldsymbol{X}, t) \end{cases} \tag{1.1}$$

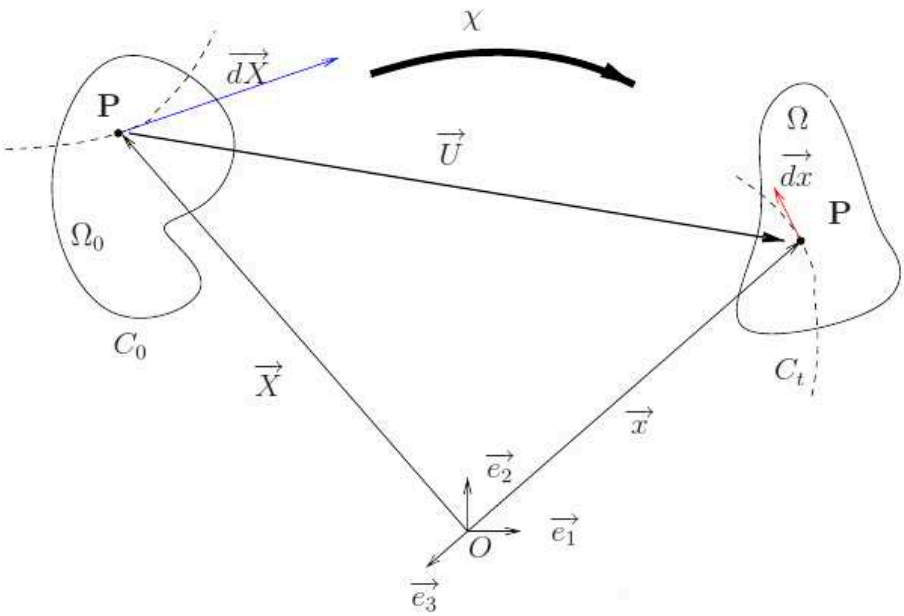

Figure 1.8: Reference and current configurations

The deformation gradient **F** is defined as :

$$\begin{aligned} d\boldsymbol{x} &= \mathbf{F} d\boldsymbol{X} \\ \mathbf{F} &= \mathbf{Grad}\, \boldsymbol{x} \end{aligned} \tag{1.2}$$

where the gradient operator **Grad** is defined with respect to the reference undeformed configuration.

The deformation χ is reversible with the condition

$$J > 0 \tag{1.3}$$

where J is the determinant of $\mathbf{F}$.
$\mathbf{F}$ is invertible, and its inverse allows to transport a tangent vector from the current configuration to the initial configuration:

$$\begin{aligned} d\boldsymbol{X} &= \mathbf{F}^{-1} d\boldsymbol{x} \\ \mathbf{F}^{-1} &= \mathbf{grad}\, \boldsymbol{X} \end{aligned} \tag{1.4}$$

where **grad** is the gradient tensor with respect to the actual deformed configuration. We introduce the spacial displacement vector $\boldsymbol{U}$ in the reference configuration as:

$$\boldsymbol{U}(\boldsymbol{X}, t) = \boldsymbol{x}(\boldsymbol{X}, t) - \boldsymbol{X} \tag{1.5}$$

A Lagrangien description (in the reference configuration) of the displacement gradient is hence given:

$$\begin{aligned} \mathbf{Grad}\boldsymbol{U} &= \mathbf{Grad}\boldsymbol{x} - \mathbf{Grad}\boldsymbol{X} \\ &= \mathbf{F} - \mathbf{I} \end{aligned} \tag{1.6}$$

We can describe the displacement gradient in the current configuration (Eulerian description) within:

$$\begin{aligned} \mathbf{grad}\boldsymbol{u} &= \mathbf{grad}\boldsymbol{x} - \mathbf{grad}\boldsymbol{X} \\ &= \mathbf{I} - \mathbf{F^{-1}} \end{aligned} \tag{1.7}$$

In the following, strain and stress tensors are briefly recalled, detailed explanations on basics of continumm mechanics can be found for example in [29][30][31].

1.3.2 Deformation Tensors

Lagrangian description (Reference Configuration C_0):
We introduce the right Cauchy Green strain tensor $\mathbf{C} = \mathbf{F}^T \mathbf{F}$. The symmetric Green Lagrange deformation tensor is defined as:

$$\mathbf{E} = \frac{1}{2}(\mathbf{C} - \mathbf{I}) \tag{1.8}$$

Using the displacement vector, this tensor is written:

$$\mathbf{E} = \frac{1}{2}\left(\mathbf{Grad}\boldsymbol{U} + (\mathbf{Grad}\boldsymbol{U})^T + \mathbf{Grad}\boldsymbol{U}\,(\mathbf{Grad}\boldsymbol{U})^T\right) \tag{1.9}$$

Eulerian description (Actual Configuration C_t):
We introduce the left Cauchy Green strain tensor $\mathbf{B} = \mathbf{F}\,\mathbf{F}^T$. The associated strain tensor is the Euler-Almansi strain tensor defined as:

$$\mathbf{A} = \frac{1}{2}(\mathbf{I} - \mathbf{B^{-1}}) \tag{1.10}$$

Invariants
Isotropic scalar-valued invariants of $\mathbf{C}$ (and $\mathbf{B}$) are written as:

$$I_1 = tr(\mathbf{C}) \tag{1.11a}$$
$$I_2 = \frac{1}{2}\left(tr(\mathbf{C})^2 - tr(\mathbf{C^2})\right) \tag{1.11b}$$
$$I_3 = det(\mathbf{C}) \tag{1.11c}$$

where tr defines the mathematical operator trace of a matrix.
Let λ_1, λ_2 and λ_3 be the eigenvalues of $\mathbf{C}$. The invariants are then written:

$$I_1 = \lambda_1 + \lambda_2 + \lambda_3 \tag{1.12a}$$
$$I_2 = \lambda_1\lambda_2 + \lambda_1\lambda_3 + \lambda_2\lambda_3 \tag{1.12b}$$
$$I_3 = \lambda_1\lambda_2\lambda_3 \tag{1.12c}$$

1.3.3 Incompressibility

The considered materials in this section are incompressible. We take into account the incompressiblity condition by imposing to the transformation χ to be volume preserving (isochoric). The volume change measure between C_0 and C_t is written:

$$dv = J\,dV \tag{1.13}$$

For an isochoric deformation, we have:

$$J = det\mathbf{F} = I_3 = 1 \tag{1.14}$$

1.3.4 Stress tensors

We consider a surface element relative to a chosen configuration. We can obtain three different description of load, with respect to the chosen configuration: Eulerien, Lagrangian and/or a mixed description.

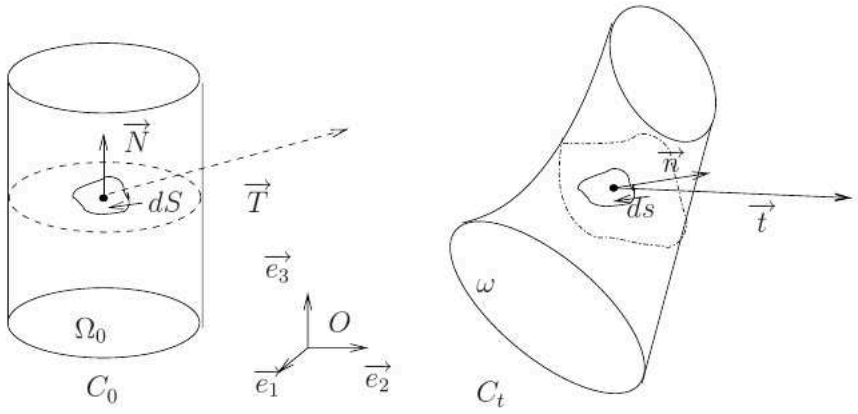

Figure 1.9: Stress vectors at different configurations

Eulerian Description

The Cauchy stress tensor $\boldsymbol{\sigma}$ is eulerian, symmetric and defined as:

$$\boldsymbol{t} = \boldsymbol{\sigma}\boldsymbol{n} \tag{1.15}$$

where $\boldsymbol{t}$ is the measured load per unit surface, and $\boldsymbol{n}$ is the normal to the element surface ds. The load per surface is then defined as:

$$d\boldsymbol{f} = \boldsymbol{t}ds = \boldsymbol{\sigma}\boldsymbol{n}ds \tag{1.16}$$

The Cauchy stress is called true stress for experimental considerations.

Mixed Description

Load per surface can be related to the reference element surface dS using :

$$d\boldsymbol{f} = \boldsymbol{T}dS = \boldsymbol{\Pi}\boldsymbol{N}dS \tag{1.17}$$

$\boldsymbol{\Pi}$ is the non-symmetric first Piola-Kirchoff stress tensor, and expresses the actual stress in the reference configuration, and related to the Cauchy stress tensor as:

$$J\boldsymbol{\sigma} = \boldsymbol{\Pi}\,\mathbf{F}^T \tag{1.18}$$

The first Piola-Kirchoff stress is called nominal stress for experimental considerations.

Lagrangian Description

Transposing all quantities to the reference configuration, we obtain:

$$d\boldsymbol{f_0} = \mathbf{F}^{-1}\, d\boldsymbol{f} \; = \mathbf{S}\, \boldsymbol{N}\, dS \tag{1.19}$$

S is the second Piola-Kirchoff stress tensor and is symmetric without physical signification. It is related to the Cauchy stress tensor as :

$$J\, \boldsymbol{\sigma} = \mathbf{FSF}^T \tag{1.20}$$

1.3.5 Equilibrium equations

The equilibrium equations are obtained from the balance of the linear and rotational momentum. The general framework of finite deformations imposes the distinction between the reference and the actual configurations. The equilibrium problem is formulated as shows fig. 1.10 and the classically considered boundary conditions are:

$$\begin{cases} \boldsymbol{u} = \boldsymbol{u}_0 & on \quad \partial\omega_u \\ \boldsymbol{t} = \boldsymbol{\sigma n} & on \quad \partial\omega_\sigma \end{cases} \tag{1.21}$$

In the reference configuration, these boundary conditions are expressed as:

$$\begin{cases} \boldsymbol{u} = \boldsymbol{u}_0 & on \quad \partial\Omega_u \\ \boldsymbol{T} = \boldsymbol{\Pi N} = & on \quad \partial\Omega_\sigma \end{cases} \tag{1.22}$$

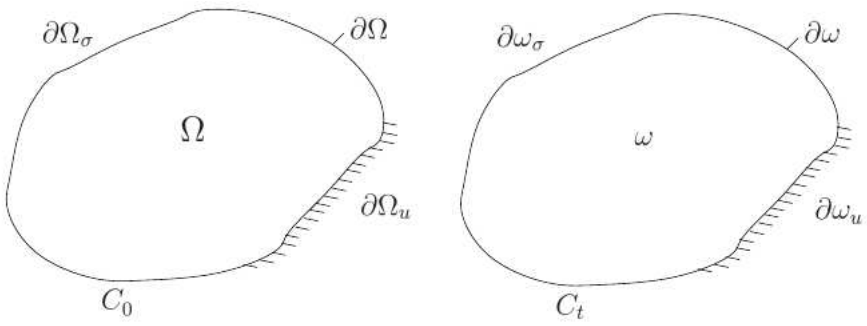

Figure 1.10: Equilibrium problem

Eulerian Description

In the actual configuration, the balance of the linear momentum is written as:

$$\int_{\omega} \rho f_i \, d\omega + \int_{\partial\omega} t_i \, ds = \int_{\omega} \rho \gamma_i \, d\omega \tag{1.23}$$

Including previously recalled stress tensors and introducing Gauss theorem, we obtain the following equilibrium equations in the actual configuration:

$$\begin{cases} \mathbf{div}(\boldsymbol{\sigma}) + \rho \mathbf{f} = \rho \ddot{\mathbf{u}} & in \quad \omega \\ \boldsymbol{u} = \boldsymbol{u}_0 & on \quad \partial\omega_u \\ \boldsymbol{t} = \boldsymbol{\sigma} \boldsymbol{n} & on \quad \partial\omega_\sigma \end{cases} \tag{1.24}$$

where **div** defines the divergence vector operator with respect to the actual configuration.

The balance of the rotational momentum provides the symmetry of the Cauchy stress $\boldsymbol{\sigma}$.

Lagrangian Description

In the actual configuration, the balance of the linear momentum is written as:

$$\int_{\Omega} \rho_0 f_i \, d\Omega + \int_{\partial\Omega} T_i \, dS = \int_{\Omega} \rho_0 \gamma_i \, d\Omega \tag{1.25}$$

Hence, we obtain the mixed equilibrium equations:

$$\begin{cases} \mathbf{Div}(\boldsymbol{\Pi}) + \rho_0 \mathbf{f} = \rho_0 \ddot{\mathbf{u}} & in \quad \Omega \\ \boldsymbol{u} = \boldsymbol{u}_0 & on \quad \partial\Omega_u \\ \boldsymbol{T} = \boldsymbol{\Pi} \boldsymbol{N} & on \quad \partial\Omega_\sigma \end{cases} \tag{1.26}$$

where **Div** defines the divergence vector operator with respect to the reference configuration.

The balance of the rotational momentum provides following:

$$\boldsymbol{\Pi} \, \mathbf{F}^T = \mathbf{F} \, \boldsymbol{\Pi}^T \tag{1.27}$$

1.4 Modeling elastic properties: Hyperelasticity

Elastomeric materials are assumed isotropic, incompressible and isothermal. In this section, only highly non-linear elastic response under large strain is considered with respect to the general theory of Hyperelasticity [32].

1.4.1 Hyperelasticity constitutive equations

A Cauchy-elastic material is one in which the stress at each point is determined only by the current state of deformation with respect to an arbitrary reference configuration [32]. It follows from this definition that the stress in a Cauchy elastic material does not depend on the path of deformation or the history of deformation, or on the time taken to achieve that deformation or the rate at which the state of deformation is reached. The definition also implies that the constitutive equations are spatially local; that is, the stress is only affected by the state of deformation in an infinitesimal neighborhood of the point in question, without regard for the deformation or motion of the rest of the material. It also implies that body forces (such as gravity), and inertial forces cannot affect the properties of the material. Hyperelatic behavior, commonly known as Green elasticity, is a special case of the Cauchy elasticity concept [33][34] and there exist a strain-energy function denoted W from which derives stress quantities. This implies that the work done during loading processes is path independent. Without recalling thermodynamical framework, this strain-energy function commonly referred to as hyperelastic potential, satisfies objectivity and material symmetry principles as written function of the deformation tensor $\mathbf{E}$ in the general case and function of invariants of $\mathbf{C}$ or $\mathbf{B}$ for isotropic materials [35]. The hyperelastic potential is obtained through :

- internal dissipation is equal to zero (elastic material)
- thermal effects are neglected (isothermal state)

By expressing the dissipation potential in the different configurations and introducing the incompressibility condition, we obtain the constitutive hyperelastic equations written as follows:

- Lagrangian description

$$\mathbf{S} = 2\,\frac{\partial W}{\partial \mathbf{C}} - p\,\mathbf{C}^{-1} \tag{1.28}$$

- Eulerian description

$$\boldsymbol{\sigma} = 2\,\mathbf{B}\,\frac{\partial W}{\partial \mathbf{B}} - p\mathbf{I} \tag{1.29}$$

- Mixed description

$$\boldsymbol{\Pi} = \frac{\partial W}{\partial \mathbf{F}} - p\mathbf{F}^{-T} \tag{1.30}$$

W can be expressed function of the invariants I_1 and I_2 [35] or of eigenvalues of C. Hence, we obtain:

$$\mathbf{S} = 2\left(\left[\frac{\partial W}{\partial I_1} + I_1\frac{\partial W}{\partial I_2}\right]\mathbf{I} - \frac{\partial W}{\partial I_2}\mathbf{C}\right) - p\mathbf{C}^{-1} \tag{1.31a}$$

$$\boldsymbol{\sigma} = 2\mathbf{B}\left(\left[\frac{\partial W}{\partial I_1} + I_1\frac{\partial W}{\partial I_2}\right]\mathbf{I} - \frac{\partial W}{\partial I_2}\mathbf{B}\right) - p\mathbf{I} \tag{1.31b}$$

$$\boldsymbol{\Pi} = 2\mathbf{F}\left(\left[\frac{\partial W}{\partial I_1} + I_1\frac{\partial W}{\partial I_2}\right]\mathbf{I} - \frac{\partial W}{\partial I_2}\mathbf{C}\right) - p\mathbf{F}^{-T} \tag{1.31c}$$

1.4.2 Hyperelastic potentials examples

Numerous forms of strain-energy functions have been proposed in the litterature and are well summarized in [24]. Some are based on statistical theories, others are purely phenomenological. There are several classification approachs for hyperelastic potentials. Firstly, we can separate those that are expressed as a function of the invariants I_1 and I_2, and those which are expressed as a function of the principal elongations λ_i. Another way of establishing a classification is to consider those whose coefficients intervene in linear form (as the generalized Rivlin model) and those whose coefficients intervene in the form of power laws (as Ogden Model). There are several forms of strain-energy function commonly used for incompressible or quasi-incompressible isotropic elastomers:

- The polynomial form and it's particular cases: the reduced polynomial form, the neo-Hookean form, the Mooney-Rivlin form, and the Yeoh form
- Ogden real exponents form
- Arruda-Boyce form
- Van der Waals form

In following, we will try to recall the general form and references for each model and its parameters.

Polynomial Form

Rivlin [12][36] extended the Mooney model [37], and proposed a Polynomial series of W:

$$W = \sum_{i=0,j=0}^{\infty} C_{ij}(I_1 - 3)^i(I_2 - 3)^j \tag{1.32}$$

where C_{ij} are material parameters and $C_{00} = 0$. This series is classically truncated to second or third order, and is used for large strain problems.

Mooney-Rivlin Model

Mooney observed that the shear response is quasi-linear [37]. This model is classicaly used for moderate strain lower than 200%. This potential has form:

$$W = C_1(I_1 - 3) + C_2(I_2 - 3) \tag{1.33}$$

where C_1 and C_2 are material parameters and are temperature dependent. We remark that this model is commonly referred to as Mooney-Rivlin model, besides, in litterature, the Mooney-Rivlin model is identified as the above mentionned Polynomial model [38].

Reduced Polynomial

Particular forms of the polynomial model can also be obtained by setting $C_{ij}, i \neq j$ coefficients to zero. If all with are set to zero, the reduced polynomial form is obtained:

$$W = \sum_{i=0}^{\infty} C_{i0}(I_1 - 3)^i \tag{1.34}$$

Omitting the I_2 dependence has been justified based on observations that the sensitivity of the strain energy function to changes in the second invariant is generally much smaller than the sensitivity to changes in the first invariant [39].

Yeoh Model

The Yeoh form [40] can be viewed as a special case of the reduced polynomial with $N = 3$:

$$W = \sum_{i=0}^{3} C_{i0}(I_1 - 3)^i \tag{1.35}$$

NeoHookean Model

The NeoHookean model [41] is the simplest proposed model for rubber, and is derived from the statistical thermodynamics of cross-linked polymer chains:

$$W = C_1(I_1 - 3) \tag{1.36}$$

This model, similar to Hooke's law, revealed good approximation of data lower than 50% of deformation, and is classically used as first test of constitutive models.

Ogden Form

The phenomenological Ogden model [13] consists on a expansion of the strain energy through a series of real powers of λ_i :

$$W = \sum_{i=1}^{N} \frac{\mu_i}{\alpha_i} (\lambda_1^{\alpha_i} + \lambda_2^{\alpha_i} + \lambda_3^{\alpha_i} - 3) \tag{1.37}$$

where the material parameters $\mu_i \, and \, \alpha_i$ should satisfy the following stability condition:

$$\mu_i \, \alpha_i > 0 \quad \forall \, i = 1, N \tag{1.38}$$

This model is one of the most widely used models for large strain problems, even with some difficulties for materials parameters identification.

Arruda-Boyce model

Commonly referred to as "8 chain model", Arruda and Boyce [42] proposed this model based on the statistical mechanics of a material with a cubic representative volume element containing eight chains along the diagonal directions. This model is isotropic and the proposed form in Abaqus is:

$$\begin{aligned} W = \mu \Bigg[& \frac{1}{2}(I_1 - 3) + \frac{1}{20\lambda_m^2}(I_1^2 - 9) + \frac{11}{1050\lambda_m^4}(I_1^3 - 27) \\ & + \frac{19}{7000\lambda_m^6}(I_1^4 - 81) + \frac{519}{67375\lambda_m^8}(I_1^5 - 243) \Bigg] \end{aligned} \tag{1.39}$$

where μ and λ_m are temperature-dependent material parameters, and the typical value of λ_m is 7.

Van Der Waals model

The use of Van Der Walls forces was firstly proposed by Wang and Guth [43] and explicitely revived in 1956 by Kilian *and al* [44], and consists on treating the rubber networks as a gaz with particules in interaction. The strain potential form was proposed later [45] and has the form:

$$W = \mu \left[-(\lambda_m^2 - 3)\left[ln(1-\eta) + \eta\right] - \frac{2}{3}a\left(\frac{\tilde{I}-3}{2}\right)^{\frac{3}{2}}\right] \tag{1.40}$$

where $\tilde{I} = (1-\beta)I_1 + \beta I_2$ is a generalized strain invariant and β is a material parameter. a is the global interaction parameter and $\eta = \sqrt{\frac{\tilde{I}-3}{\lambda_m^2-3}}$ whith λ_m is the so-called "locking stretch".

1.5 Modeling dissipative properties: viscoelasticity

Within the section dedicated to the phenomenology of elastomers, we have highlighted a dissipative behavior of rubber-like materials due to their viscoelastic nature [16]. In this section, we will recall the general framework of viscoelasticity aiming to take into account the dissipation effects. In fact, viscoelastic materials are those for which the relationship between stress and strain depends on time or, in the frequency domain, on frequency. This section is organised in two part: while the first is dedicated to the linear viscoelastic behavior and to some basic rheological models describing this dissipative behavior, the second investigates the finite strain viscoelasticity and some proposed models within the main two approachs commonly used in this framework: integral based approach and internal variables approach.

1.5.1 Linear viscoelasticity

Viscoelastic materials are those for which the relationship between stress and strain depends on time. Linear viscoelastic materials are those for which there is a linear relationship between stress and strain, and the linear viscoelasticity theory have a sens of "idealization" for this class of materials. The effects of creep (evolution of the strain in response to a stress step) and of relaxation (evolution of the stress in response to a deformation step) evoked in fig. 1.3 call on the concept of "memory" of viscoelastic materials. The linear viscoelastic behavior can be defined from the data of one of these response functions with care to linearity and Boltzmann superposition principle. The stress (respectively strain) is hence linear functional in the whole history of deformation (respectively stress).
The constitutive equation for an isotropic linear viscoelastic material is:

$$\boldsymbol{\sigma}(t) \;=\; \int_0^t \lambda(t-\tau)\, tr(\dot{\boldsymbol{\epsilon}})(\tau)\, d\tau\, \mathbf{I} \;+\; \int_0^t 2\mu(t-\tau)\, \dot{\boldsymbol{\epsilon}}(\tau)\, d\tau \tag{1.41}$$

where λ and μ are the lamé parameters [35], that explicitely defines the relaxation functions.
A commonly used approach is to seperate the stress into deviatoric and spherical parts [46] for near incompressible materials:

$$\begin{cases} \mathbf{s}(t) = \boldsymbol{\sigma}(t) - \frac{1}{3} tr\boldsymbol{\sigma}(t)\, \mathbf{I} \\ \mathbf{e}(t) = \boldsymbol{\epsilon}(t) - \frac{1}{3} tr\boldsymbol{\epsilon}(t)\, \mathbf{I} \end{cases} \tag{1.42}$$

$\mathbf{e}(t)$ (respectively $\mathbf{s}(t)$) is the deviatoric part of the deformation tensor (respectively stress tensor).
The constitutive equation could then be written as:

$$\begin{cases} \mathbf{s}(t) = \int_0^t 2\mu(t-\tau)\,\dot{\mathbf{e}}(\tau)\,d\tau \\ tr\boldsymbol{\sigma}(t) = 3\int_0^t K(t-\tau) tr\dot{\boldsymbol{\epsilon}}(\tau)\,d\tau \end{cases} \tag{1.43}$$

where K is the bulk modulus.
An alternative form of eq. (1.41) for incompressible materials can be:

$$\boldsymbol{\sigma}(t) = \int_0^t 2\mu(t-\tau)\,\dot{\mathbf{e}}(\tau)\,d\tau - p(t)\mathbf{I} \tag{1.44}$$

and $\mu(t)$ is function of relaxation, and this equation can be written for creep. To approximate this relaxation function, we present some basic rheological models in linear viscoelasticity.

1.5.1.1 Rheological models in linear viscoelasticity

Viscoelasticity is the property of materials that exhibit both viscous and elastic characteristics when undergoing deformation. Within linear viscoelasticiy, the elastic property is modeled by a linear spring while the viscous part is modeled by a newtonian fluid dashpot, as shows section 1.5.1.1.

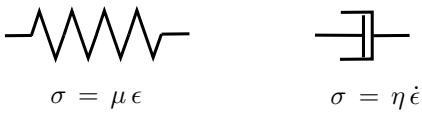

Figure 1.11: Rheology basic elements in viscoelasticity

In order to correctly represent the complex behavior of viscoelastic materials, these rheological elements are assembled in series or in parallel. For elements in parallel, the relaxation function of the set is the sum of the relaxation functions of the elements (all the elements undergo the same strain, the total stress is the sum of the stress on each element). For the elements in series, the creep function of the set is the sum of the creep functions of the elements (the same stress is supported by all the elements, but the total strain is the sum of the strains of each element). In the following, we briefly recall relaxation functions issued from some classic models in litterature.

Maxwell model This model consists on a series assembly of the previously mentionned rheological elements as shows fig. 1.12. This model is able to model a viscoelastic fluid behavior but not a viscoelastic solid.

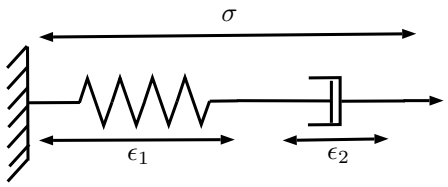

Figure 1.12: Mawxell model

As mentionned above, the same stress is supported by all the elements, but the total strain is the sum of the strains of each element:

$$\begin{cases} \sigma(t) = \mu\,\epsilon_1(t) \\ \sigma(t) = \eta\,\dot{\epsilon_2}(t) \\ \epsilon(t) = \epsilon_1(t) + \epsilon_2(t) \end{cases} \tag{1.45}$$

The governing equation of this model is:

$$\dot{\sigma} + \frac{\mu}{\eta}\sigma = \mu\dot{\epsilon} \tag{1.46}$$

The instantaneous response is given as: $\sigma_0 = \mu\epsilon_0$. The relaxation kernel of this model is given as:

$$\mu(t) = \mu e^{(\frac{-t}{\tau})} \tag{1.47}$$

with $\tau = \frac{\eta}{\mu}$ is the relaxation time.

Kelvin model The Kelvin model, as shows fig. 1.13, consists of a spring and dashpot in parallel, so that the strain experienced by the spring is the same as that experienced by the dashpot:

$$\begin{cases} \sigma_1(t) = \mu\,\epsilon(t) \\ \sigma_2(t) = \eta\,\dot{\epsilon}(t) \\ \sigma(t) = \sigma_1(t) + \sigma_2(t) \end{cases} \tag{1.48}$$

This model is mainly used to explain the creep behaviour of viscoelastic materials meanwhile it poses the limitation of not supporting the instantaneous deformations.

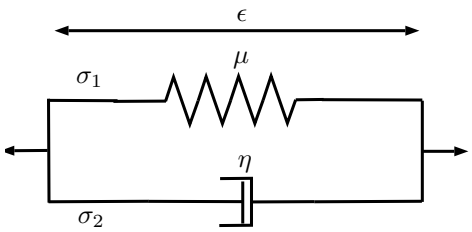

Figure 1.13: Kelvin model

The governing equation is written as:

$$\sigma \;=\; \eta\dot{\epsilon} + \mu\epsilon \tag{1.49}$$

Standard linear solid (SLS) model The standard linear solid model (also referred to as Zener model) effectively combines the Maxwell model and a Hookean spring in parallel, as shows fig. 1.14. A viscous material is modeled as a spring and a dashpot in series with each other, both of which are in parallel with a lone spring. For this model, the governing constitutive relation is:

$$\dot{\sigma} \;+\; \frac{\mu}{\eta}\sigma \;-\; \frac{\mu_\infty\,\mu}{\eta}\epsilon \;=\; (\mu_\infty + \mu)\dot{\epsilon} \tag{1.50}$$

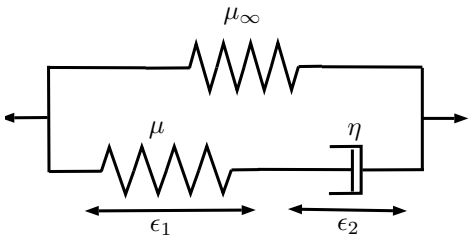

Figure 1.14: SLS model

The relaxation kernel issued from this model is:

$$\begin{aligned}\mu(t) &= \mu_\infty \;+\; \mu e^{\left(\frac{-t}{\tau}\right)} \\ &= \mu_\infty \left(1 + \tfrac{\mu}{\mu_\infty}\, e^{\left(\frac{-t}{\tau}\right)}\right)\end{aligned} \tag{1.51}$$

For a relaxation test, the long time response ($t \to \infty$) of this model is found to be $\sigma = \mu_\infty\,\epsilon_0$, which justifies the denomination of "infinite elasticity" given to the first spring.

Generalized maxwell model The Generalized Maxwell model also known as the Maxwell–Wiechert model is the most general form of the linear model for viscoelasticity [47]. It takes into account that the relaxation does not occur at a single time, but at a distribution of times. This model consists of a parallel assembly of n Maxwell models and a NeoHookean spring, as shows fig. 1.15. This leads to a model

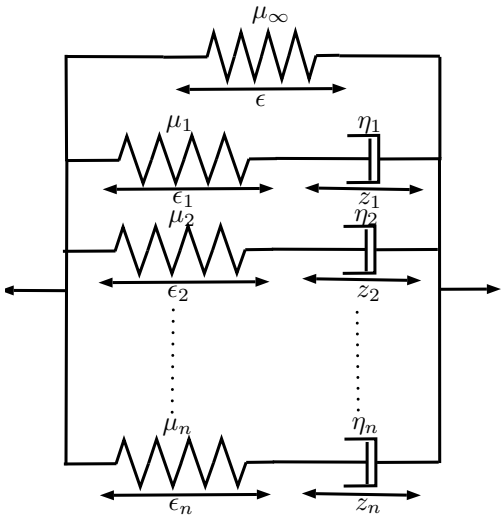

Figure 1.15: Maxwell–Wiechert model

having the same properties as the SLS model, but more capable of smoothing the experimental data. The relaxation kernel is written as:

$$\begin{aligned} \mu(t) = & \ \mu_\infty + \sum_{i=1}^{n} \mu_i e^{(\frac{-t}{\tau})} \\ & = \mu_\infty \left(1 + \sum_{i=1}^{n} \frac{\mu_i}{\mu_\infty} e^{(\frac{-t}{\tau})}\right) \end{aligned} \tag{1.52}$$

This general form is commonly referred to as Prony serie. In the frequency domain, we apply an excitation having the form $\epsilon = \epsilon_0 e^{(i\omega t)}$ and we seek for a solution of the same form $\sigma = \sigma_0 e^{(i\omega t)}$. More accurately, we apply a Fourier transform of eq. (1.44) after introducing the Prony serie

$$\sigma(t) = \mu_\infty \int_0^t \left(1 + \sum_{i=1}^{n} \frac{\mu_i}{\mu_\infty} e^{(\frac{-(t-s)}{\tau_i})}\right) \dot{\epsilon}(s)\, ds \tag{1.53}$$

The obtained stress has the form:

$$\sigma(\omega) \ = \ i\omega\epsilon_0\, g^*(\omega)\, e^{(i\omega t)} \tag{1.54}$$

where $g^*(\omega)$ stands for the Fourier transform of the normalized shear modulus. The obtained dynamic modulus is hence written:

$$\begin{aligned} g^*(\omega) &= \sum_{i=1}^{n} \int_0^{\infty} \frac{\mu_i}{\mu_\infty} e^{(\frac{-t}{\tau_i})} e^{-(i\omega t)} dt \\ \mu^*(\omega) &= \mu_\infty + \sum_{i=1}^{n} \frac{i\omega\mu_i}{\frac{1}{\tau_i}+i\omega} \end{aligned} \tag{1.55}$$

1.5.2 Finite strain viscoelasticity

The framework of the large deformations is a context that adds a difficulty in the description of the viscoelastic behavior. Modeling strain-rate dependent response of rubber materials is derived following different approachs which can be classified according to different criterions. In this section, we made use of the following criterions: The first one is related to the formulation of the model which can be integral based or differential/internal-variables based, while the second criterion is the time-strain separability or factorability [48][49] which is frequently introduced in the formulation of finite strain viscoelastic constitutive models and afford a large theoretical simplicity.

1.5.2.1 Integral based formulation

The integral-based framework is founded on an extension of the Boltzmann superposition principle to finite strain. The stress quantity is decomposed to an hyperelastic part corresponding to the instantaneous/equilibrium stress response, and an overstress quantity expressed as an heriditary integral including a measure of material's memory through relaxation functions. From an historically point of view, multiple-integral representation of the finite strain viscoelastic behavior have been originally proposed by Green and Rivlin [50][51], in a general form commonly referred to as functional Volterra series. This work has been followed by other contributions: [52], [53], [54], [55] and more recently [56], among others. Multiple-integral models are known to be generally non seperable [57] and mainly hardly identifiable.
An example for this class of models is the model proposed by [54]. After introducing

incompressibility condition, and in term of second Piola-Kirchoff stress:

$$\begin{aligned}\mathbf{S}(t) = -p\,\mathbf{C}^{-1} &+ \int_{-\infty}^{t} r_1(t-\tau)\dot{\mathbf{E}}(\tau)\,d\tau \\ &+ \int_{-\infty}^{t}\int_{-\infty}^{t} r_2(t-\tau_1, t-\tau_2)\,\dot{\mathbf{E}}(\tau_1)\dot{\mathbf{E}}(\tau_2)\,d\tau_1 d\tau_2 \\ &+ \int_{-\infty}^{t}\int_{-\infty}^{t}\int_{-\infty}^{t} r_3(t-\tau_1, t-\tau_2, t-\tau_3)\,tr\left(\dot{\mathbf{E}}(\tau_1)\dot{\mathbf{E}}(\tau_2)\right)\dot{\mathbf{E}}(\tau_3)\,d\tau_1 d\tau_2 d\tau_3 \\ &+ \int_{-\infty}^{t}\int_{-\infty}^{t}\int_{-\infty}^{t} r_4(t-\tau_1, t-\tau_2, t-\tau_3)\,\dot{\mathbf{E}}(\tau_1)\dot{\mathbf{E}}(\tau_2)\dot{\mathbf{E}}(\tau_3)\,d\tau_1 d\tau_2 d\tau_3 + ...\end{aligned} \tag{1.56}$$

where the r_i designate the i order Volterra kernel which have to be chosen carefully to estimate the viscoelastic behavior.
Meanwhile, the constitutive theory of finite linear viscoelasticity [58] have been of a major contribution within this framework, and small deviations away from the thermodynamic equilibrium are assumed. The proposed models with respect to this theory are generally of single integral presentation and have been widely investigated, as by [59], [60], [61] and[62], for the simplicity they afford to enginnering applications. Some of most used models of this contruction type which are seperable and do not require hard identification procedure could be found in [63], [64], [65] and [66]. As examples of models of single interal formulation, we can find:

- Christensen model [67]

$$\boldsymbol{\sigma} = -p\mathbf{I} + 2\mathbf{B}\frac{\partial W}{\partial \mathbf{B}} + \mathbf{F}\,G_0\int_0^t g_1(t-s)\frac{\partial \mathbf{E}(\mathbf{s})}{\partial s}ds\mathbf{F}^T \tag{1.57}$$

- QLV model [68]

$$\boldsymbol{\sigma} = -p\mathbf{I} + 2\mathbf{B}\frac{\partial W}{\partial \mathbf{B}} + \mathbf{F}G_0\int_0^t g_1(t-s)\,\frac{\partial \mathbf{S}}{\partial s}\,ds\,\mathbf{F}^T \tag{1.58}$$

- Hallquist model [69] (implemented in LS-DYNA)

$$\boldsymbol{\sigma}^{Fg} = -p\mathbf{I} + 2\mathbf{B}\frac{\partial W}{\partial \mathbf{B}} - \mathbf{F}G_0\int_0^t \frac{\partial g_1(t-s)}{\partial(t-s)}\,\beta_1\mathbf{C}^{-1}(s)\,ds \tag{1.59}$$

- Yang et al model [70]

$$\boldsymbol{\sigma}^{Fg} = -p\mathbf{I} + 2\mathbf{B}\frac{\partial W}{\partial \mathbf{B}} - \mathbf{F}G_0 \int_0^t \frac{\partial g_1(t-s)}{\partial(t-s)} \left(\beta_1 + \beta_2 \mathbf{I}_2(s)\right) \mathbf{C}^{-1}(s)\, ds \tag{1.60}$$

where G_0 is the instantaneous shear modulus, g_i are the dimensionless Prony series parameters and β_i are material parameters.

In the work of [71], a seperable model adapted for high strain rates was introduced, meanwhile, other contributors [62] have found that it shows some shortcomings owing to a zero Young's modulus in the undeformed configuration. We denote that a new class of quasi-linear models, consisting on a generalization of fung's models [68] describing nonlinear viscoelastic response of materials, have been latterly proposed by [72][73] where the linearized strain is expressed in terms of a nonlinear measure of the stress. Within this framework, other models are found to be non seperable as [74], [75], [26] and [76] among others. The recently proposed model by [77] offers the ability to be seperable or non seperable according to the choice of some variables.

1.5.2.2 Differential and internal variables model

The second framework, differential/internal-variables, consists on a 3D generalization of the 1D rheological models with large deformations. Whithin this framework, two different approachs could be considered: differential models without thermodynamics considerations [14], and the thermodynamically consistent internal-variables approach [78][79]. Considering differential approach, some of these models could be classified according to the seperability criterion to: seperable [80], [81], non-seperable that leads to integral [82] and non-seperable that does not lead to integral [83]. The second approach, internal-variables, was originally proposed by [84] and [85] as generalization of the work of Biot [86]. This approach have been more investigated mid 1970s by [78][79], inspired by the work of [87] on elasto-plastic deformations. This thermodynamically consistent approach consists on a multiplicative decomposition of deformation gradient into elastic and inelastic parts, and one can take either the "over-stress" or the inelastic strain as an internal variable. The key point to develop models of this form is the choice of the evolution equation for the internal variables which is not evident nor unique. The particularity of these models is that in some cases they could lead to an integral equation, and specially some contributors introduced linear evolution equations for the internal variables: seperable models including works of [88], [89], [85] and [90], and non seperable models as [84]. Even

thought some models could take the integral form and are seperable, they are found to be hardly identifiable and require a large number of material parameters except the Simo model. Examples of non seperable internal-variables models that don't lead to an integral equation would include the work of [91], [23], [92], [93], [94] among others.

1.6 Conclusion

Within this chapter, we tried to present a sort of review for the mechanical behavior of elastomeric materials. We firstly recalled the phenomenological behavior of elastomers which are known to be of high deformability and posessing dissipative capabilities. Those materials are widely used in industrial context, even with non mastered phenomena and experimental investigations pointing out lots of non linear effects. Modeling elastomers behavior correctly should be done within the framework of finite strain viscoelaticiy. In the second part of this chapter, we recalled basic concepts of this description, with uncoupled elastic and viscous effects. The next chapter will be dedicated to experimental investigation on three rubber-like materials. In fact, to well design the industrial compound or device, a suitable choice of elastomeric material is a primary future, combining stiffness properties and damping requirements. To this end, this survey will be carried on candidate mixtures chosen with respect to those requirements.

Chapter 2

Experimental investigation on three rubber-like materials

Contents

2.1 Introduction

In the previous chapter, we highlighted that elastomers are widely used in industry due to their mechanical properties particularly their damping capabilities[6][4]. Subjected to complex combinations of manufacturing and service loadings, elastomers show the fact of undergoing severe loading conditions [95]. It has been pointed out through experimental investigations that rubber-like materials show lots of non linear behaviors [3]. Estimating the damping capability is a primary feature to be considered in many engineering applications and to design industrial compounds efficiently, it is of major importance to measure the sensitivity of the dynamic response to the influencing parameters [96].
This chapter is dedicated to a series of experimental observations on three vulcanized rubber materials : Natural Rubber NR, Bromobutyl BIIR and a mix of both NR/BIIR. The considered materials are intended to the specified damping application.Firstly, we present the considered materials and the furnished parameters, the experimental set-up as well as the used procedures for an efficient specimens testing.

The following section reports the experimental results for the monotonic and dynamic investigation of the three elastomers. In order to evaluate the hysterisis response, cyclic tests are presented. The Mullins effect have been studied by many authors whith different approaches [23][21][97] and it is to denote that for the intended industrial application, a preconditionning procedure is applied to eliminate this effect. Since the rubber-like material's behavior is pronounced to be rate-dependent, multistep tests were used to approach the nonlinear elastic equilibrium with a good approximation. Relaxation tests were conducted in order to identify the viscoelastic behavior of the tested materials, which is time dependent none deformation dependent i.e time-strain separable [48][49]. In the same section, dynamic tests are presented. Herein, we intentionally avoid the Payne Effect [25], which consists on a dynamic amplitude dependent softening effect [26]. Both frequency and temperature dependence were evaluated and discussed. Within this investigation, a coupled temperature-frequency dependence is highlighted. Increasing frequency leads to shift the glass transition temperature to higher values [98]. Moreover, the influence of the static predeformation on the dynamic response were investigated [99]. Conclusions are drawn concerning a comparison of the materials properties, with consideration to the industrial applications.

2.2 Materials and specimens

2.2.1 Materials

The aim of this experimental investigation is the characterization of some candidate rubber-like materials, that have to satisfy some requirements from mechanical properties as well as degazage and cleanliness imposed by **ESA standard ECSS Q-70-02A**. It should also be emphasized that the mixture must have a good capability for molding, and good adhesion to metal insert. The chosen vulcanized rubber-like materials throughout this work are:

- a filled natural rubber NR vulcanizate
- a filled bromo butyl BIIR vulcanizate
- a mix of both precedent filled rubbers NR/BIIR vulcanizate

The considered rubbers were provided by " *EMAC Technical Rubber Compounds*". The mechanical behavior of the three materials is known to be incompressible hyper-visco elastic [3][16][100], as highlighted in Chapter 1.

Tables 2.1 to 2.3 summarizes the measured hardness and the furnished vulcanization and strength parameters. The manufacturer also provided curemeter curves, shown in figs. 2.1 to 2.3, for vulcanization, on MDR 2000 Moving Die Rheometer which is designed to test mixed rubber and capable of measuring rubber compound cure under isothermal test conditions with constant strain and frequency.

	NR	BIIR	NR/BIIR
Shore A	41	30	27

Table 2.1: Measured hardness

	Test Temp °C	Test time min	ML dNm	MH dNm	ts_1 min	ts_2 min	t_{10} min	t_{50} min	t_{90} min
NR	160	5	0.82	7.73	1.08	1.20	1.02	1.36	2.31
BIIR	160	10	1.6	3.83	3.85	6.48	0.1	4.06	6.56
NR/BIIR	160	10	1.06	2.90	5.76		2.90	5.57	8.20

Table 2.2: Vulcanization parameters

	R.Fracture MPa	A.Fracture %	M@50% MPa	M@100% MPa	M@200% MPa	M@300% MPa
NR	20.7	683	0.73	1.04	1.62	2.4
BIIR	13.5	902	0.47	0.78	1.28	1.84
NR/BIIR	9.77	920	0.48	0.66	1.03	1.42

Table 2.3: Strength properties

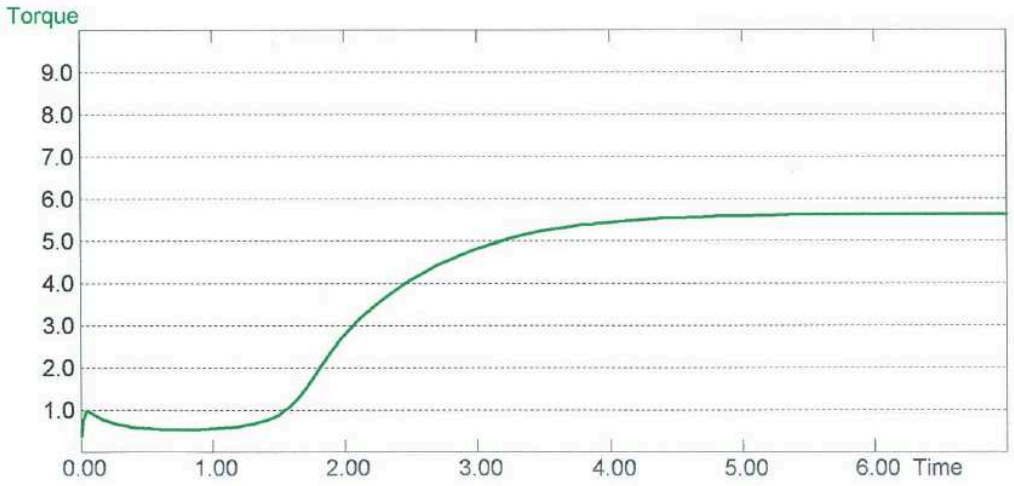

Figure 2.1: NR rheometer response

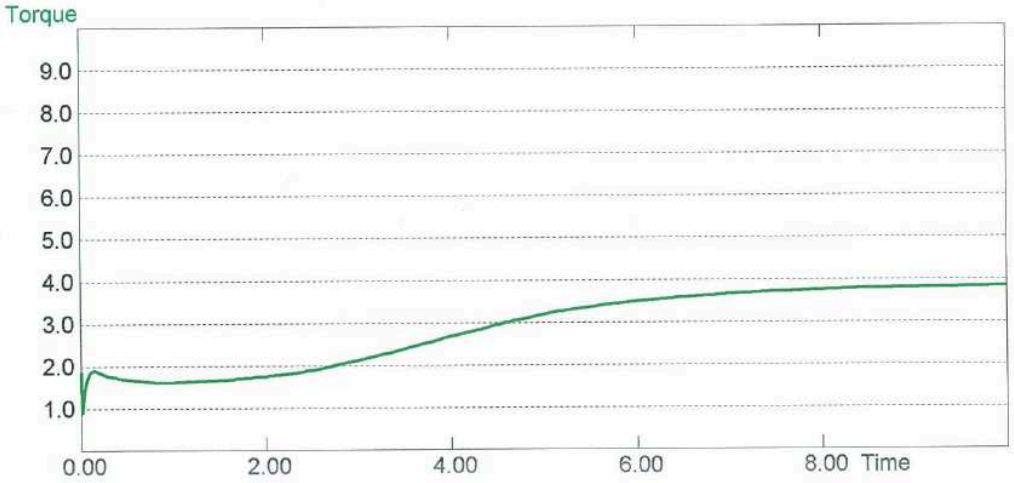

Figure 2.2: BIIR rheometer response

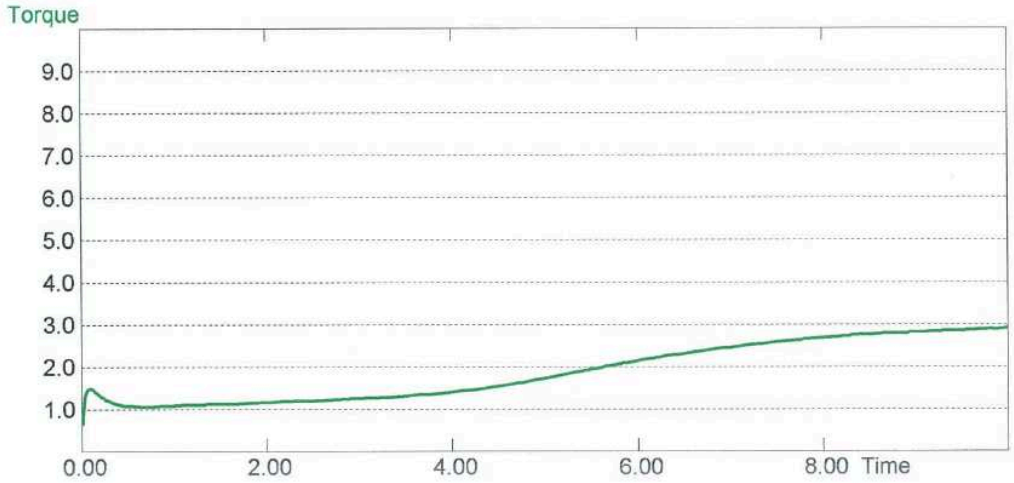

Figure 2.3: NR/BIIR rheometer response

2.2.2 Experimental devices

The objective of this section is to present the material available to us to carry out the mechanical characterization of our candidate materials.

2.2.2.1 Traction Machine

Traction machines are commonly used in the rubber industry to control the tensile traction characteristics of materials such as stress and strain till break. For monotonic testing, we made use of the Instron 3345 single-column compression traction

machine which is particularly suitable for traction and compression tests of elastomeric materials, with force ranges of less than 5 kN. This testing machine is used for its precision :

- 100: 1 force range (use of 1.0% force sensor capacity without loss of accuracy)
- Strain rate 0.001-500 mm.min^{-1}
- Data acquisition rate of 500 Hz
- Vertical test area of 1123 mm (44.2 in)

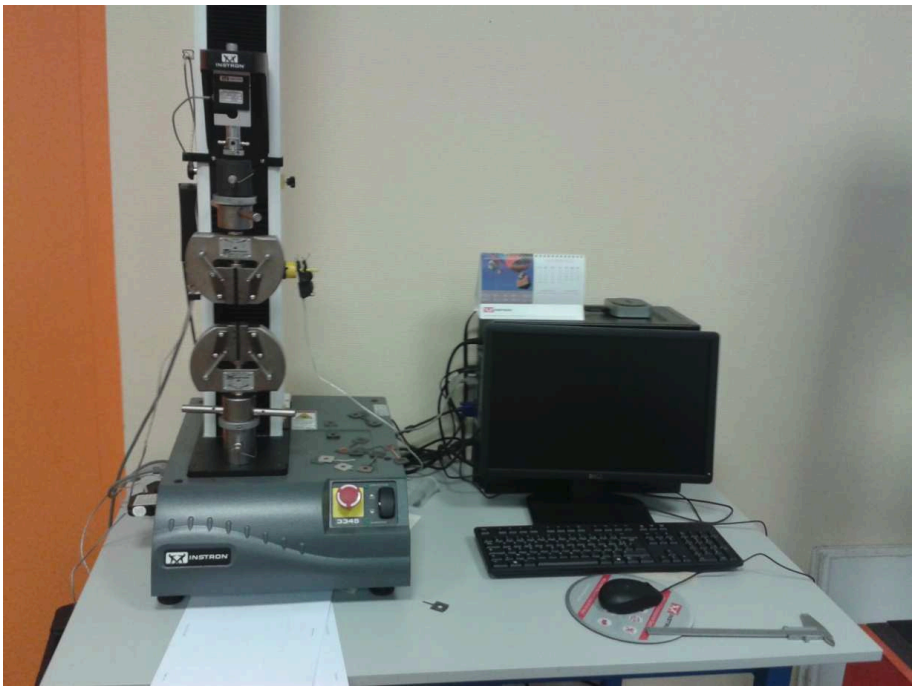

Figure 2.4: Instron 3345 testing machine

2.2.2.2 Visco-analyzer

The Metravib DMA 50N shown in fig. 2.5 allows to characterize dynamic behavior of materials:

- Maximum force 50N
- Maximum displacement +/- 3mm
- Frequency range 10^{-3}-100 Hz
- Temperature range -100→+500 °C
- Temperature rate range +/-0.1 → +/-10 °C min^{-1}

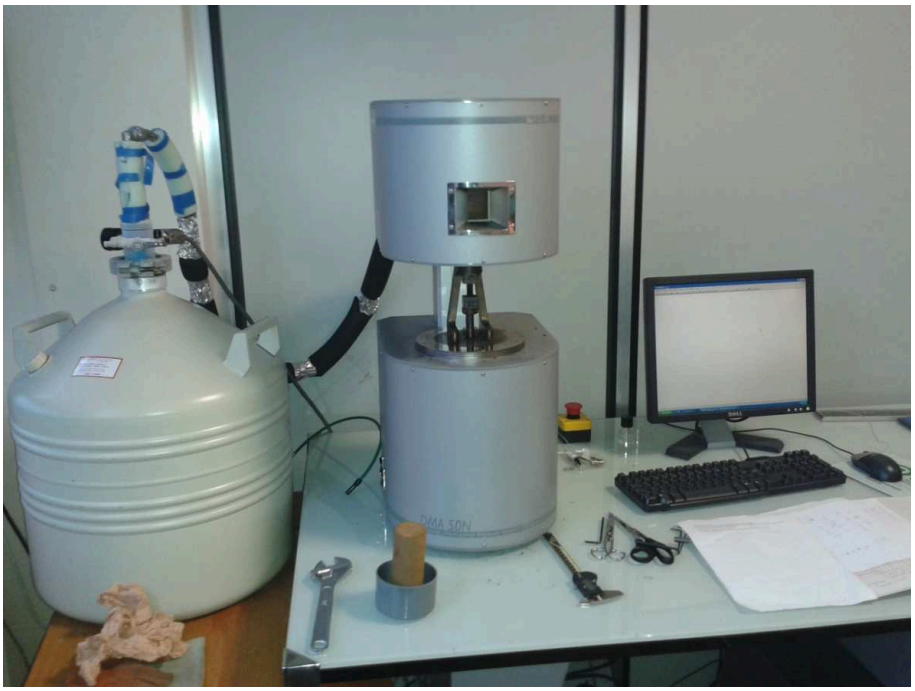

Figure 2.5: Metravib DMA 50N testing machine

2.2.3 Differential scanning calorimetry

Differential scanning calorimetry, commonly named DSC and developed by [101], is a thermoanalytical technique in which the difference in the amount of heat required to increase the temperature of a sample and reference is measured as a function

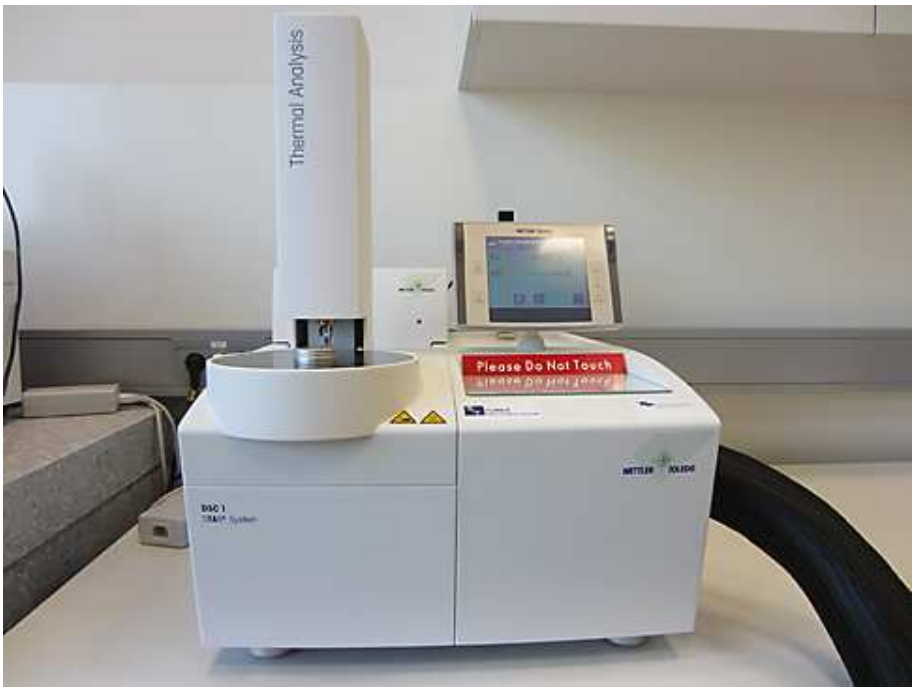

Figure 2.6: DSC machine

of temperature. Both the sample and reference are maintained at nearly the same temperature throughout the experiment. Generally, the temperature program for a DSC analysis is designed such that the sample holder temperature increases linearly as a function of time. The reference sample should have a well-defined heat capacity over the range of temperatures to be scanned. DSC is used widely for examining polymeric materials to determine their thermal transitions.

2.2.4 Test specimens

According to the tests carried out during this part, different geometries of test specimens were used. These are all obtained from a 2.3 mm thick plates molded in compression in which the test pieces are cut-out with a punch.

2.2.4.1 Haltère type 2 specimen

The Haltère type 2 specimen (fig. 2.7), commonly referred to as H2 Specimen, was used for monotonic tension tests. These specimens are normalized according to **ISO 37 standard**.

Figure 2.7: H2 Specimen (ISO 37 standard)

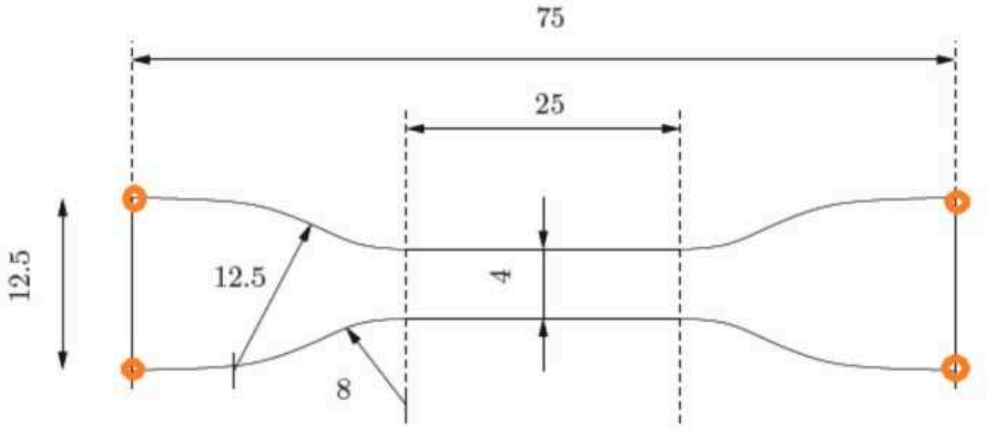

Figure 2.8: H2 Specimen dimensions in mm

2.2.4.2 Quad-shear samples

The Quad-shear test specimen [102] consists of four rubber parts glued on four rectangular metallic fittings, as shows fig. 2.9. This specimen is used for monotonic shear tests

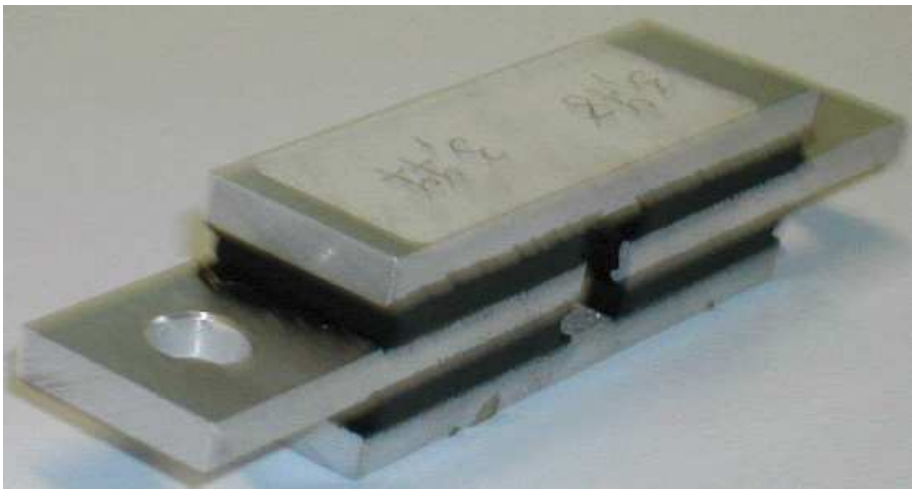

Figure 2.9: Quad-shear sample

2.2.4.3 DMA double shear specimen

The DMA double-shear test piece consists of three metal fittings on which two cylindrical rubber parts are glued. This test piece will be used to quantify the viscous behavior of our materials. Due to some testing difficulties for thermal testing, we substituted the steel reinforcements by aluminium ones to gain on adherance between rubber/glue/reinforcement, as shows fig. 2.10

Figure 2.10: specimen preparation

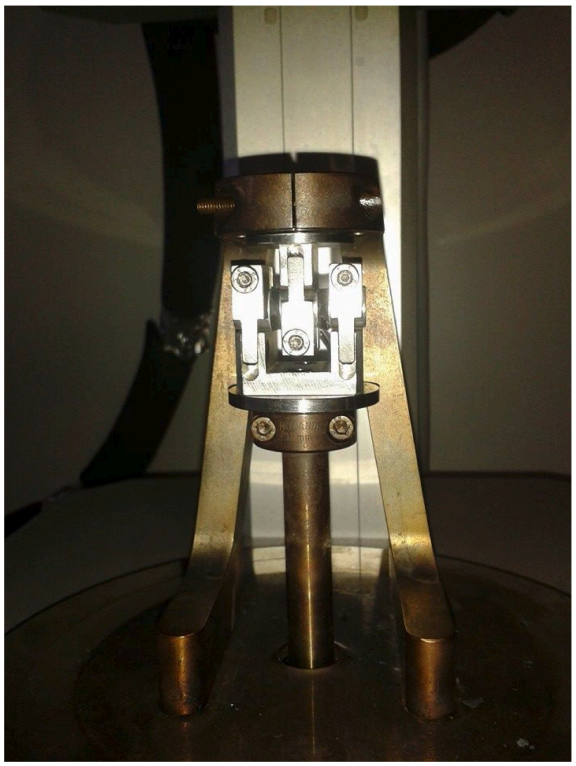

Figure 2.11: DMA shear specimen holder

2.2.4.4 DSC sample

DSC samples are analysed in small metal pans, designed for optimal thermal conductivity and minimum reaction with the sample. Pans may be open, pin-hole, covered or sealed

Figure 2.12: DSC pans

2.3 Experimental procedure

2.3.1 Monotonic testing

The monotonic tests aims to identify the hyperelastic behavior of the three vulcanized rubber materials. Taking different loading paths into account, sets of experiments including uniaxial tension and simple shear tests were carried out on an Instron 3345 Table machine. The tension tests were performed using standardized Haltere type 2 specimens, as shows fig. 2.8. Shear tests were achieved with the use of quad-shear specimens holders [102][9], as shows fig. 2.9, with four elastomeric inserts of 25mm height, 15mm wide and 2.3mm thick cut out from plates. An industrial cyanoacrylate fast-acting adhesive was used to hold the assembly. Note that preliminary tests showed that the shear occurs on inserts none on glue. The monotonic experiments were performed at room temperature under displacement control, and the engineering strain was calculated assuming an homogeneous deformations on the whole specimen. At least three tests were carried out for each loading path.
For the uniaxial tension, the specimens were loaded till 500% of deformation under strain-rates of 10% min^{-1}, 100% min^{-1} and 200% min^{-1}. Avoiding that the shear occurs on glue, the shear tests were loaded till 100% of deformation at 5% min^{-1}, 10% min^{-1} and 20% min^{-1}. Focusing on the equilibrium hyperelastic stress response, we make use of multistep experiments at different strains with holding periods of 10 minutes during which the applied strain was held constant[23], as shows fig. 2.13.
It is important to underline that a preconditioning procedure allows to not consider the Mullins effect, that is known to be a stress softening of virgin specimens in the first loading cycles [21][103]. The elastomeric samples were subjected to 5 loading-unloading cycles, under a constant strain-rate of 100% min^{-1} for uniaxial tension and 10% min^{-1} for shear loadings.

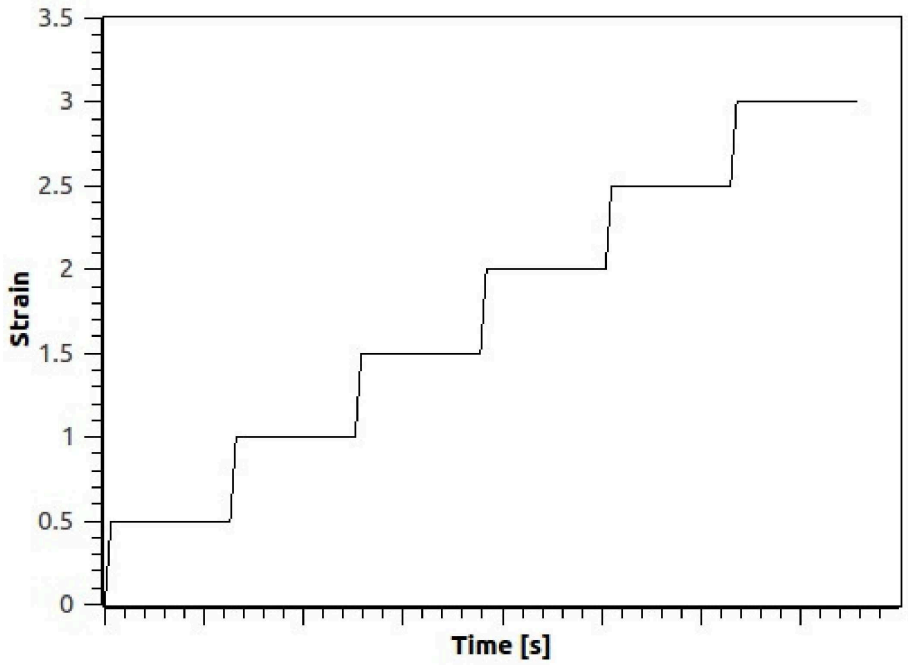

Figure 2.13: Strain history for monotonic testing

2.3.2 DMA tests

To identify the time-dependent viscoelastic behavior, stress relaxation experiments were conducted on a Metravib DMA machine of load capacity 50N by mean of the double shear specimens holder as shown in fig. 2.11. It consists on an assembly of metallic cylinders with elastomers sheet cut out of plates of 10mm diameter and 2.3 mm thickness, as shown in fig. 2.10. The experimental procedure consists on deforming the specimen with a traverse rate of 100% min^{-1} at different strains levels, ranging from 10% to 50%, and holding the assembly for four hours. An hysteresis is seen to quickly vanish and the steady relaxation response is measured.
Investigating the dynamic properties of the considered elastomers, the experimental procedure consists on superimposing a simple shear predeformation and a sinusoidal strain after sufficient relaxation time of about 10 mn as:

$$\epsilon(t) = \epsilon_0 + \triangle\epsilon.sin(\omega t) \tag{2.1}$$

where ϵ_0 denotes the predeformation and $\triangle\epsilon$ the strain amplitude.
To consider the frequency-dependence of the material's behavior, frequency sweep tests with stepwise changing frequency from 0.1Hz up to 40Hz at constant predefor-

mation were used. Furthermore, the predeformation-dependence was investigated through imposing different levels of prestrain levels from 10% up to 30% [104]. The dynamic deformation amplitude was set as maximum dynamic strain is less than 1%, in order to avoid another softening effect, the so-called Payne-effect [25][105]. The Payne-effect is an amplitude dependent stress softening that leads to a decrease of the storage modulus for increasing dynamic strain amplitude and a maximum of the loss modulus at middle strains. Since elastomers are known to be sensitive to thermal environement, dynamic investigation were conducted with a temperature sweep from -100 °C to 100 °C with a temperature rate of 2 °C per minute.

2.4 Experimental results and discussion

2.4.1 Monotonic Tests

2.4.1.1 The Mullins Effect

To investigate the softening behavior of virgin specimens, loading-unloading cycles were applied under a constant strain rate of 100% min^{-1}. During this process, a maximum of stress is reached in the first cycle [22]. The second cycle shows a significant decrease in the stress value. Figures 2.14 and 2.15 show cyclic responses of the three filled rubbers, under tension and shear modes, respectively. One can observe that the mechanical softening occurs until a quasi-stationary loop is reached [21][102][23]. Both BIIR and NR/BIIR reached this loop beginning from the third cycle. NR exhibit continuous non-linear softening effect and reached the stationary loop at the fifth cycle.

2.4.1.2 Strain-rate dependence

The three elastomers exhibit strain-rate dependence in the studied range of deformation. Increasing deformation rate leads to a higher stress, till a glassy hyperelastic response is obtained [106][107][108]. Figure 2.16 shows that NR is dependent for all the applied strain-rates while BIIR exhibit the glassy behavior for strain-rates higher than 100% /min. The NR/BIIR material shows a slight dependence, with maximum deviation of 5%. Moreover, for BIIR and NR/BIIR, this dependence is seen to be pronounced for high strains, higher than 200% of deformation.

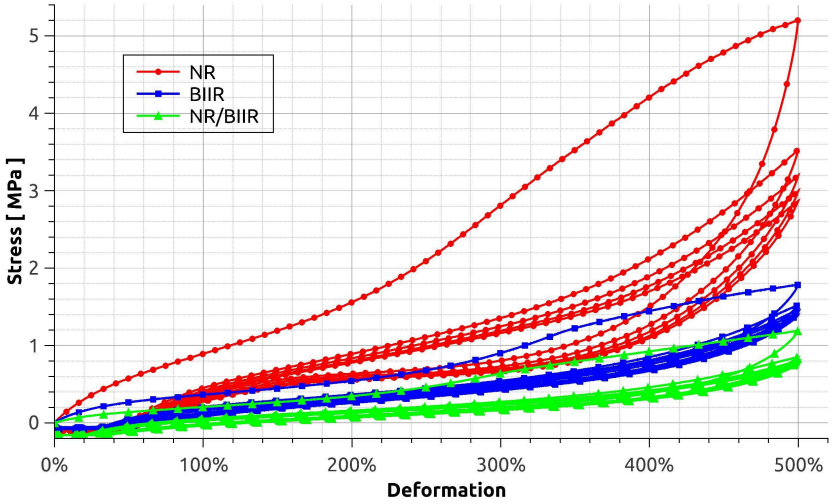

Figure 2.14: Uniaxial tension cyclic loading

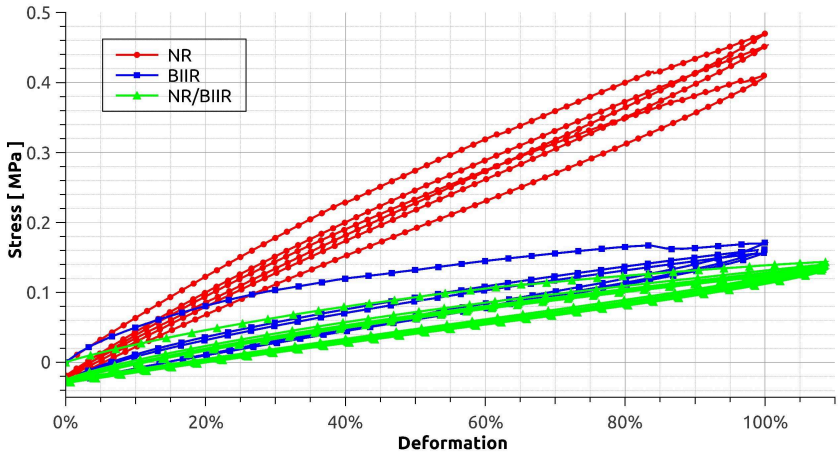

Figure 2.15: Simple shear cyclic loading

Focusing on the hyperelastic equilibrium stress-strain curve, the constant strain-rate was interrupted by several holding times, with a duration of 10 minutes. Many authors [23][98] suggest that there exists a unique equilibrium response, approached in an asymptotic sense, as the strain rate goes to zero. In our experiments, we have seen that the value of stress reached at the end of each relaxation period is approximately constant at the lower strain-rate. The set of these points is defined as the time-independent equilibrium hyper-elastic stress-strain curve, as shows fig. 2.17. Figure 2.18 graphically shows the equilibrium response of the three elastomers. The

NR is seen to be the stiffest material while NR/BIIR is the softer. The reason of this softening is not clear, but could be related to the vulcanization parameters.

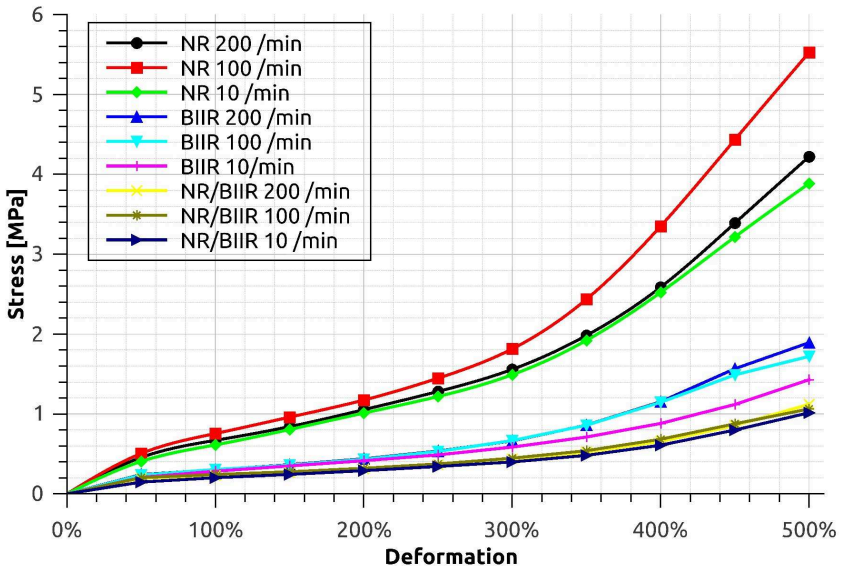

Figure 2.16: Non-equilibrium tension stress response at different strain-rates

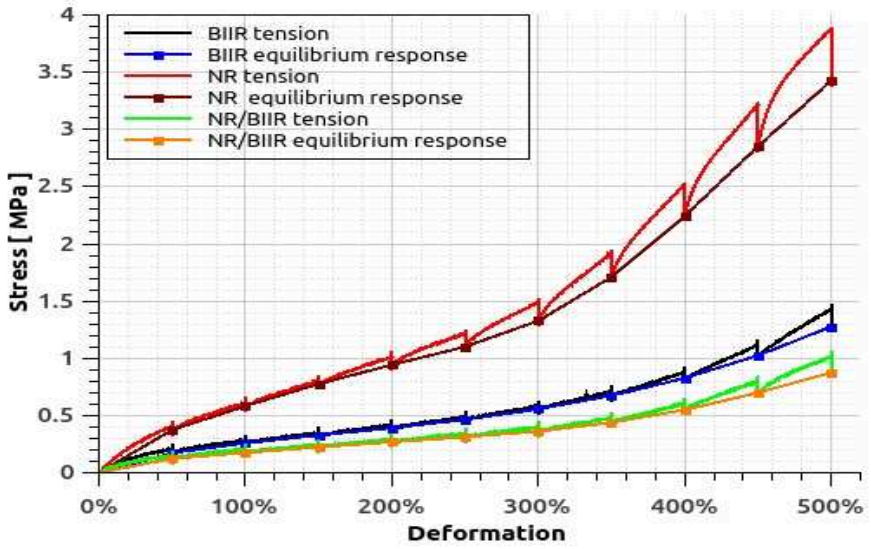

Figure 2.17: Definition of the equilibrium stress-strain curve for the tension mode

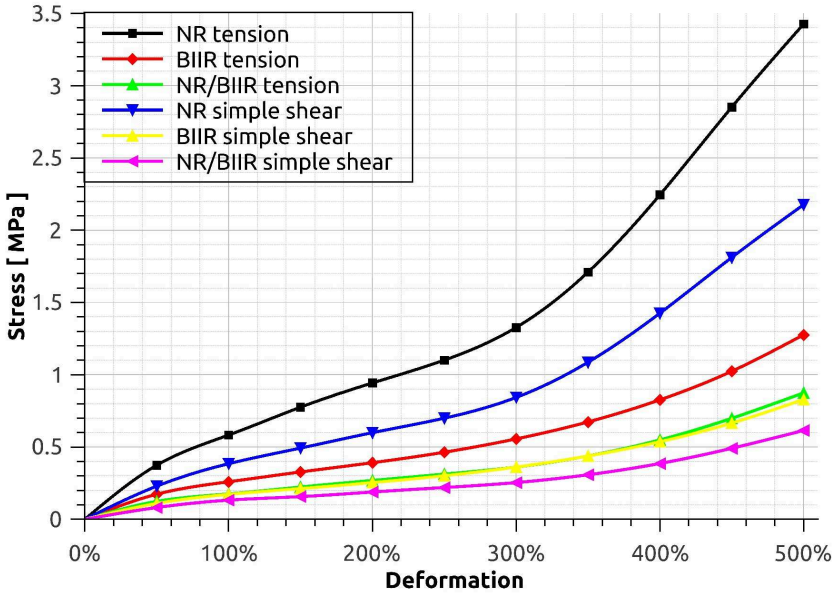

Figure 2.18: Time independent equilibrium stress-strain curve of the three materials

2.4.2 Stress Relaxation

When vulcanized rubbers are deformed, the stress gradually decreases with time [6][16]. In other circumstances, when viscoelastic materials are subjected to a constant stress, the resulting deformation is seen to increase continuously, which is the creep phenomena [6][109]. Stress relaxation experiments were conducted on simple shear specimens, measuring the stress over four hours of relaxation for different constant strains. Figures 2.19 to 2.21 show that the three materials relax and the shift from the levels of maintained strain is quasi linear. Direct comparison of the three materials shows that the relaxation of the natural rubber NR is less obvious than the Bromobutyl filled materials (BIIR and NR/BIIR).

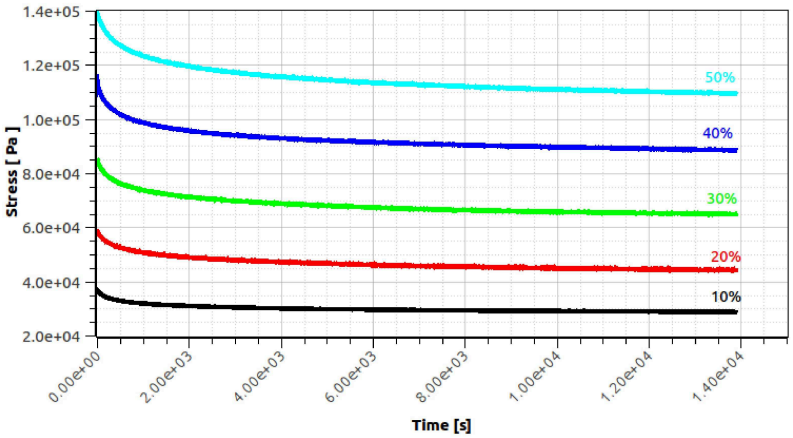

Figure 2.19: Relaxation stress response: BIIR

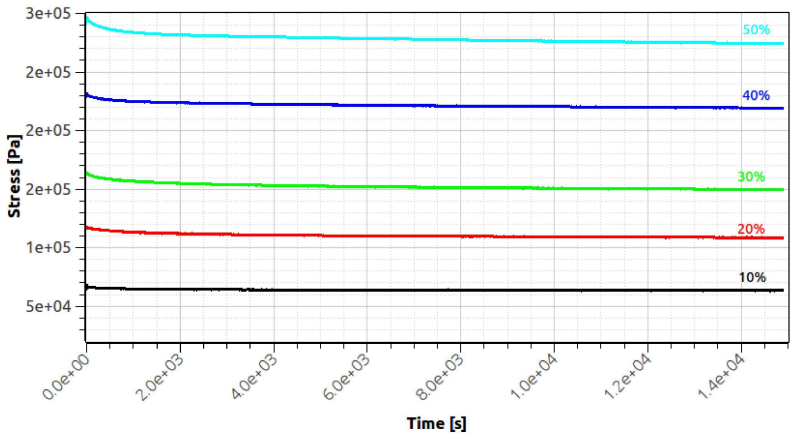

Figure 2.20: Relaxation stress response: NR

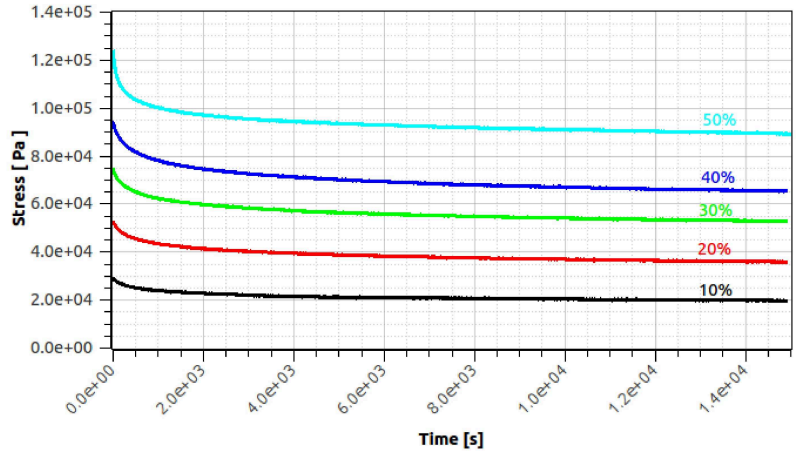

Figure 2.21: Relaxation stress response: NR/BIIR

2.4.3 Time-Strain separability

The time-strain separability in viscoelastic materials [48][49] is not a rule derived from fundamental principles but merely an hypothesis based on experimental phenomena, stress relaxation for long times. In constitutive modeling, time-strain separability has been extensively employed because of its theoretical simplicity and practical convenience [110]. Within our experimental survey, the time-strain separability is confirmed by normalized stress relaxation curves, and graphically shown in figs. 2.22 to 2.24. The normalized stress response is seen to be independent of the deformation. For each material, the different curves form an "envelop" with a maximum deviation of 5%. The three materials exhibit only time dependent behavior none deformation dependence, and the stress could hence be written:

$$\sigma(t, \epsilon) = f(t) \, . \, g(\epsilon) \tag{2.2}$$

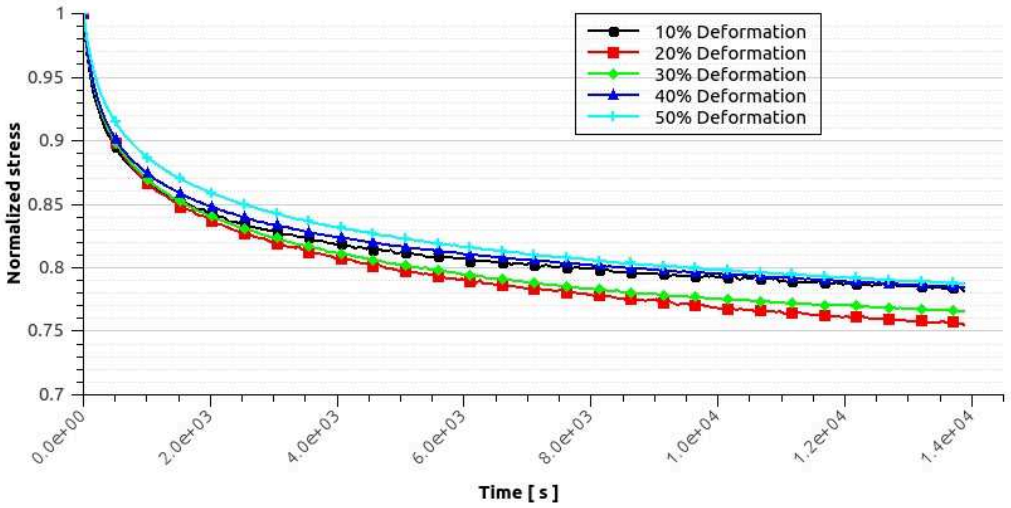

Figure 2.22: Normalized relaxation stress: BIIR

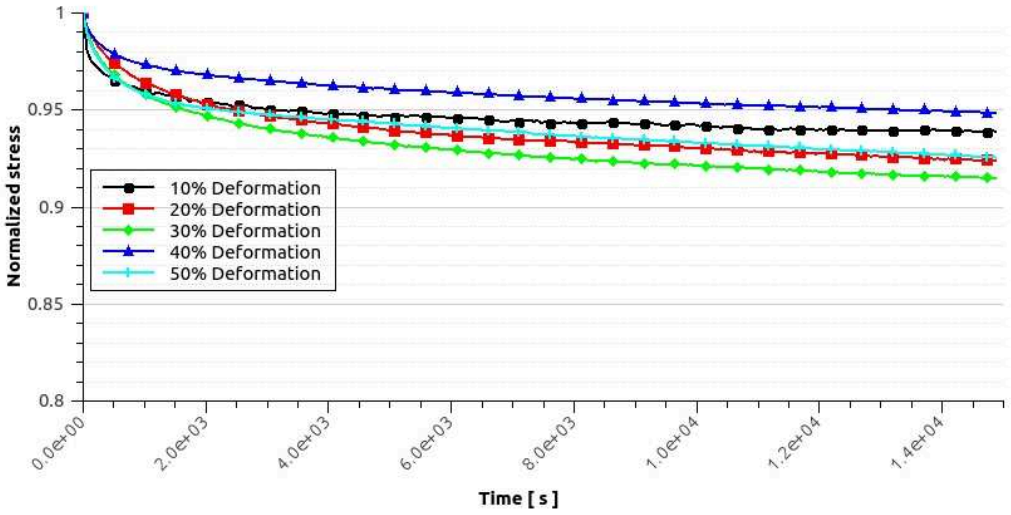

Figure 2.23: Normalized relaxation stress: NR

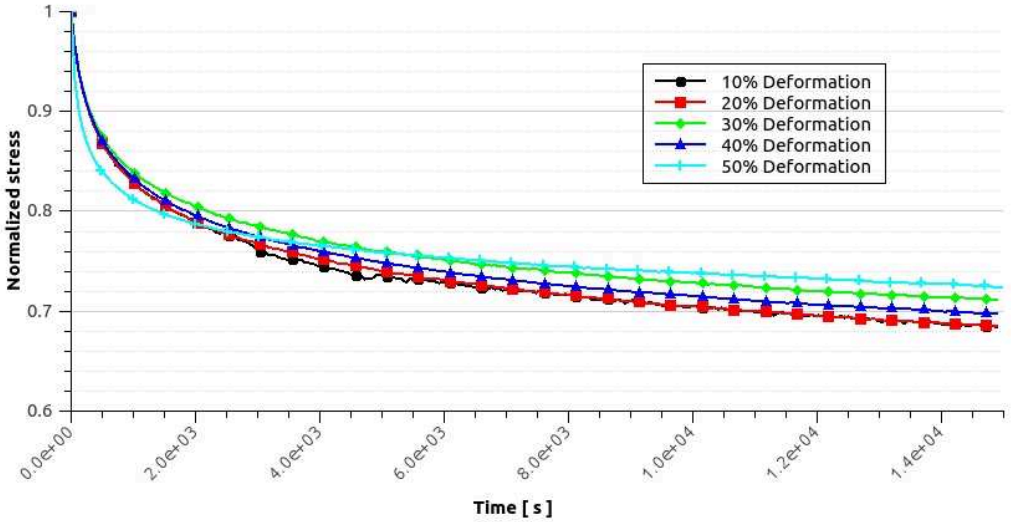

Figure 2.24: Normalized relaxation stress: NR/BIIR

2.4.4 Temperature effect on dynamic properties

The variation of dynamic mechanical properties (storage modulus and loss factor) with temperature provide fundamental knowledge for understanding the filled rubber characteristics [26][111]. As mentioned above, we performed temperature sweep test for the three materials, at a small dynamic strain amplitude to avoid the Payne effect. The results are shown in figs. 2.25 and 2.30. At low temperature, the shear storage modulus is at its maximum, and the loss factor at its minimum. This is the glassy state of the material. Increasing the temperature, the storage modulus decreases suddenly and the loss factor reach its maximum. The maximum point of the this factor defines the glass transition temperature. For higher frequencies, the behavior is stable and not too dependent of temperature compared to the previous areas. This domain is called the "rubbery plateau" [112]. In fact, the glass transition were measured for the three materials using the peak for the loss factor at 1 Hz as measure. The three materials exhibit the same response, with different glass transition temperatures varying from -55 °C for the NR, -45 °C for the BIIR, -40 °C for the NR/BIIR. There exist important differences between the Tg values depending on the measurement method [113][114] (DSC, DMA).
The value of the glass transition temperature is shown, for example in fig. 2.30, to be sensitive to frequency. Increasing the frequency leads to a higher glass transition temperature. The T_g is seen to be shifted approximately with 4 °C per decade of frequency. This effect can be explained by the work of [16][115][116], resuming that dynamic mechanical properties of certain thermo-rheologically simple materials depend on a single variable combining the temperature and frequency effects.

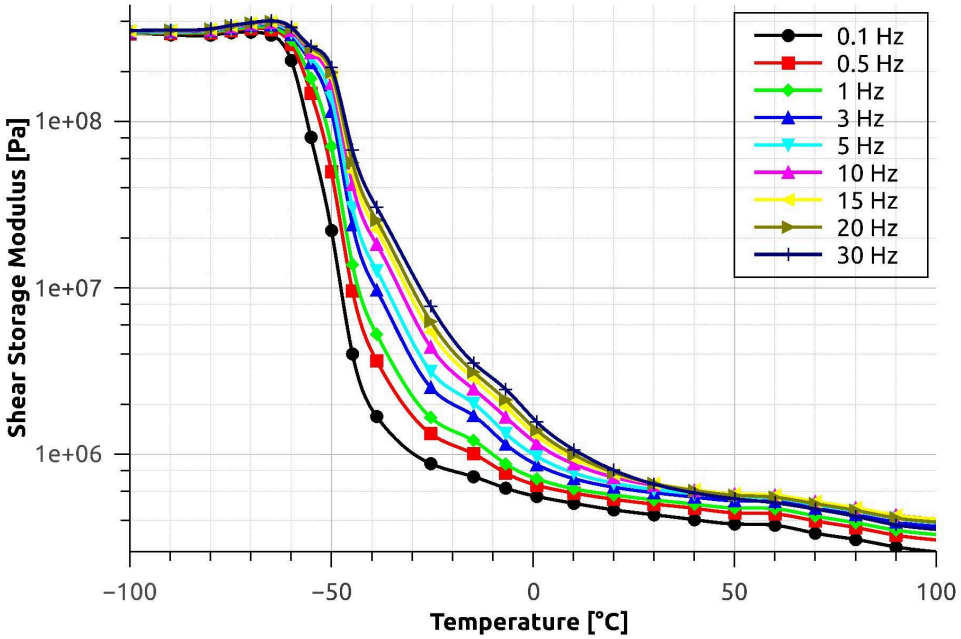

Figure 2.25: Shear storage modulus vs temperature at different frequencies: BIIR

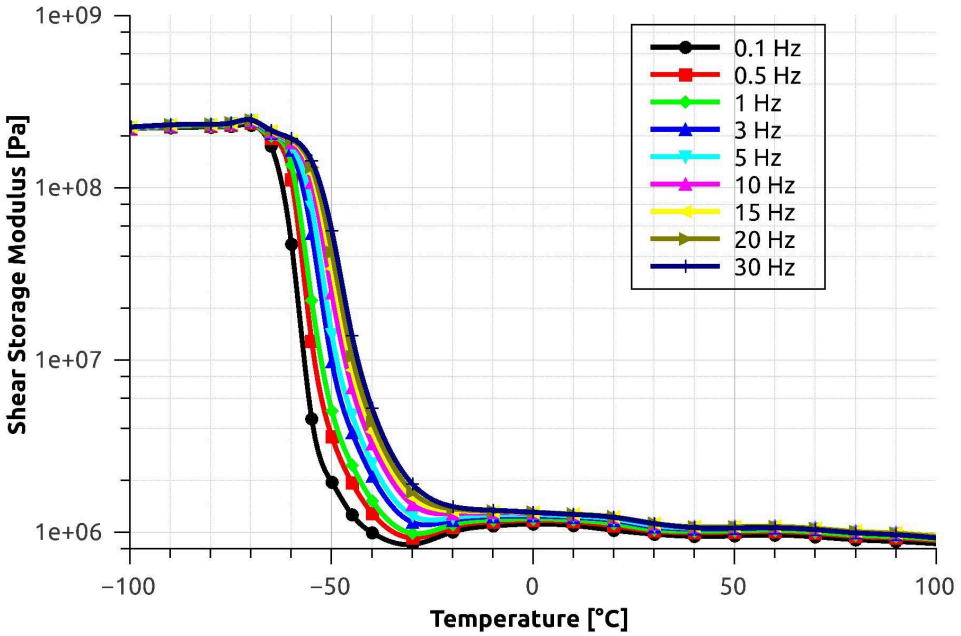

Figure 2.26: Shear storage modulus vs temperature at different frequencies: NR

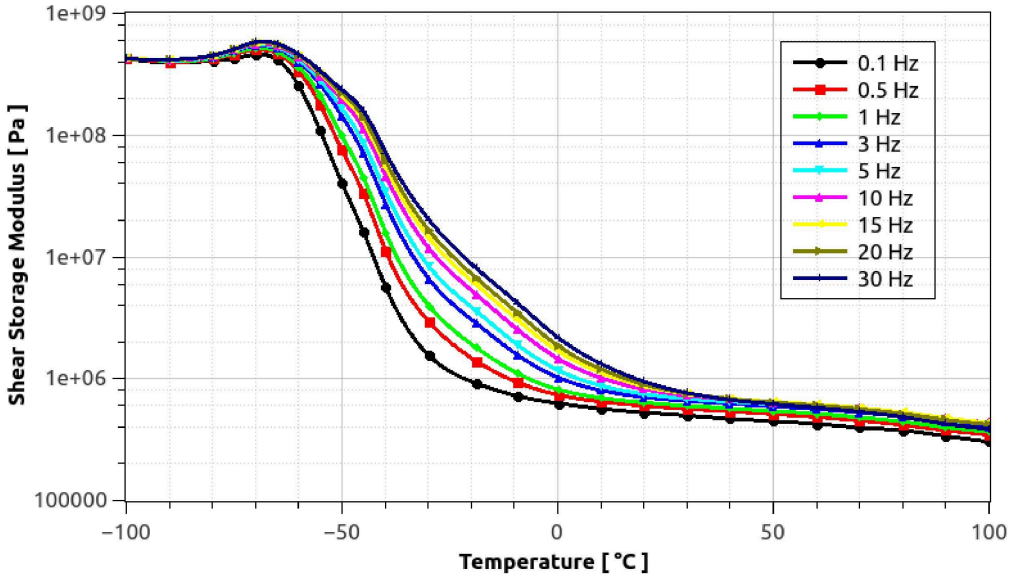

Figure 2.27: Shear storage modulus vs temperature at different frequencies: NR/BIIR

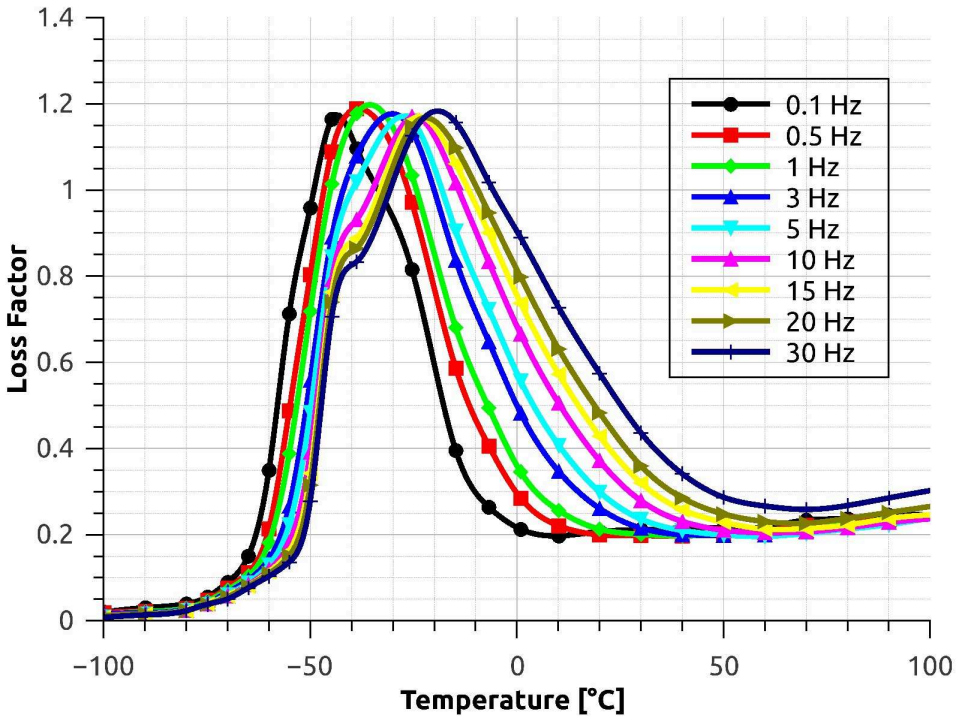

Figure 2.28: Loss factor vs temperature at different frequencies: BIIR

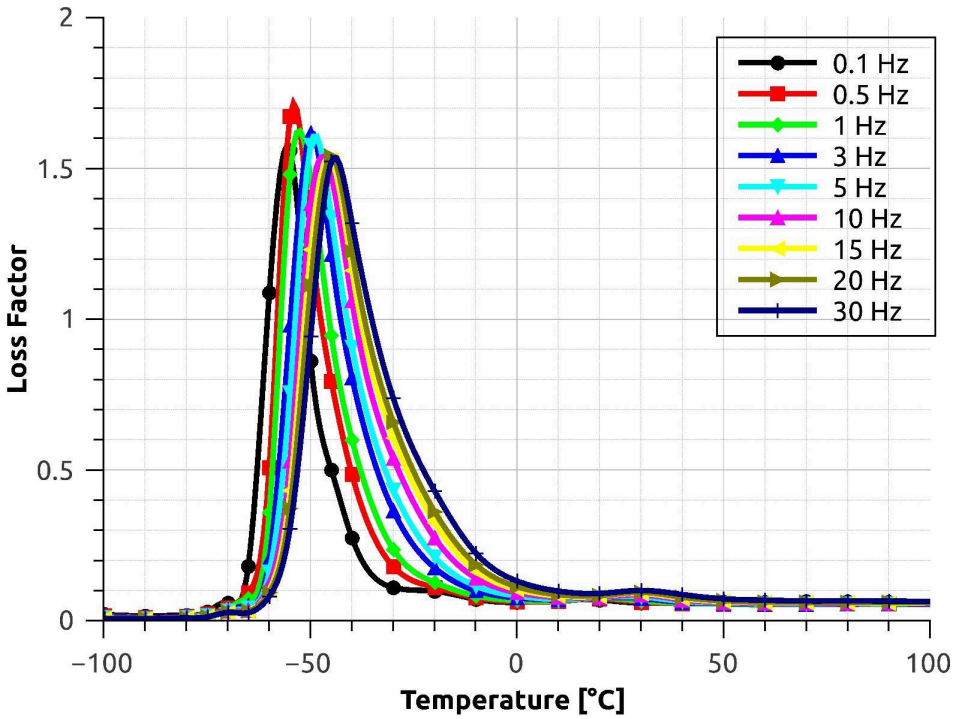

Figure 2.29: Loss factor vs temperature at different frequencies: NR

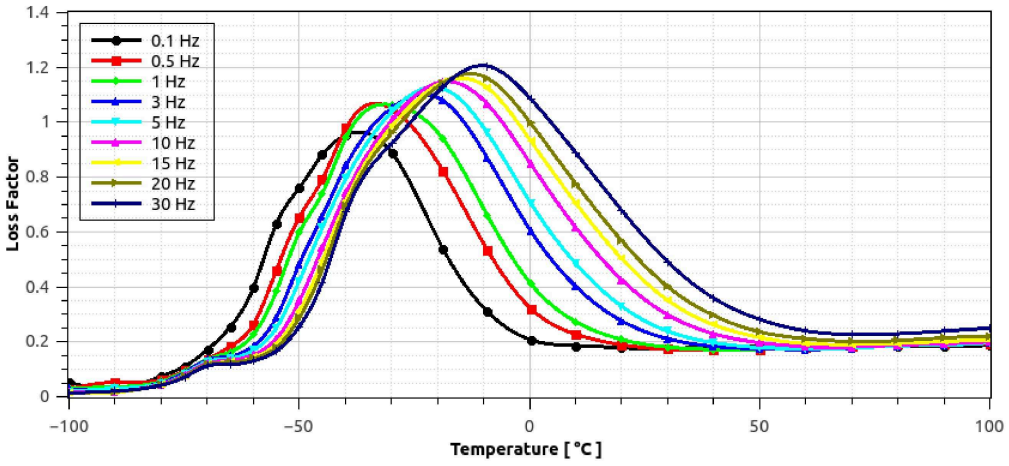

Figure 2.30: Loss factor vs temperature at different frequencies: NR/BIIR

2.4.5 Glass transition temperature

The glass transition were measured for the three materials using the peak for the loss factor at 1 Hz as measure. The three materials exhibit the same response, with different glass transition temperatures varying from -55 °C for the NR, -45 °C for the BIIR, -40 °C for the NR/BIIR. There exist important differences between the Tg values depending on the measurement method [113][114] (DSC, DMA). Table 2.4 summarizes the measured glass transition temperatures with both methods, while figs. 2.31, 2.33 and 2.34 graphically report the DSC thermal response to a temperature slope of 10 °C/min rate.

	DSC	DMA
NR	-63.02 °C	-55 °C
BIIR	-64.76 °C	-45 °C
NR/BIIR	-62.43 °C	-40 °C

Table 2.4: Glass transition temperatures: Comparison DSC and DMA

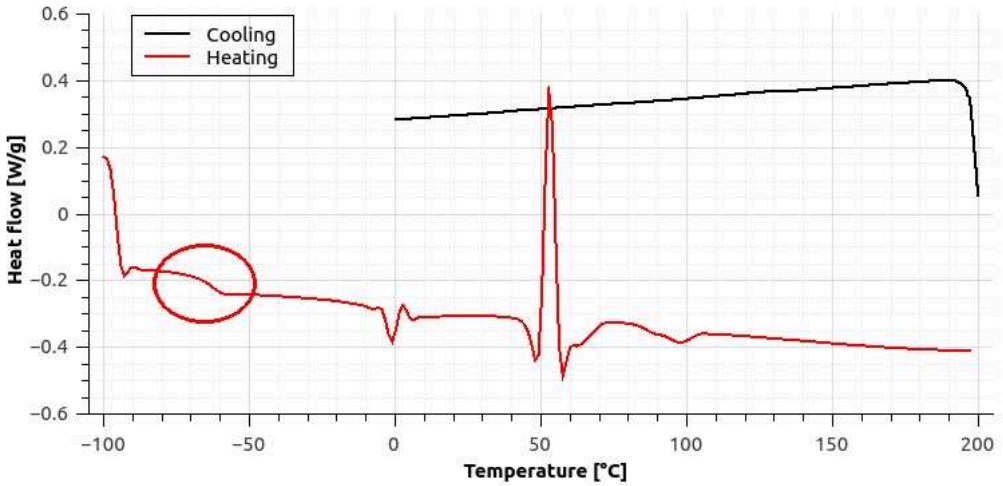

Figure 2.31: DSC curve: BIIR

Figure 2.32: DSC Glass transition technique: BIIR

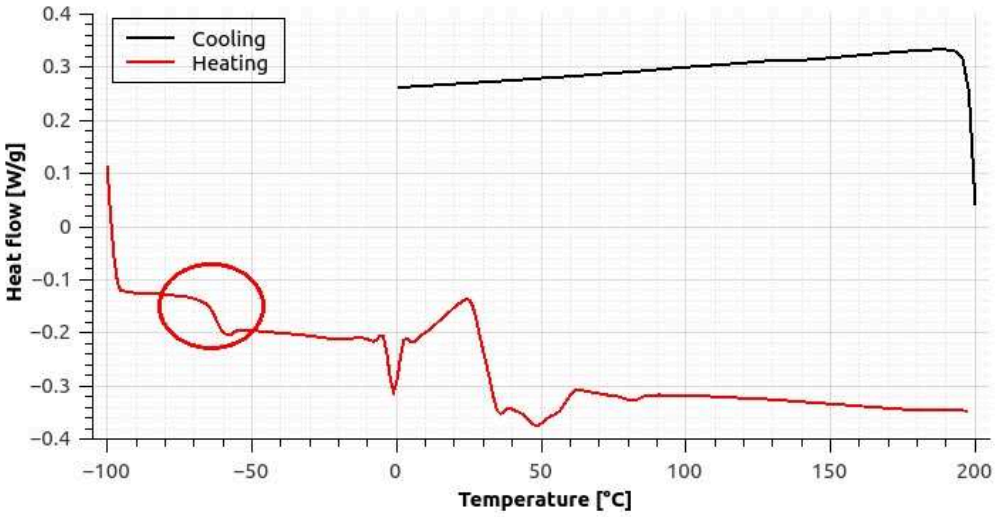

Figure 2.33: DSC curve: NR

2.4.6 Time-Temperature superposition principle: Master curves

To investigate the frequency-dependent material behavior, frequency sweep tests from 0.1Hz up to 40Hz were performed at room temperature of about 23 °C. Increasing the frequency range is accessible via the time-temperature superposition principle, which states that the effect of temperature is the same as applying a

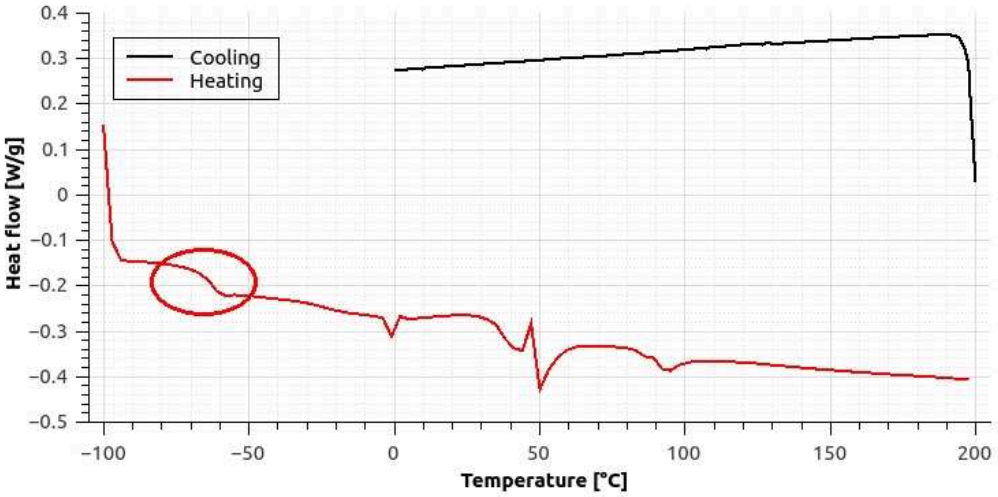

Figure 2.34: DSC curve: NR/BIIR

shifting to the timescale [117][105]. This superposition principle is used to determine temperature-dependent mechanical properties of linear viscoelastic materials from known properties at a reference temperature [6]. The elastic moduli of typical amorphous polymers increase with loading rate but decrease when the temperature is increased. Fortunately, curves of the instantaneous modulus as a function of time do not change shape as the temperature is changed but appear only to shift left or right. This implies that a master curve at a given temperature can be used as the reference to predict curves at various temperatures by applying a shift operation. The application of the principle typically involves the following steps:

1. experimental determination of frequency-dependent curves of isothermal viscoelastic mechanical properties at several temperatures and for a small range of frequencies

2. computation of a translation factor to correlate these properties for the temperature and frequency range

3. experimental determination of a master curve showing the effect of frequency for a wide range of frequencies

The translation factor is often computed using an empirical relation. To this end and to consider a wide range of frequency (10^{-2} till 10^{7} Hz), we make use of the

WLF (William-Landel and Ferry) model [117], which takes the following form:

$$log(a_T) = \frac{-C_1(T - T_r)}{C_2 + (T - T_r)} \tag{2.3}$$

where T is the temperature, T_r is a reference temperature chosen to construct the compliance master curve and C_1, C_2 are the WLF law material constants adjusted to fit the values of the superposition parameter a_T. The alternative model suggested by Arrhenius [118] was not used herein.
The figs. 2.35 to 2.40 summarizes the experimental determination of frequency-dependent curves of isothermal properties. Table 2.5 summarizes the determined coefficients for the WLF model.

	C_1	C_2	T_r°C
NR	2.6	75.5	3.2
BIIR	11.6	212	23.3
NR/BIIR	7.3	166.2	28

Table 2.5: WLF parameters for the three materials

Shear storage modulus and loss factor show the same behavior for the three materials, as illustrated in figs. 2.41 and 2.42. At low frequencies, the shear storage modulus and the loss factor are seen to be of low values. Increasing frequency in the way that higher frequencies lead to greater modulus, but it is shown that the loss modulus increases with frequency till reaching a maximum and decreasing since. As mentioned above, the compounds are relevant to a damping application. Comparing the behavior of the three materials to the dynamic excitation, fig. 2.41 shows that the three materials exhibit nearly the same shear storage modulus dependence to frequency, except that the Natural Rubber NR shear modulus is quietly constant under the frequency of 3000 Hz, and increases after. The loss factor is that part significant to damping property. In fig. 2.42, BIIR and NR/BIIR have better damping properties than the NR for low frequencies. For very high frequencies (near 1E5 Hz), the NR is relevant to a more damping ability.

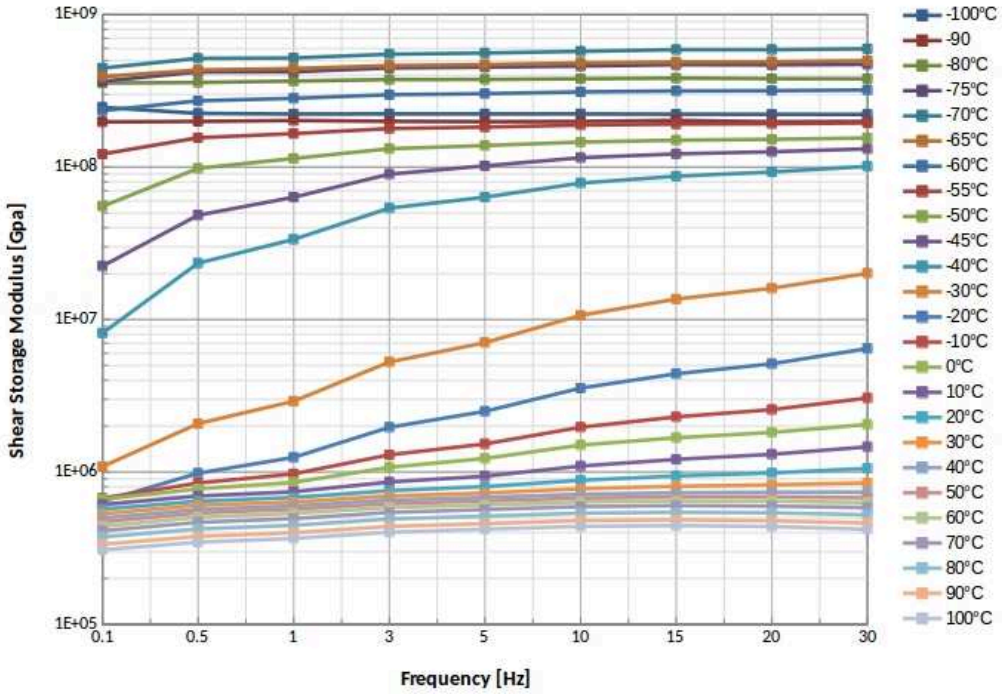

Figure 2.35: Isothermal Shear storage modulus: BIIR

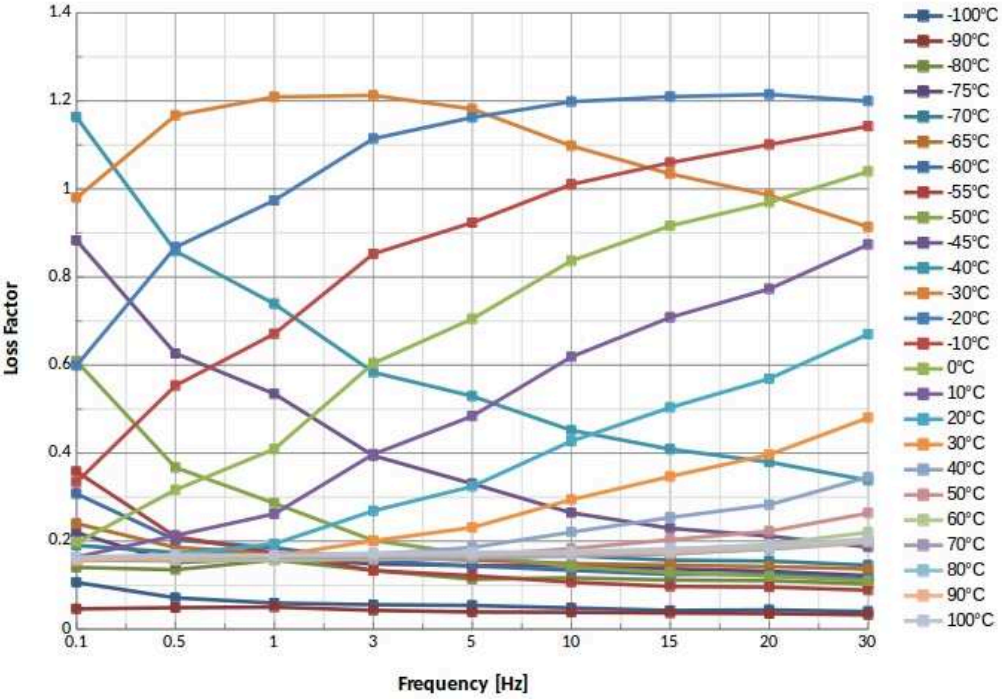

Figure 2.36: Isothermal Loss factor: BIIR

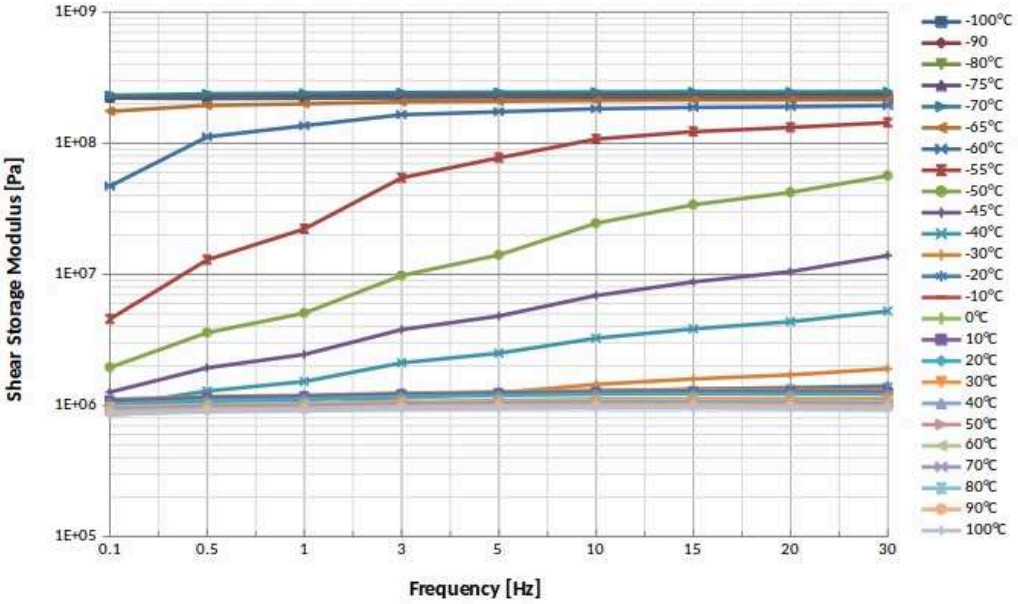

Figure 2.37: Isothermal Shear storage modulus: NR

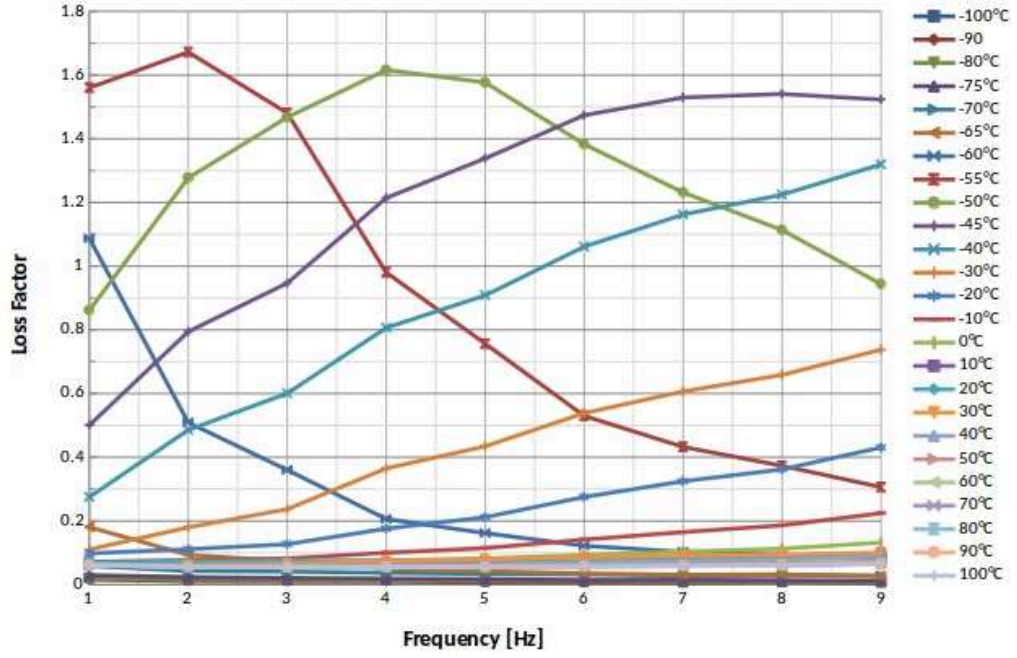

Figure 2.38: Isothermal Loss factor: NR

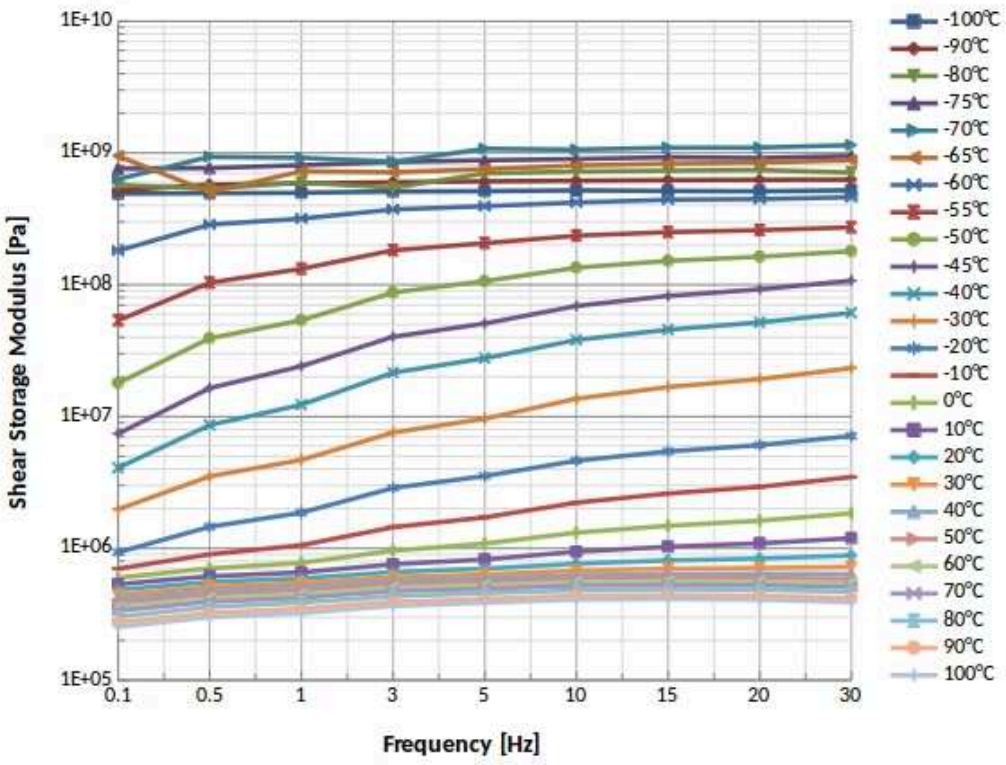

Figure 2.39: Isothermal Shear storage modulus: NR/BIIR

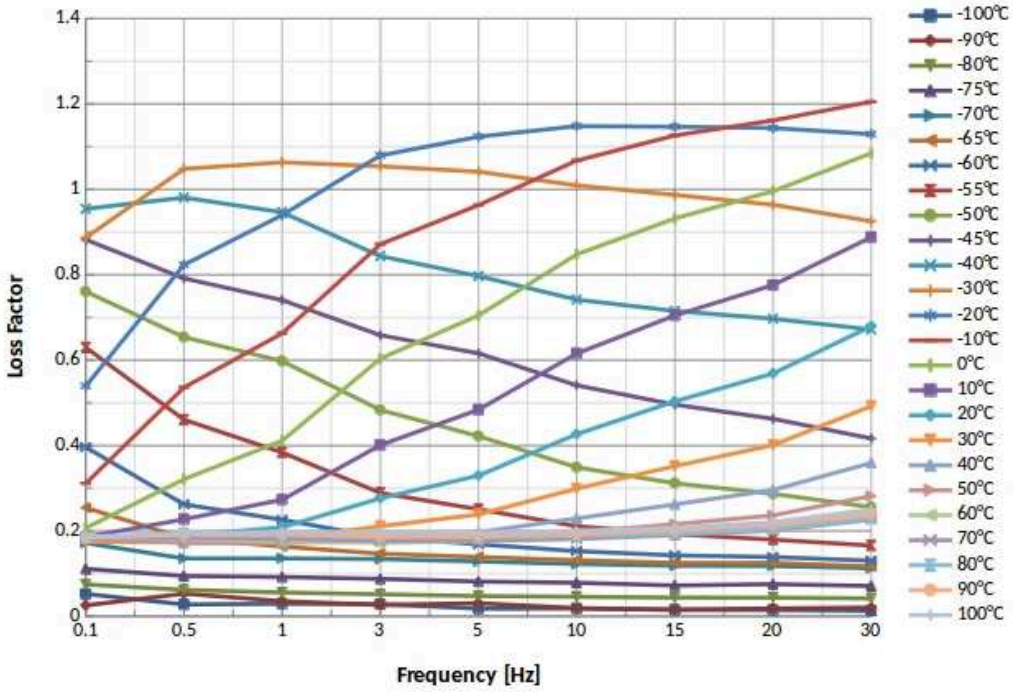

Figure 2.40: Isothermal Loss factor: NR/BIIR

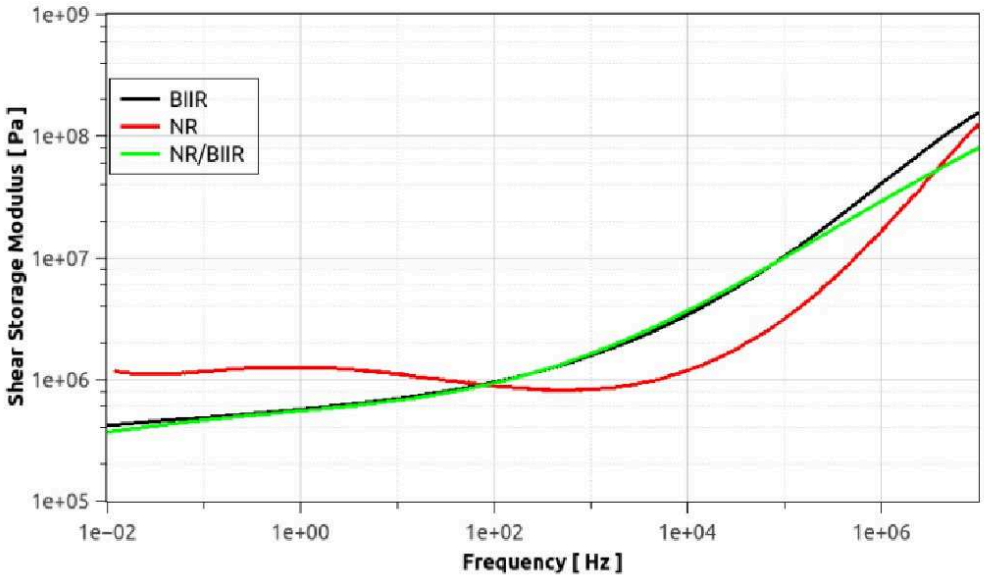

Figure 2.41: Shear storage modulus Master curves, comparison of the three materials

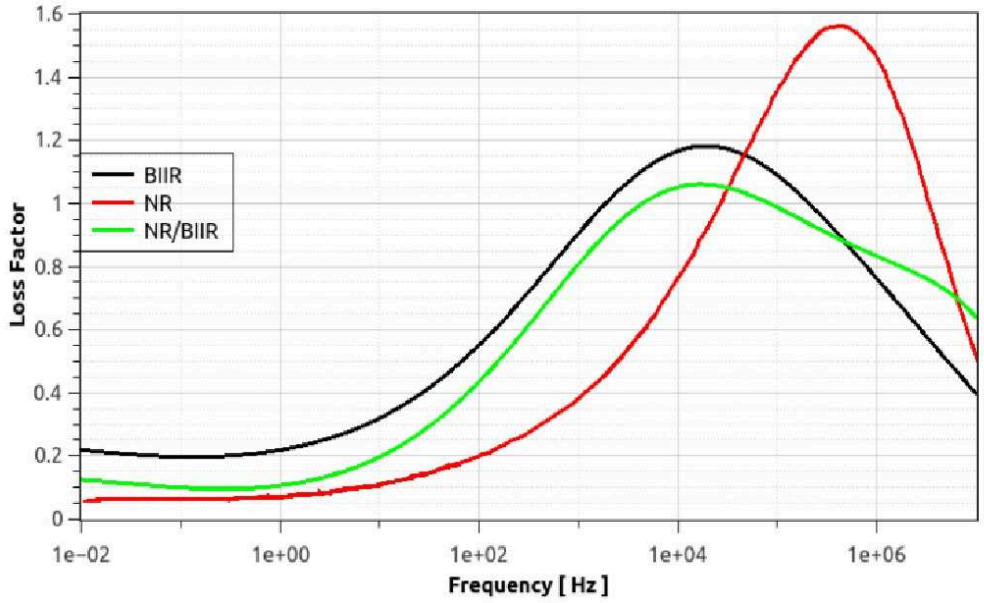

Figure 2.42: Loss factor Master curves, comparison of the three materials

2.4.7 Static predeformation effect on dynamic properties

Depending on the applications, rubber compounds are generally used at a predeformed configuration [9]. Several authors [22][49][115] have investigated this phenomena, and defined three zones: a linear domain, transition zone and nonlinear domain of dependency, depending on the amount of installed predeformation. The three tested materials exhibit predeformation-dependence. In term of shear storage modulus, the experimenntal curves in figs. 2.43 to 2.45 show that increasing the static predeformation leads to a lower storage modulus. Greater predeformation leads to a softening phenomenon. The decrease between 0% and 10% of predeformation is greater than the one between 20% of predeformation and 30% of predeformation for the tested materials. Interested by the loss factor, increasing installed predeformation for both NR and BIIR decreases the loss factor, as graphically shown in figs. 2.46 and 2.47. For the NR/BIIR, increasing predeformation leads to a higher damping factor as shows fig. 2.48. In relation with authors observations mentioned above, we can define the deformation zones as:

- Deformation less than 10% corresponding to the linear domain, the curves are qualitatively the same with a slight transition
- From 10% to 20% of deformation corresponding to the transition domain, where the transition is of a greater amount
- Deformation greater than 20% corresponding to the non linear domain

Fig. 2.43 and Fig. 2.46 exhibits the prestrain-dependence behavior of the Bromobutyl BIIR. The experimental curves show that increasing the static predeformation leads to a lower storage modulus and loss factor. Greater predeformation leads to a lower softening in term of shear storage modulus. The decrease between 0% and 10% of predeformation is greater than the one between 20% of predeformation and 30% of predeformation. The loss factor's dependency exhibits the same phenomena. Therefore, the softening of the material is non linear.

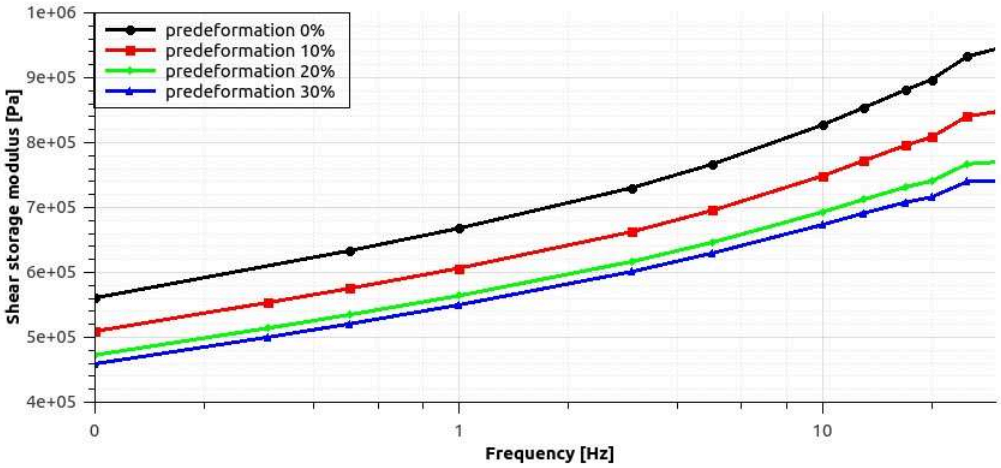

Figure 2.43: Shear modulus frequency and predeformation dependence: BIIR

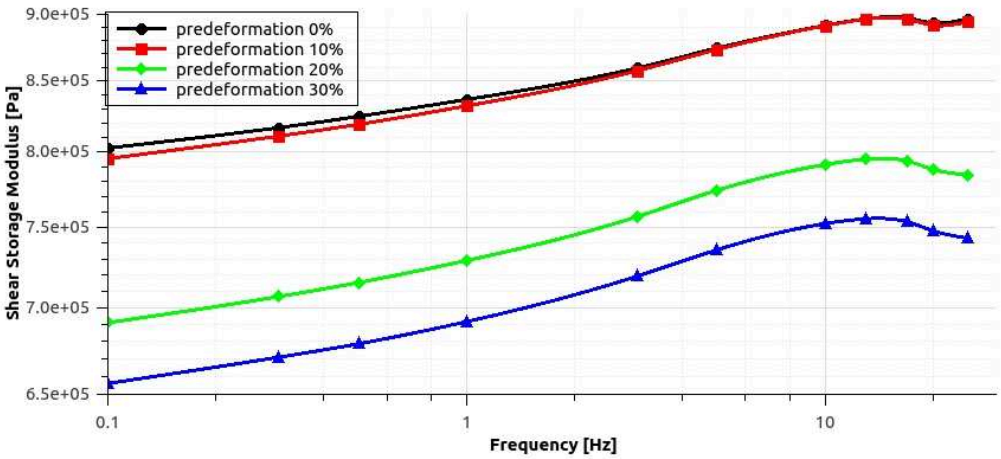

Figure 2.44: Shear modulus frequency and predeformation dependence: NR

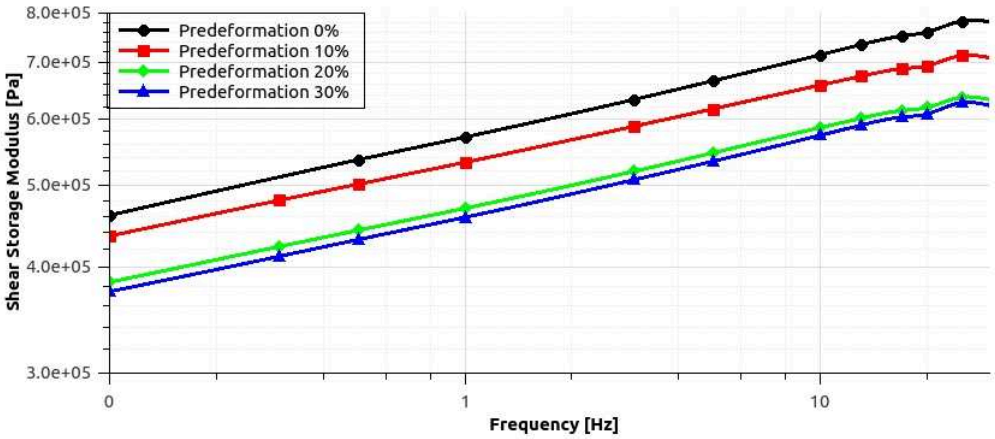

Figure 2.45: Shear modulus frequency and predeformation dependence: NR/BIIR

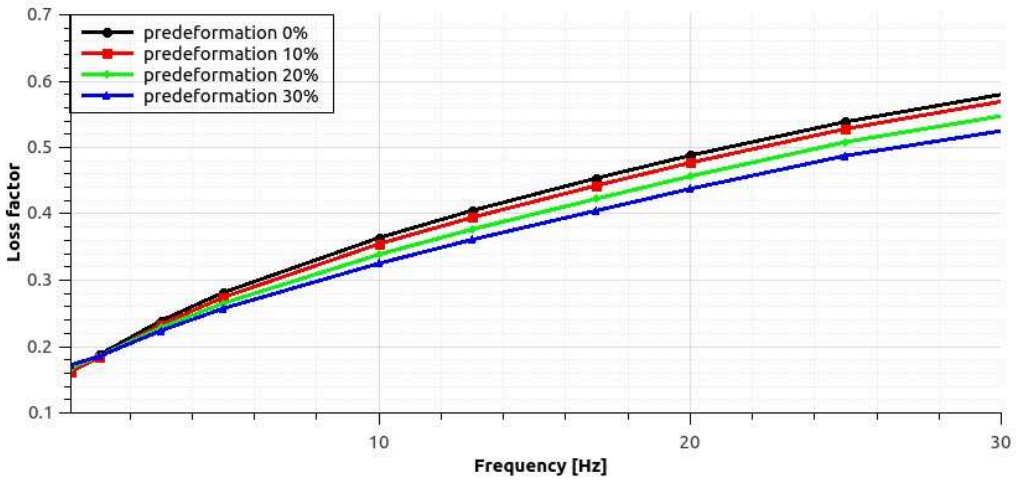

Figure 2.46: Loss factor frequency and predeformation dependence: BIIR

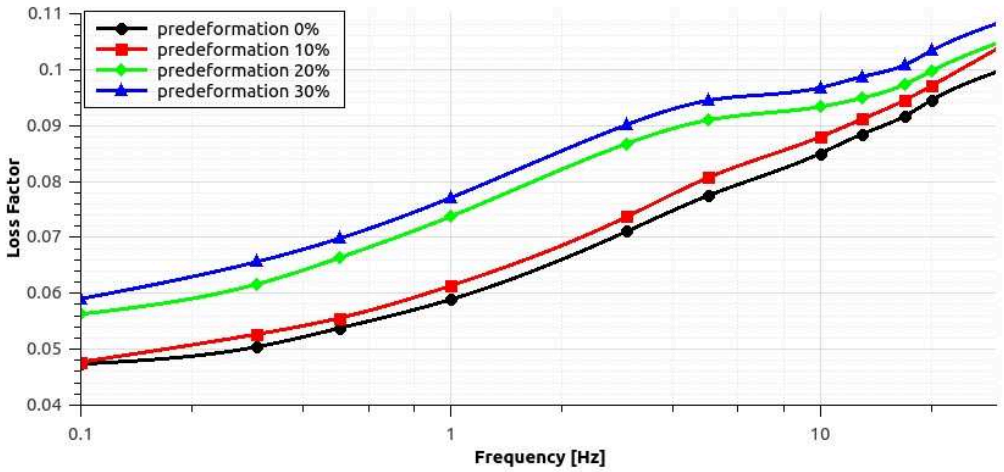

Figure 2.47: Loss factor frequency and predeformation dependence: NR

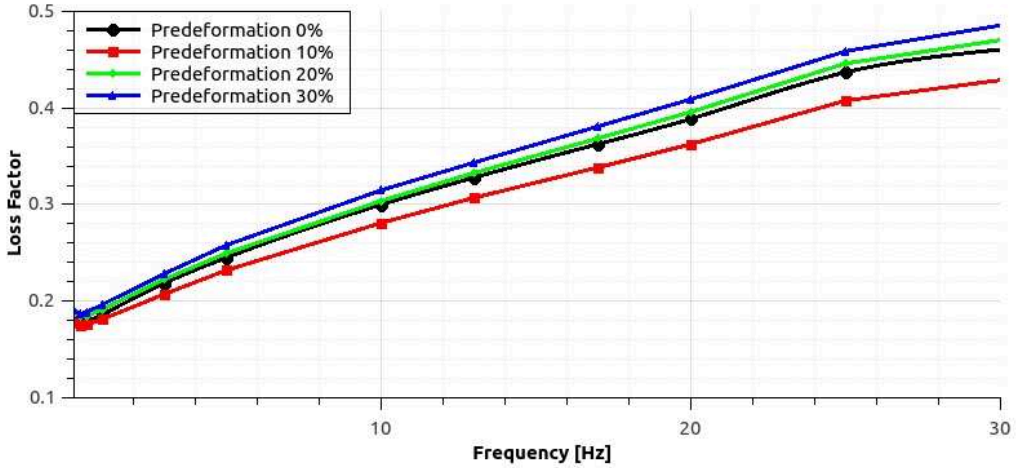

Figure 2.48: Loss factor frequency and predeformation dependence: NR/BIIR

2.5 Conclusions

The intention of this chapter is to investigate the mechanical behavior of the filled rubber materials, at different frequency, temperature and predeformation levels used for the intented engineering application. The materials behavior is characterized by non-linear elasticity combined with viscoelasticity, and a weak equilibrium hysteresis. Within this experimental investigation, for the monotonic tests, it has been shown that the Mullins effect vanishes after the three to five loading cycles and a quasi-stationary equilibrium is then reached. The three materials exhibit rate-dependence properties, and the hyperelastic equilibrium response was identified with the presented technique. Since application of superimposed predeformation with a small sinusoidal strain is widely common in engineering applications, the viscoelastic properties of the three vulcanized materials, for different levels of predeformation, were investigated. The experimental data show that material behaviors depend on frequency, temperature and the predeformation level. Conducting the tests over a wide range of temperature and using the time-temperature equivalence principle lead to characterize the materials damping as a function of frequency and temperature over the range encountred in engineering applications. Experimental observations printed out from this work are resumed as:

- NR offers the highest stiffness while it shows the lowest damping ability in the intented service domain. It can offer the maximum damping factor for high frequencies. It has been found that increasing predeformation leads to the highest softening in terms of shear storage modulus.
- In contrast with NR, BIIR offers the highest damping factor and the lowest stiffness. The softening of BIIR with increasing predeformation is moderate.
- The softening of NR/BIIR observed during monotonic tests is not clear, and could be due to vulcanization parameters. Meanwhile, it offers mid-range dynamic properties. This material shows the ability to be softer and acquire a higher damping ability with increasing predeformation.

With these experimental findings, the focus in the next chapter will be made on the predictive capabilities of some hyper-visco-elastic models which are widely used for rubber-like material. Within the proposed experimental database, the following investigation will be carried in time and frequency domains.

Chapter 3

Comparison of Some Integral-based seperable Hyper-visco-elastic models

Contents

3.1 Introduction

Modeling strain-rate dependent response of rubber materials is mainly derived following two different frameworks based on the phenomenological approach, and one can reffer to the well detailed introduction of [119] for more details. As recalled in Chapter 1, the constitutive theory of finite linear viscoelasticity [58] have been of a major contribution and is founded on an extension of the Boltzmann superposition principle to finite strain. The stress quantity is decomposed to an equilibrium part corresponding to the stress response at highly slow rate, and an overstress quantity expressed as an heriditary integral including a measure of material's memory through relaxation function [120]. Based on experimental observations, the time-strain separability or factorability assumption [57][110] is frequently introduced in the formulation of finite strain viscoelasticity constitutive models and afford a large theoretical simplicity. The second approach consists on decomposition of deformation gradient into elastic and inelastic parts [121], and in which the elastic part derives from an hyperelasticity model while the viscoelastic overstressed part is related to the so-called internal strain, determined by an evolution equation [78][79][122][23]. The objective of this chapter is to propose an analysis of the predictive capabilities of some models for engineering applications. The choice is made herein on some heriditary integral-based constitutive models in time and frequency domains, under the separability assumption [48][49]. This work is instigated by the experimental investigation made in chapter 2. Moreover, the choice of the considered models is motivated by the fact that these models do not require a special identification procedure and all parameters have been identified using Abaqus Evaluate Module. Conclusion for time domain and frequency domain analysis as described in [64] and [123] are drawn, with focus on the capability of the considered models to predict dynamic properties in term of storage modulus and loss factor with respect to the predeformation levels.

3.2 Seperable Finite Strain Viscoelastic Models under consideration

3.2.1 Models under consideration

In the present work, some of major contributions finite strain viscoelastic models involving heriditary integral have been considered under the seperability assumption. This choice is motivated by the experimental observation confirming the seperability assumption, as mentionned above. Models are chosen so as to not require a special identification procedure. All parameters have been identified using Abaqus Evaluate Module. The models under consideration are:

- Christensen model (3.1a), applicable for moderate and large strain ranges, consists on a viscoelastic generalisation of the kinetic theory of rubber elasticity with specific attention to stress-imposed problems [67]
- Fosdick & Yu model [65](3.1b), based on the QLV model, consists on a simple convolution between the Cauchy stress tensor $\boldsymbol{\sigma(t)}$ and the relative Green-Saint-Venant deformation gradient $\mathbf{E_t(s)}$
- a solid extension of the K-BKZ model (3.1c), based on an hyperelastic part and a K-BKZ fluid [63] for the viscous part. This model have been proposed investigated in a recent work [124] for monotonic and relaxation response.
- Simo model (3.1d), proposed in 1987 [88], based on an uncouple volumetric and deviatoric response over any range of deformation, with decomposition of the stress tensor into initial and nonequilibrium parts. We denote that the Simo model is used in finite element software Abaqus [125]

We have considered two other models, that analysis have shown that:

– Fung's model, commonly referred to as Quasi Linear Viscoelastic QLV model [68], is one of the most used models as a simple way to incorporate nonlinearity and time dependence in a simplified integral model. This model is intended specially for biological tissues, and can find application for elastomers. Analysis of this model have shown that, for an incompressible material, we hold the same expression as the Simo model.

– Yang et al. model was proposed in 2000, and is an extension of the BKZ model [70]. This model is mainly issued for very high strain-rates. Considering the A_5 term as zero in the originally proposed model, we denote that the expression is the same as Fosdick and Yu model.

We consider an homogeneous, isotropic and incompressible material. Intending to have the same parameters number for the hyperelastic part, we make use of a generalisation of some models originally introduced with respect to a NeoHookean material. Moreover, introduced an extension of the original versions of single relaxation time in some models to a Prony's series of at least 3 characteristic times. The constitutive relations for respectively Christensen, Fosdick & Yu , K-BKZ and Simo models are:

$$\boldsymbol{\sigma}^{Ch} = -p\mathbf{I} + 2\mathbf{B}\frac{\partial W}{\partial \mathbf{B}} + \mathbf{F}\, G_0 \int_0^t g_1(t-s)\frac{\partial \mathbf{E}(\mathbf{s})}{\partial s} ds \mathbf{F}^T \tag{3.1a}$$

$$\boldsymbol{\sigma}^{FY} = -p\mathbf{I} + 2\mathbf{B}\frac{\partial W}{\partial \mathbf{B}} + G_0 \int_0^t g_1(t-s)\frac{\partial \mathbf{E}_t(s)}{\partial s} ds \tag{3.1b}$$

$$\boldsymbol{\sigma}^{BKZ} = -p\mathbf{I} + 2\mathbf{B}\frac{\partial W}{\partial \mathbf{B}} - 2\,\mathbf{F}\, G_0 \int_0^t g_1(t-s)\frac{\partial \mathbf{C}^{-1}}{\partial s} ds\, \mathbf{F}^T \tag{3.1c}$$

$$\begin{aligned}\boldsymbol{\sigma}^{Si} = &-p\mathbf{I} + 2\mathbf{B}\frac{\partial W}{\partial \mathbf{B}}\frac{1}{g_\infty} + \\ &dev\left[\int_0^t \frac{\partial g_1(s)}{\partial s}\mathbf{F}_t^{-1}(t-s)\frac{2}{g_\infty}\mathbf{B}(t-s)\frac{\partial W}{\partial \mathbf{B}}\mathbf{F}_t^{-T}(t-s)\, ds\right]\end{aligned} \tag{3.1d}$$

(3.1e)

The convolution integral-based approach is based on the relative deformation gradient $\mathbf{F}_t(s) = \mathbf{F}(s)\mathbf{F}^{-1}(t)$ which is the deformation gradient at the current time s at the current configuration. For the Simo model, the "dev" operator is defined as: $dev(.) = (.) - \left(\frac{1}{3}(.) : \mathbf{I}\right)\, \mathbf{I}$.

We recall the first Piola-Kirchoff stress $\boldsymbol{\Pi}$, which is called nominal stress and expresses the actual stress in the reference configuration. This stress is related to the Cauchy stress tensor as:

$$\boldsymbol{\sigma} = \boldsymbol{\Pi}\,\mathbf{F}^T \tag{3.2}$$

Using eq. (1.31c), stress-stretch relationships corresponding to simple test for an hyperelastic material can be derived:

- Uniaxial Tension:

$$\Pi = 2\left(\lambda - \frac{1}{\lambda^2}\right)\left(\frac{\partial W}{\partial I_1} + \frac{\partial W}{\partial I_2}\frac{1}{\lambda}\right) \tag{3.3}$$

- Pure Shear:

$$\Pi = 2\left(\lambda - \frac{1}{\lambda^3}\right)\left(\frac{\partial W}{\partial I_1} + \frac{\partial W}{\partial I_2}\right) \tag{3.4}$$

Detailed expressions for simple tests and equations in the framework of hyperlasticity can be found in [38].

3.2.2 Identification Procedure

Identification of materials parameters consists on fitting theoretical solution T^{th} with experimental data T^{test}. Abaqus offers an evaluation module [126]: Given experimental data, the material constants are determined through a least-squares-fit procedure, which minimizes the relative error in stress. For the N nominal stress–nominal strain data pairs, the relative error measure e is minimized:

$$e = \sum_{i=1}^{N}\left(1 - \frac{T_i^{th}}{T_i^{test}}\right)^2 \tag{3.5}$$

Moreover, Abaqus offers the possibility to check the material stability limits using the Drucker criterion [127].

3.2.3 Transformations under consideration

The available experimental data are for an uniaxial tension test and a simple shear test, so we have considered the following motions:

3.2.3.1 Uniaxial Tension

We consider an uniaxial tension test. The transformation has the form:

$$x_1 = \lambda(t)\, X_1 \qquad x_2 = \frac{1}{\sqrt{\lambda_t}}\, X_2 \qquad x_3 = \frac{1}{\sqrt{\lambda_t}}\, X_3 \tag{3.6}$$

The deformation gradient and the right Cauchy-Green strain tensor have components:

$$\mathbf{F}(t) = \begin{bmatrix} \lambda(t) & 0 & 0 \\ 0 & \frac{1}{\sqrt{\lambda(t)}} & 0 \\ 0 & 0 & \frac{1}{\sqrt{\lambda(t)}} \end{bmatrix} \quad \mathbf{C}(t) = \mathbf{B}(t) = \begin{bmatrix} \lambda^2(t) & 0 & 0 \\ 0 & \frac{1}{\lambda(t)} & 0 \\ 0 & 0 & \frac{1}{\lambda(t)} \end{bmatrix} \tag{3.7}$$

The hydrostatic pressure is eliminated through the relation:

$$\sigma_{tension} = \sigma_{11} - \sigma_{22} \tag{3.8}$$

since $\sigma_{22} = 0$.

The obtained constitutive equations for uniaxial tension motion are then:

$$\begin{aligned} \sigma^{Ch}_{tension}(t) &= 2\left(\lambda(t)^2 - \frac{1}{\lambda(t)}\right)\left(\frac{\partial W}{\partial I_1} + \frac{1}{\lambda(t)}\frac{\partial W}{\partial I_2}\right) \\ &\quad + \frac{G_0}{2}\lambda(t)^2 \int_0^t g_1(t-s)\frac{\partial \lambda^2(s)}{\partial s}ds \\ &\quad - \frac{G_0}{2\lambda(t)} \int_0^t g_1(t-s)\frac{\partial \frac{1}{\lambda(s)}}{\partial s}ds \end{aligned} \tag{3.9a}$$

$$\begin{aligned} \sigma^{FY}_{tension}(t) &= 2\left(\lambda(t)^2 - \frac{1}{\lambda(t)}\right)\left(\frac{\partial W}{\partial I_1} + \frac{1}{\lambda(t)}\frac{\partial W}{\partial I_2}\right) \\ &\quad + \frac{G_0}{2\lambda(t)^2} \int_0^t g_1(t-s)\frac{\partial \lambda^2(s)}{\partial s}ds \\ &\quad - \frac{G_0}{2}\lambda(t) \int_0^t g_1(t-s)\frac{\partial \frac{1}{\lambda(s)}}{\partial s}ds \end{aligned} \tag{3.9b}$$

$$\begin{aligned} \sigma^{BKZ}_{tension}(t) &= 2\left(\lambda(t)^2 - \frac{1}{\lambda(t)}\right)\left(\frac{\partial W}{\partial I_1} + \frac{1}{\lambda(t)}\frac{\partial W}{\partial I_2}\right) \\ &\quad + \frac{2G_0}{\lambda(t)} \int_0^t g_1(t-s)\frac{\partial \lambda(s)}{\partial s}ds \\ &\quad - 2G_0\lambda(t)^2 \int_0^t g_1(t-s)\frac{\partial \frac{1}{\lambda(s)^2}}{\partial s}ds \end{aligned} \tag{3.9c}$$

$$\begin{aligned} \sigma^{Si}_{tension}(t) &= \frac{2}{g_\infty}\left(\lambda(t)^2 - \frac{1}{\lambda(t)}\right)\left(\frac{\partial W}{\partial I_1} + \frac{1}{\lambda(t)}\frac{\partial W}{\partial I_2}\right) \\ &\quad + \frac{2}{g_\infty}\left(\lambda(t)^2 - \frac{1}{\lambda(t)}\right) \int_0^t \dot{g}_1(s)\left(\frac{\partial W}{\partial I_1} + \frac{1}{\lambda(t-s)}\frac{\partial W}{\partial I_2}\right)ds \\ &\quad - \frac{2}{\lambda(t)g_\infty} \int_0^t \dot{g}_1(s)\frac{\partial W}{\partial I_2}\lambda^2(t-s)ds \end{aligned} \tag{3.9d}$$

3.2.3.2 Simple Shear motion

Considering a simple shear motion, the non-symmetric deformation gradient has components:

$$\mathbf{F}(t) = \begin{bmatrix} 1 & \gamma(t) & 0 \\ 0 & 1 & 0 \\ 0 & 0 & 1 \end{bmatrix} \tag{3.10}$$

The right and left Cauchy-Green strain tensor:

$$\mathbf{C}(t) = \begin{bmatrix} 1 & \gamma(t) & 0 \\ \gamma(t) & 1+\gamma^2(t) & 0 \\ 0 & 0 & 1 \end{bmatrix} \quad \mathbf{B}(t) = \begin{bmatrix} 1+\gamma^2(t) & \gamma(t) & 0 \\ \gamma(t) & 1 & 0 \\ 0 & 0 & 1 \end{bmatrix} \tag{3.11}$$

The obtained constitutive equations for a simple shear motion are then:

$$\begin{aligned} \sigma_{12}^{Ch}(t) = 2\gamma(t)\left(\frac{\partial W}{\partial I_1} + \frac{\partial W}{\partial I_2}\right) + \frac{G_0}{2}\int_0^t g_1(t-s)\frac{\partial \gamma(s)}{\partial(s)}ds \\ + \frac{G_0}{2}\gamma(t)\int_0^t g_1(t-s)\frac{\partial \gamma^2(s)}{\partial(s)}ds \end{aligned} \tag{3.12a}$$

$$\sigma_{12}^{FY}(t) = 2\gamma(t)\left(\frac{\partial W}{\partial I_1} + \frac{\partial W}{\partial I_2}\right) + \frac{G_0}{2}\int_0^t g_1(t-s)\frac{\partial \gamma(s)}{\partial(s)}ds \tag{3.12b}$$

$$\sigma_{12}^{BKZ}(t) = 2\gamma(t)\left(\frac{\partial W}{\partial I_1} + \frac{\partial W}{\partial I_2}\right) + 2\,G_0\int_0^t g_1(t-s)\frac{\partial \gamma(s)}{\partial(s)}ds \tag{3.12c}$$

$$\begin{aligned} \sigma_{12}^{Si}(t) = \frac{2}{g_\infty}\gamma(t)\left(\frac{\partial W}{\partial I_1} + \frac{\partial W}{\partial I_2}\right) - \frac{2}{g_\infty}\int_0^t \frac{\partial g_1(s)}{\partial s}\frac{\partial W}{\partial I_2}\gamma(t-s)\,ds \\ + \frac{2}{g_\infty}\gamma(t)\int_0^t \frac{\partial g_1(s)}{\partial s}\left(\frac{\partial W}{\partial I_1} + 2\frac{\partial W}{\partial I_2}\right)ds \end{aligned} \tag{3.12d}$$

3.3 Prediction of purely hyperelastic response

There are several forms of strain energy potentials available in Abaqus to model incompressible or quasi-incompressible isotropic elastomers [128]:

- The polynomial form and it's particular cases: the reduced polynomial form, the neo-Hookean form, the Mooney-Rivlin form, and the Yeoh form
- Ogden real exponents form
- Arruda-Boyce form
- Van der Waals form

Comparison results are graphically shown in fig. 3.1. For a given model, a unique set of material parameters must be able to reproduce set of experimental data with good appproximation. In the considered deformation range, we observed that:

- Arruda Boyce model, Van der Walls and Yeoh models have shown slightly the same response in uniaxial or shear modes. These models are seen to underestimate the uniaxial tension nominal stress and over estimate the shear one. Nevertheless, the response have the same curvature as experimental data and the maximum measured error for highest strains is of about 18%.
- Mooney-Rivlin and NeoHookean potentials are seen not able to predict experimental data. The response is quasi-linear for both models. An acceptable range of deformation for both models can be less than 150% of deformations.
- The reduced polynomiam model with N=6 is seen to have a response similar to Arruda-Boyce model. It under-estimate tension stress and over-estimate the shear stress. Nevertheless, at moderate of large strains, the models is seen to have some instabilities, and the origin of some curvatures (as shown in Figure) is not clear.
- Both Ogden (N=3) and Polynomial(N=2) strain energy potentials are seen to give a well approximated response of the experimental data for a large strain loading. For moderate strains (approximately 300% in shear), the Polynomial model is seen unable to fit the curvature. Ogden model exhibit a slight under-estimation of the tension stress and an over-estimation of the shear stress. Nevertheless, the measured error is acceptable.

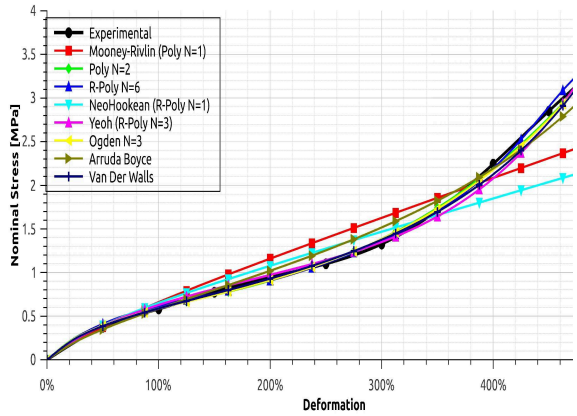

(a) NR Uniaxial

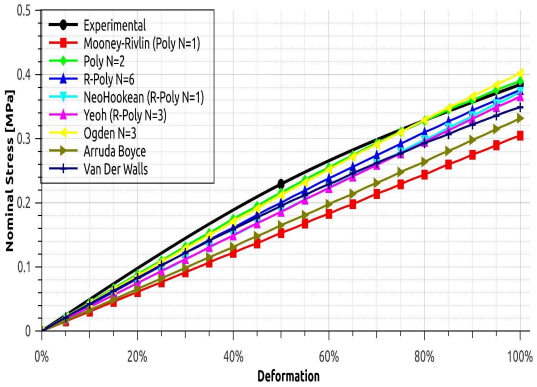

(b) NR Simple Shear

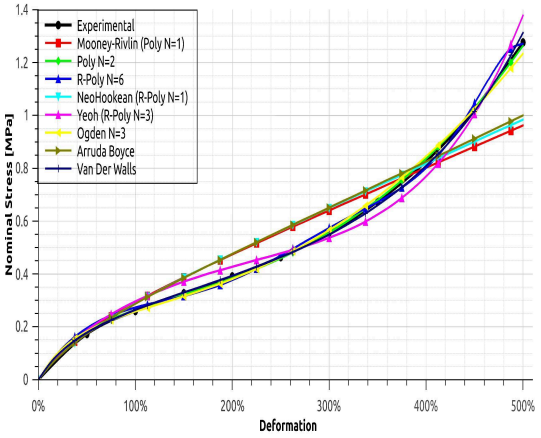

(c) BIIR Uniaxial

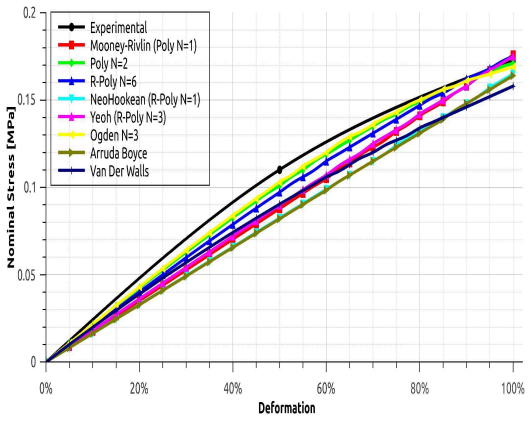

(d) BIIR Simple Shear

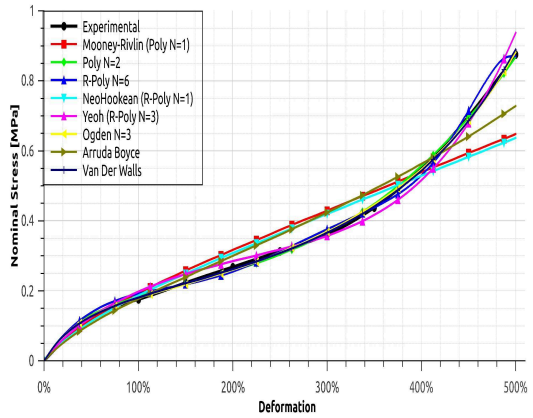

(e) NR/BIIR Uniaxial

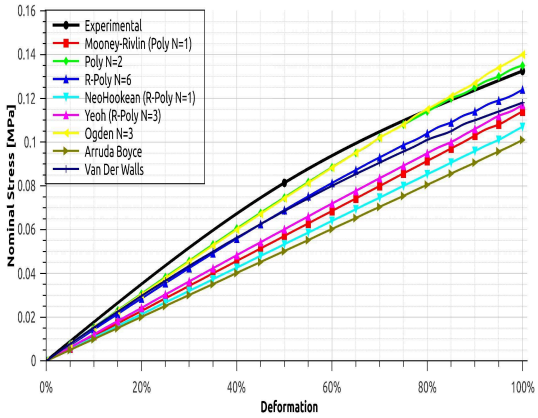

(f) NR/BIIR Simple Shear

Figure 3.1: Comparison of experimental data and different hyperelastic strain energy potentials response

3.4 Predictive capabilities of relaxation experiments

The evaluation of the prony series is available in the abaqus evaluation module [126] for normalized shear stress relaxation experiments, with a specification on the maximum relative error which we have chosen to be of 10^{-2}. We make use of the normalized stress relaxation curves for the three materials at mean deformation level (30%).

The deformation taken into account for relaxation tests is less than 50% of deformation. For simplification reasons, and since experimental data are well approximated in this range, we consider in this section Neo-Hookean, Mooney-Rivlin and 2^{nd} order Polynomial hyperelastic potentials.

For a stress relaxation test:

$$\gamma(t) = \gamma_0 H(t) \tag{3.13}$$

where $H(t)$ is the Heaviside function. This equation is to be introduced in the governing shear equations eqs. (3.12a) to (3.12d). Considering NeoHookean, Mooney-Rivlin and 2^{nd} order polynomial hyperelastic potential, the following equations are hence obtained:

Neo-Hookean potential:

$$\sigma_{12}^{Ch}(t) = 2\gamma_0\, C_{10} + \frac{G_0}{2}\gamma_0 g_1(t) + \frac{G_0}{2}\gamma_0^3 g_1(t) \tag{3.14a}$$

$$\sigma_{12}^{FY}(t) = 2\gamma_0\, C_{10} + \frac{G_0}{2}\gamma_0 g_1(t) \tag{3.14b}$$

$$\sigma_{12}^{BKZ}(t) = 2\gamma_0\, C_{10} + 2G_0\gamma_0 g_1(t) \tag{3.14c}$$

$$\sigma_{12}^{Si}(t) = \frac{2}{g_\infty}\gamma_0 C_{10} + \frac{2}{g_\infty}\gamma_0 C_{10}\,[g_1(t) - g_1(0)] \tag{3.14d}$$

Mooney-Rivlin potential:

$$\sigma_{12}^{Ch}(t) = 2\gamma_0\ (C_{10} + C_{01}) + \frac{G_0}{2}\gamma_0 g_1(t) + \frac{G_0}{2}\gamma_0^3 g_1(t) \tag{3.15a}$$

$$\sigma_{12}^{FY}(t) = 2\gamma_0\ (C_{10} + C_{01}) + \frac{G_0}{2}\gamma_0 g_1(t) \tag{3.15b}$$

$$\sigma_{12}^{BKZ}(t) = 2\gamma_0\ (C_{10} + C_{01}) + 2G_0\gamma_0 g_1(t) \tag{3.15c}$$

$$\sigma_{12}^{Si}(t) = \frac{2}{g_\infty}\gamma_0\,(C_{10} + C_{01}) + \frac{2}{g_\infty}\gamma_0\,(C_{10} + C_{01})\,[g_1(t) - g_1(0)] \tag{3.15d}$$

2^{nd} order Polynomial potential

$$\begin{aligned}\sigma_{12}^{Ch}(t) &= 2\gamma_0\left(C_{10}+2C_{20}\gamma_0^2+C_{11}\gamma_0^2+C_{01}+2C_{02}\gamma_0^2+C_{11}\gamma_0^2\right)\\ &\quad+\frac{G_0}{2}\gamma_0 g_1(t)+\frac{G_0}{2}\gamma_0^3 g_1(t)\end{aligned} \tag{3.16a}$$

$$\begin{aligned}\sigma_{12}^{FY}(t) &= 2\gamma_0\left(C_{10}+2C_{20}\gamma_0^2+C_{11}\gamma_0^2+C_{01}+2C_{02}\gamma_0^2+C_{11}\gamma_0^2\right)\\ &\quad+\frac{G_0}{2}\gamma_0 g_1(t)\end{aligned} \tag{3.16b}$$

$$\begin{aligned}\sigma_{12}^{BKZ}(t) &= 2\gamma_0\left(C_{10}+2C_{20}\gamma_0^2+C_{11}\gamma_0^2+C_{01}+2C_{02}\gamma_0^2+C_{11}\gamma_0^2\right)\\ &\quad+2G_0\gamma_0 g_1(t)\end{aligned} \tag{3.16c}$$

$$\begin{aligned}\sigma_{12}^{Si}(t) &= \frac{2}{g_\infty}\gamma_0\left(C_{10}+2C_{20}\gamma_0^2+C_{11}\gamma_0^2+C01+2C_{02}\gamma_0^2+C_{11}\gamma_0^2\right)\\ &\quad+\frac{2}{g_\infty}\gamma_0\left(C_{10}+2C_{20}\gamma_0^2+C_{11}\gamma_0^2+C_{01}+2C_{02}\gamma_0^2+C_{11}\gamma_0^2\right)\\ &\quad[g_1(t)-g_1(0)]\end{aligned} \tag{3.16d}$$

Relaxation equilibrium response For a very long relaxation time i.e $t\to\infty$, the relaxation equations for the considered hyperelastic potentials give the following equilibrium expressions:

$$\sigma_{12}^{Neo-Hook\,Equil} = 2C_{10}\gamma_0 \tag{3.17a}$$

$$\sigma_{12}^{MR\,Equil} = 2\left(C_{10}+C_{01}\right)\gamma_0 \tag{3.17b}$$

$$\sigma_{12}^{Poly\,Equil} = 2\left(C_{10}+2C_{20}\gamma_0^2+C_{11}\gamma_0^2+C01+2C_{02}\gamma_0^2+C_{11}\gamma_0^2\right)\gamma_0 \tag{3.17c}$$

Comparison results are reported on figs. 3.2 to 3.4 :

- Considering the NeoHookean hyperelastic potential, the models are seen to well reproduce the relaxation test data for low deformation level. For higher deformation levels, the predicted response is seen to be overestimated. This can be dedicated to the few hyperelastic model parameters, which is clearly not able to predict the long-term vicoelastic response with good accuracy.

- Considering the Mooney-Rivlin hyperelastic potential, the response of the models improves. With materials BIIR and NR/BIIR, as shows figs. 3.3b and 3.4b, the response is well approximated at 10% and 30% of deformations. This hyperelastic model still can't predict the long-term stress for the NR model since the response between the two deformation levels stress response is not really linear.

- The 2^{nd} order Polynomial hyperelastic model offers the best prediction for the long-term relaxation stress response. The measured error between experimental test data and predicted data is of an acceptable level.

- The major difference of the considered hyper-visco-elastic models is seen for the hysteritic part. Focusing on figs. 3.2c, 3.3c and 3.4c, the Simo model is seen to offer a good fidelity to approximate low times stress. Christensen and Fosdick & Yu models underestimate the hysteritic stress level while the BKZ model is observed to highly overestimate the instantaneous relaxation stress.

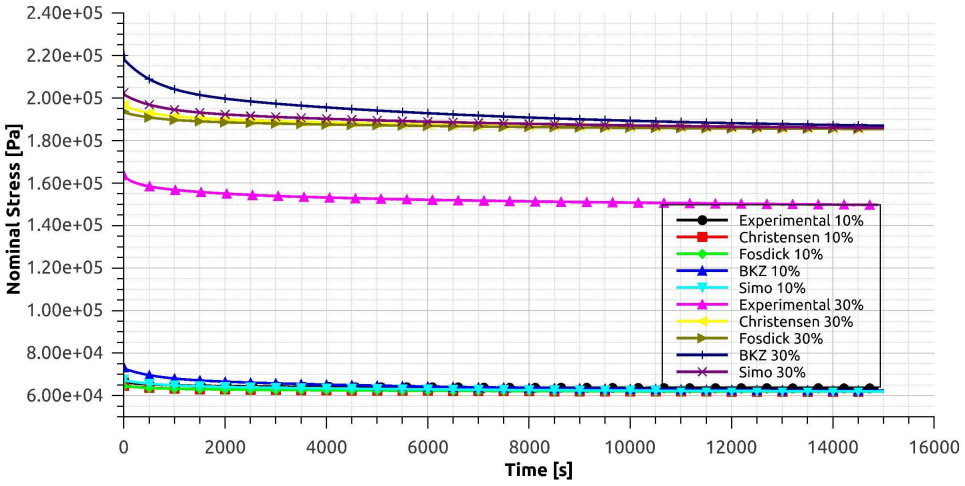

(a) NeoHook

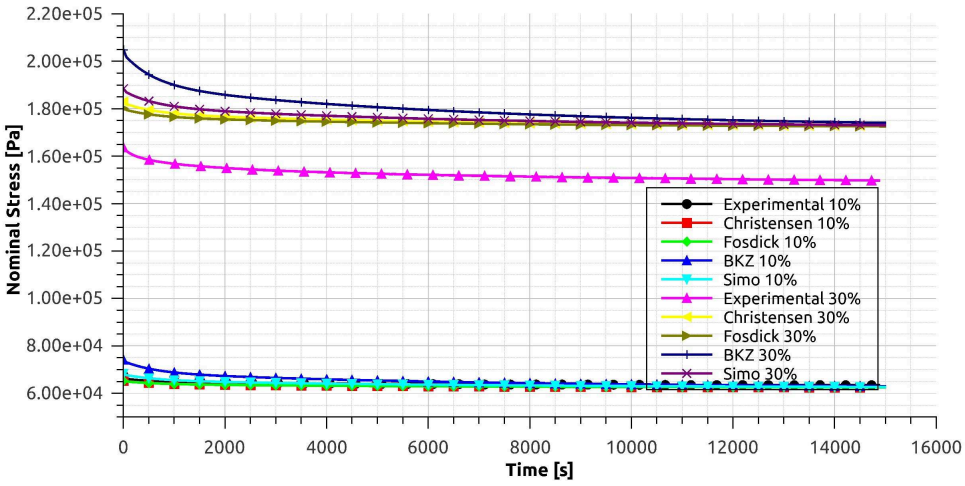

(b) Mooney-Rivlin

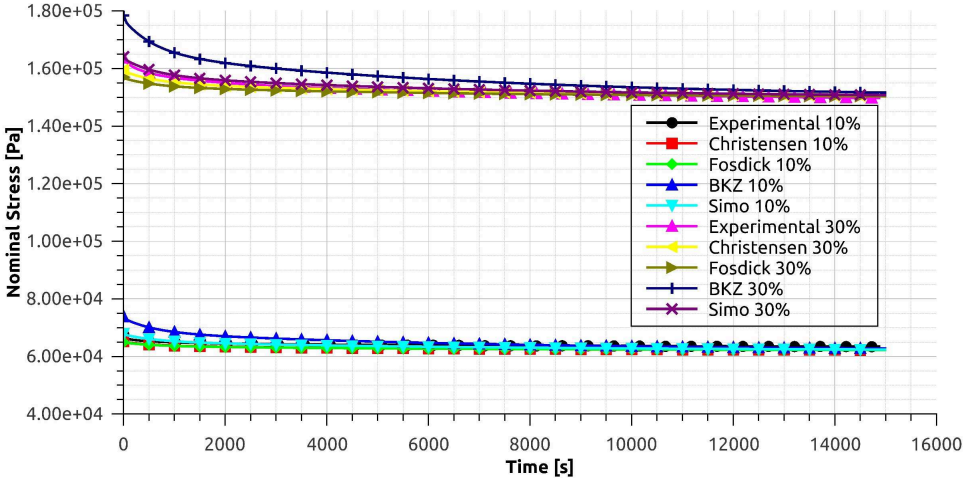

(c) 2^{nd} Order Polynomial

Figure 3.2: Comparison of the models relaxation response with different hyperelastic models: Material NR

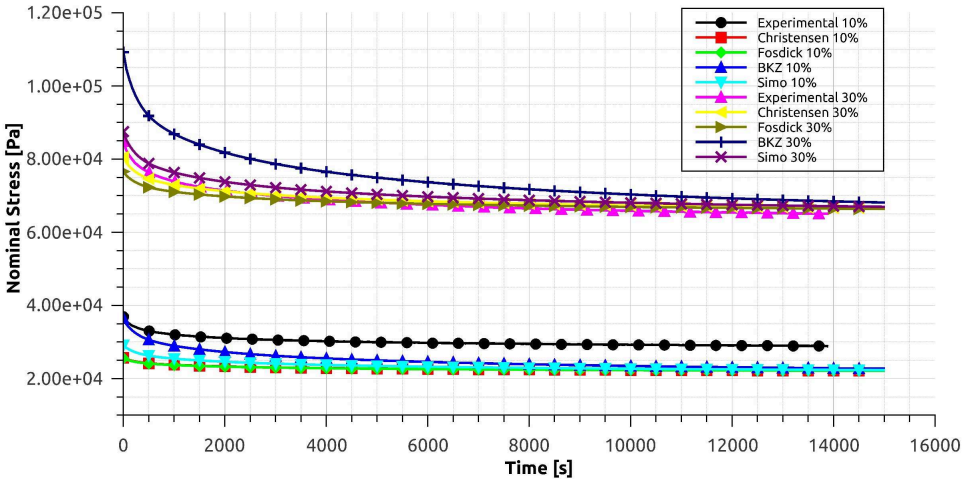

(a) NeoHook

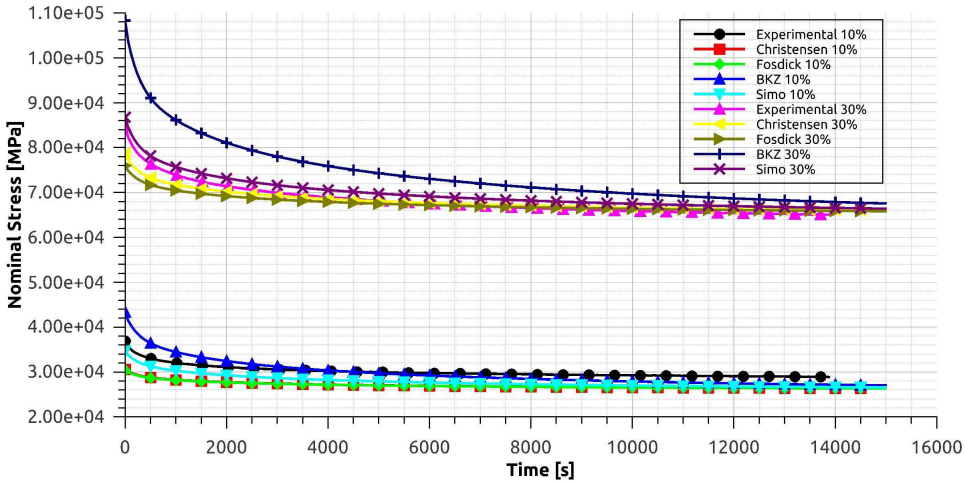

(b) Mooney-Rivlin

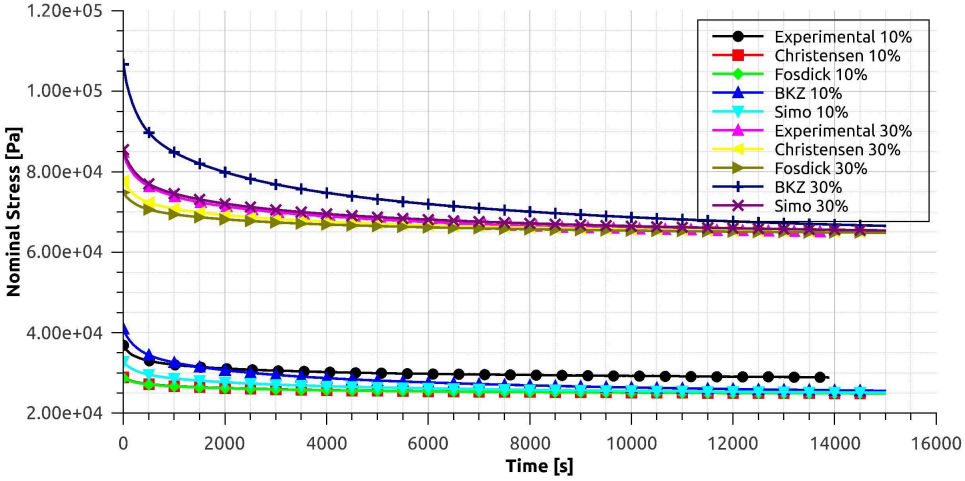

(c) 2^{nd} Order Polynomial

Figure 3.3: Comparison of the models relaxation response with different hyperelastic models: Material BIIR

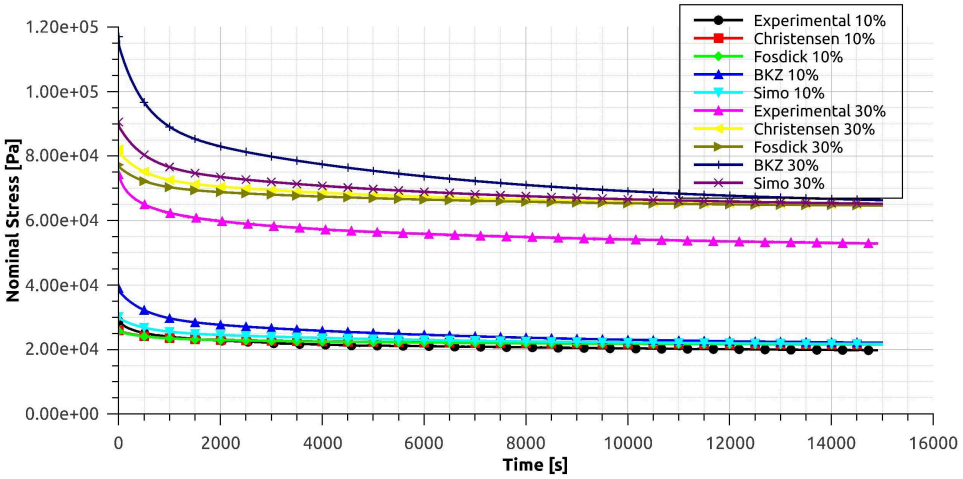

(a) NeoHook

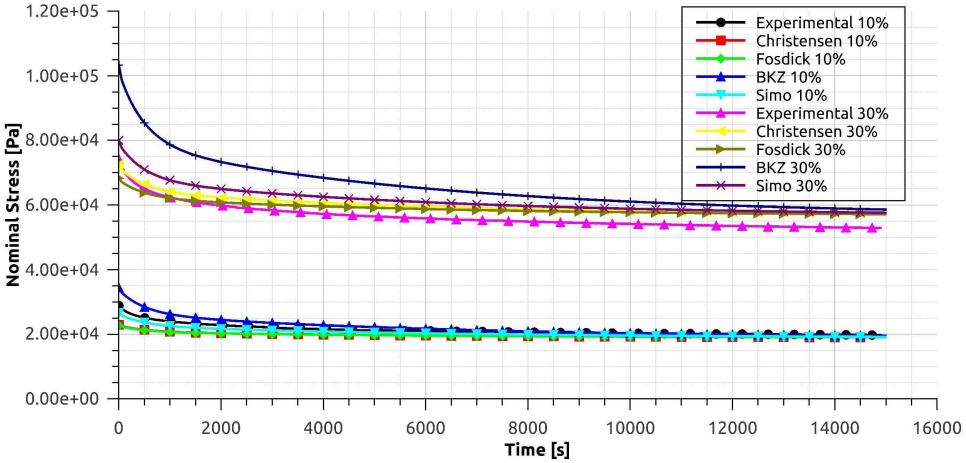

(b) Mooney-Rivlin

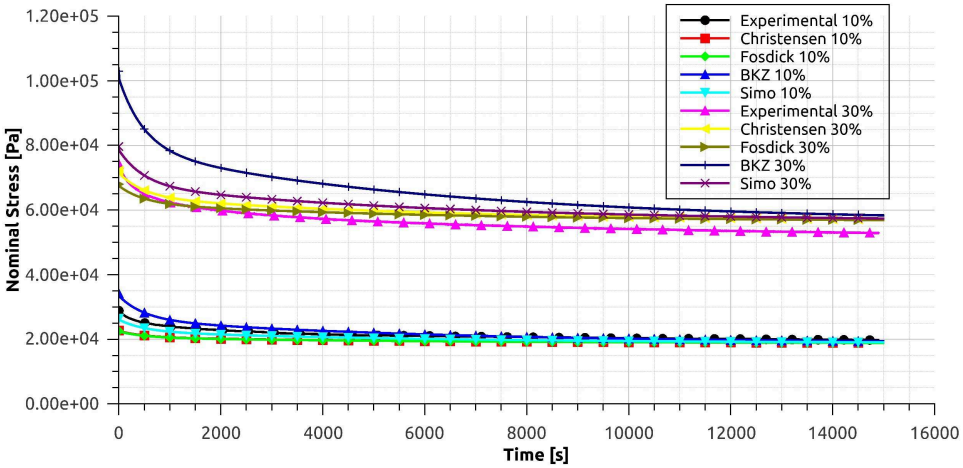

(c) 2^{nd} Order Polynomial

Figure 3.4: Comparison of the models relaxation response with different hyperelastic models: Material NR/BIIR

3.5 Predictive capabilities of monotonic experiments

3.5.1 Monotonic uniaxial tension

In this section we hold the choice of the polynomial hyperelasic form and its particular cases NeoHookean and Mooney-Rivlin.

NeoHookean Potential

$$\begin{aligned}\sigma^{Ch}_{tension}(t) &= 2\left(\lambda(t)^2 - \frac{1}{\lambda(t)}\right) C_{10} \\ &\quad + \frac{G_0}{2}\lambda(t)^2 \int_0^t g_1(t-s)\frac{\partial \lambda^2(s)}{\partial s} ds \\ &\quad - \frac{G_0}{2\lambda(t)} \int_0^t g_1(t-s)\frac{\partial \frac{1}{\lambda(s)}}{\partial s} ds \end{aligned} \tag{3.18a}$$

$$\begin{aligned}\sigma^{FY}_{tension}(t) &= 2\left(\lambda(t)^2 - \frac{1}{\lambda(t)}\right) C_{10} \\ &\quad + \frac{G_0}{2\lambda(t)^2} \int_0^t g_1(t-s)\frac{\partial \lambda^2(s)}{\partial s} ds \\ &\quad - \frac{G_0}{2}\lambda(t) \int_0^t g_1(t-s)\frac{\partial \frac{1}{\lambda(s)}}{\partial s} ds \end{aligned} \tag{3.18b}$$

$$\begin{aligned}\sigma^{BKZ}_{tension}(t) &= 2\left(\lambda(t)^2 - \frac{1}{\lambda(t)}\right) C_{10} \\ &\quad + \frac{2G_0}{\lambda(t)} \int_0^t g_1(t-s)\frac{\partial \lambda(s)}{\partial s} ds \\ &\quad - 2G_0\lambda(t)^2 \int_0^t g_1(t-s)\frac{\partial \frac{1}{\lambda(s)^2}}{\partial s} ds \end{aligned} \tag{3.18c}$$

$$\begin{aligned}\sigma^{Si}_{tension}(t) &= \frac{2}{g_\infty}\left(\lambda(t)^2 - \frac{1}{\lambda(t)}\right) C_{10} \\ &\quad + \frac{2}{g_\infty}\left(\lambda(t)^2 - \frac{1}{\lambda(t)}\right) C_{10} \int_0^t \dot{g}_1(s) ds \end{aligned} \tag{3.18d}$$

Mooney-Rivlin Potential

$$\begin{aligned}\sigma^{Ch}_{tension}(t) &= 2\left(\lambda(t)^2-\frac{1}{\lambda(t)}\right)\left(C_{10}+\frac{1}{\lambda(t)}C_{01}\right)\\ &\quad+\frac{G_0}{2}\lambda(t)^2\int_0^t g_1(t-s)\frac{\partial\lambda^2(s)}{\partial s}ds\\ &\quad-\frac{G_0}{2\lambda(t)}\int_0^t g_1(t-s)\frac{\partial\frac{1}{\lambda(s)}}{\partial s}ds\end{aligned} \tag{3.19a}$$

$$\begin{aligned}\sigma^{FY}_{tension}(t) &= 2\left(\lambda(t)^2-\frac{1}{\lambda(t)}\right)\left(C_{10}+\frac{1}{\lambda(t)}C_{01}\right)\\ &\quad+\frac{G_0}{2\lambda(t)^2}\int_0^t g_1(t-s)\frac{\partial\lambda^2(s)}{\partial s}ds\\ &\quad-\frac{G_0}{2}\lambda(t)\int_0^t g_1(t-s)\frac{\partial\frac{1}{\lambda(s)}}{\partial s}ds\end{aligned} \tag{3.19b}$$

$$\begin{aligned}\sigma^{BKZ}_{tension}(t) &= 2\left(\lambda(t)^2-\frac{1}{\lambda(t)}\right)\left(C_{10}+\frac{1}{\lambda(t)}C_{01}\right)\\ &\quad+\frac{2G_0}{\lambda(t)}\int_0^t g_1(t-s)\frac{\partial\lambda(s)}{\partial s}ds\\ &\quad-2G_0\lambda(t)^2\int_0^t g_1(t-s)\frac{\partial\frac{1}{\lambda(s)^2}}{\partial s}ds\end{aligned} \tag{3.19c}$$

$$\begin{aligned}\sigma^{Si}_{tension}(t) &= \frac{2}{g_\infty}\left(\lambda(t)^2-\frac{1}{\lambda(t)}\right)\left(C_{10}+\frac{1}{\lambda(t)}C_{01}\right)\\ &\quad+\frac{2}{g_\infty}\left(\lambda(t)^2-\frac{1}{\lambda(t)}\right)\int_0^t \dot{g}_1(s)\left(C_{10}+\frac{1}{\lambda(t-s)}C_{01}\right)ds\\ &\quad-\frac{2}{\lambda(t)g_\infty}C_{01}\int_0^t \dot{g}_1(s)\lambda^2(t-s)ds\end{aligned} \tag{3.19d}$$

2^{nd} order Polynomial Potential

$$\begin{aligned}\sigma^{Ch}_{tension}(t) &= 2\left(\lambda(t)^2-\frac{1}{\lambda(t)}\right)\Big[C_{10}+2C_{20}(I_1-3)+C_{11}(I_2-3)\\ &\quad+\frac{1}{\lambda(t)}\left(C_{01}+2C_{02}(I_2-3)+C_{11}(I_1-3)\right)\Big]\\ &\quad+\frac{G_0}{2}\lambda(t)^2\int_0^t g_1(t-s)\frac{\partial\lambda^2(s)}{\partial s}ds\\ &\quad-\frac{G_0}{2\lambda(t)}\int_0^t g_1(t-s)\frac{\partial\frac{1}{\lambda(s)}}{\partial s}ds\end{aligned} \tag{3.20a}$$

$$\begin{aligned}\sigma^{FY}_{tension}(t) = 2\left(\lambda(t)^2 - \frac{1}{\lambda(t)}\right)\Bigg[&C_{10} + 2C_{20}(I_1-3) + C_{11}(I_2-3)\\ &+\frac{1}{\lambda(t)}\left(C_{01} + 2C_{02}(I_2-3) + C_{11}(I_1-3)\right)\Bigg]\\ &+\frac{G_0}{2\lambda(t)^2}\int_0^t g_1(t-s)\frac{\partial\lambda^2(s)}{\partial s}ds\\ &-\frac{G_0}{2}\lambda(t)\int_0^t g_1(t-s)\frac{\partial\frac{1}{\lambda(s)}}{\partial s}ds\end{aligned} \tag{3.20b}$$

$$\begin{aligned}\sigma^{BKZ}_{tension}(t) = 2\left(\lambda(t)^2 - \frac{1}{\lambda(t)}\right)\Bigg[&C_{10} + 2C_{20}(I_1-3) + C_{11}(I_2-3)\\ &+\frac{1}{\lambda(t)}\left(C_{01} + 2C_{02}(I_2-3) + C_{11}(I_1-3)\right)\Bigg]\\ &+\frac{2G_0}{\lambda(t)}\int_0^t g_1(t-s)\frac{\partial\lambda(s)}{\partial s}ds\\ &-2G_0\lambda(t)^2\int_0^t g_1(t-s)\frac{\partial\frac{1}{\lambda(s)^2}}{\partial s}ds\end{aligned} \tag{3.20c}$$

$$\begin{aligned}\sigma^{Si}_{tension}(t) = \frac{2}{g_\infty}\left(\lambda(t)^2 - \frac{1}{\lambda(t)}\right)\Bigg[&C_{10} + 2C_{20}(I_1-3) + C_{11}(I_2-3)\\ &+\frac{1}{\lambda(t)}\left(C_{01} + 2C_{02}(I_2-3) + C_{11}(I_1-3)\right)\Bigg]\\ &+\frac{2}{g_\infty}\left(\lambda(t)^2 - \frac{1}{\lambda(t)}\right)\int_0^t \dot{g}_1(s)\Bigg[C_{10} + 2C_{20}(I_1-3) + C_{11}(I_2-3)\\ &+\frac{1}{\lambda(t-s)}\left(C_{01} + 2C_{02}(I_2-3) + C_{11}(I_1-3)\right)\Bigg]ds\\ &-\frac{2}{\lambda(t)g_\infty}\int_0^t \frac{\partial g_1(s)}{\partial s}\left(C_{01} + 2C_{02}(I_2-3) + C_{11}(I_1-3)\right)\lambda^2(t-s)ds\end{aligned} \tag{3.20d}$$

Since the available experimental data for uniaxial tension are only for monotonic testing, we consider the elongation function as:

$$\lambda(t) = 1 + \dot{\lambda}\, t \tag{3.21}$$

with $\dot{\lambda} = cst$. The integration of those equations have been done using numerical approximation methods [129].

The response of monotonic tension nominal stress ($\mathbf{\Pi}$) for each material are reported in figs. 3.5 to 3.7. The considered models present the capability to take into account a strain rate effect, with higher stain rates leading to a higher stress at same defor-

mation level. Considering a NeoHookean or a Mooney-Rivlin hyperelastic potential, the predicted data are seen to be non accurate, and all the models could not predict the second inflection point. Considering the 2^{nd} Order Polynomial hyperelastic potential, we made the following observations:

- All the considered models are able to predict a strain-rate effect.
- The Christensen model is seen to highly overestimate the nominal stress level for high strains, not to exceed 100% of deformation for the BIIR and the NR/BIIR materials as shows figs. 3.6e, 3.6f, 3.7e and 3.7f. For the NR material, this model was able to predict the stress level with accepted overestimation and the error increases as strain-rate increases.
- Fosdick & Yu model is seen to underestimate the stress level for the three materials, and has the lowest stress level through all models. Nevertheless, the predicted level is seen to be acceptable.
- Both BKZ and Simo models were able to give a better approximation of the stress level. The prediction is quite good and the predicted stress is in a good range.

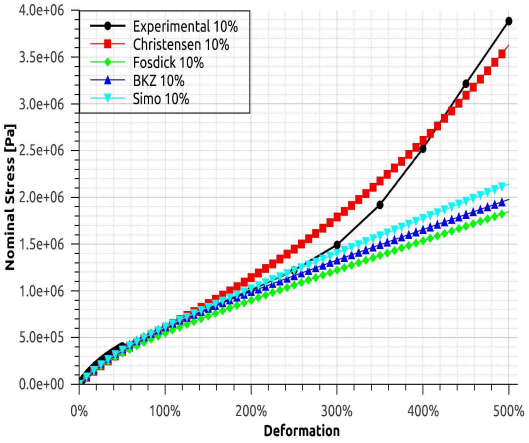

(a) NR 10% min NeoHookean

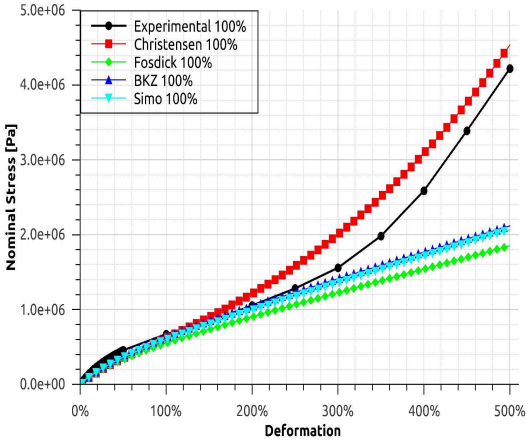

(b) NR 100% min NeoHookean

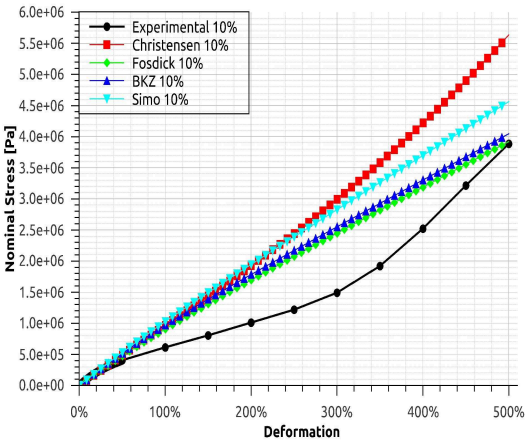

(c) NR 10% min Mooney

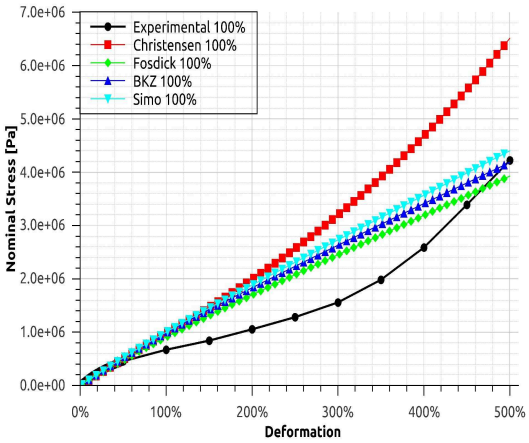

(d) NR 100% min Mooney

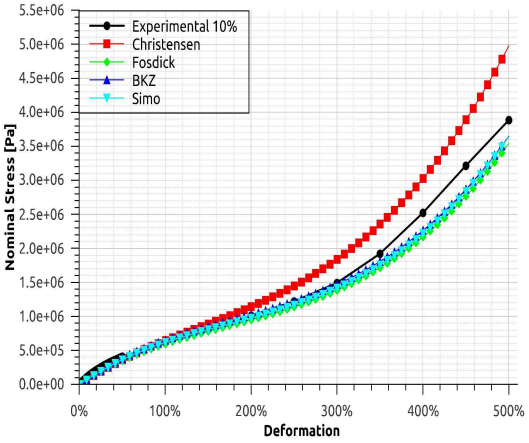

(e) NR 10% min Poly

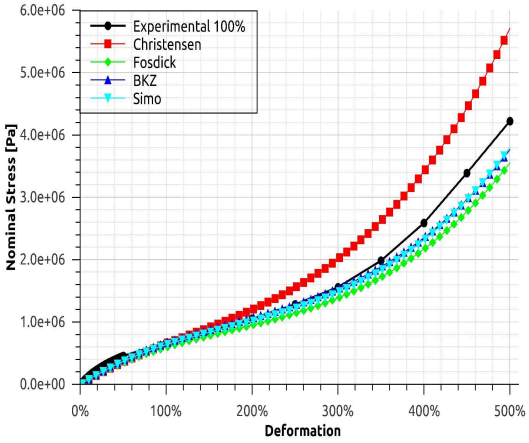

(f) NR 100% min Poly

Figure 3.5: NR monotonic tension models response, for NeoHookean, Mooney-Rivlin and Polynomial Hyperelastic Potentials

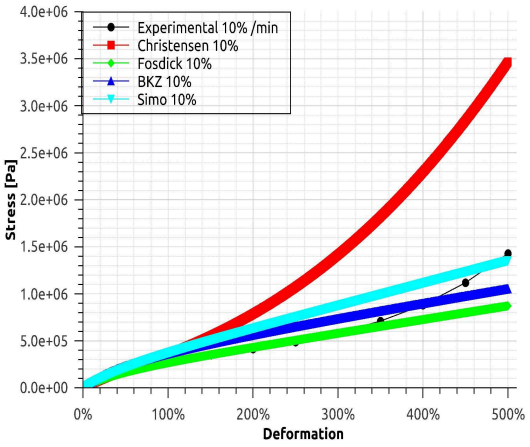

(a) BIIR 10% min NeoHookean

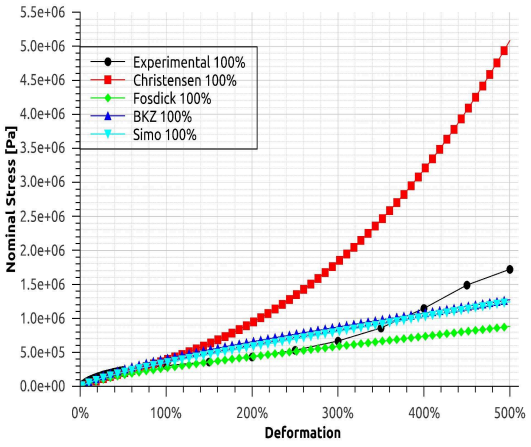

(b) BIIR 100% min NeoHookean

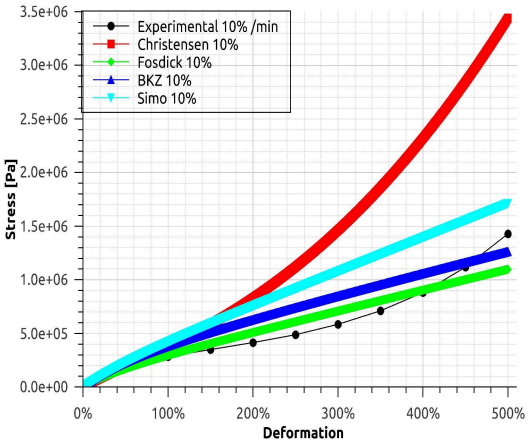

(c) BIIR 10% min Mooney

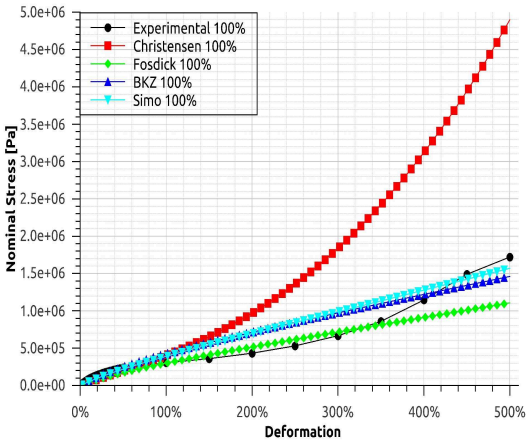

(d) BIIR 100% min Mooney

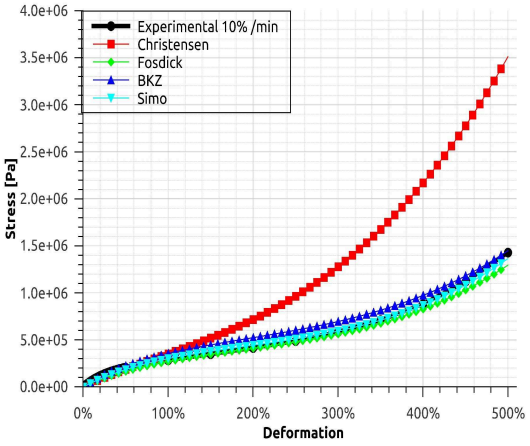

(e) BIIR 10% min Poly

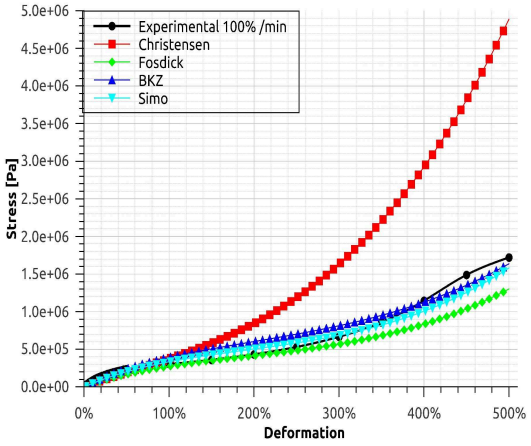

(f) BIIR 100% min Poly

Figure 3.6: BIIR monotonic tension models response, for NeoHookean, Mooney-Rivlin and Polynomial Hyperelastic Potentials

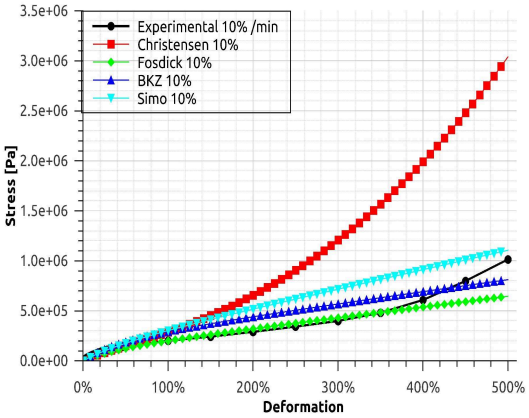

(a) NRBIIR 10% min NeoHookean

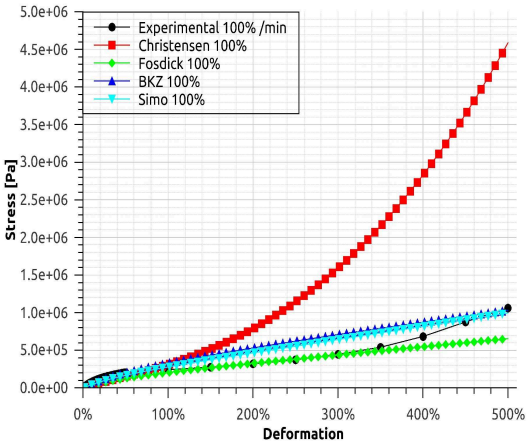

(b) NRBIIR 100% min NeoHookean

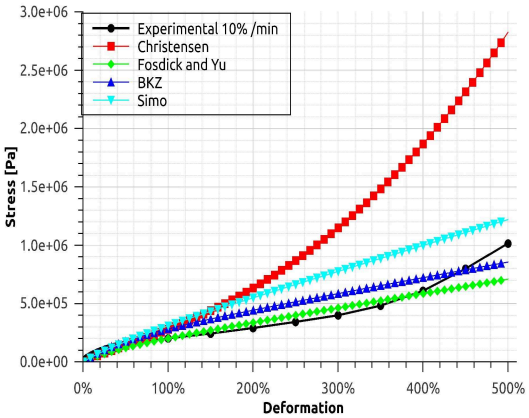

(c) NRBIIR 10% min Mooney

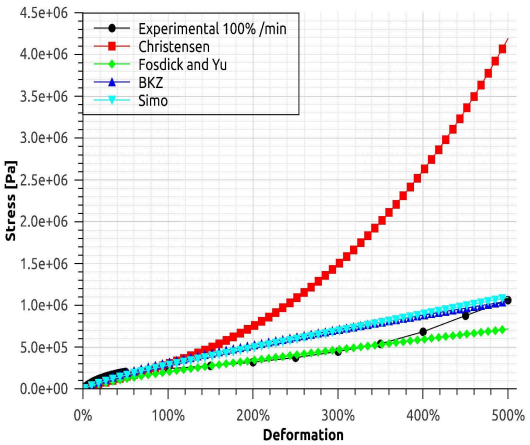

(d) NRBIIR 100% min Mooney

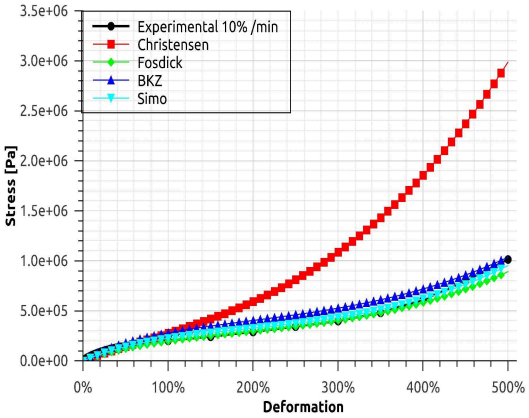

(e) NRBIIR 10% min Poly

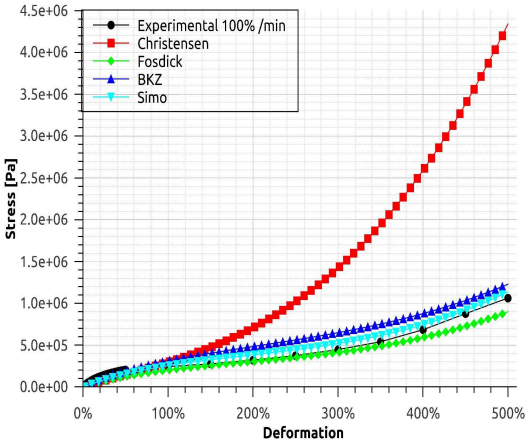

(f) NRBIIR 100% min Poly

Figure 3.7: NRBIIR monotonic tension models response, for NeoHookean, Mooney-Rivlin and Polynomial Hyperelastic Potentials

3.5.2 Monotonic simple shear

For a monotonic simple shear motion, we consider:

$$\gamma(t) = \gamma_0 t \tag{3.22}$$

We introduce this equation into eqs. (3.12a) to (3.12d) to obtain the constitutive equations for a monotonic simple shear motion:

NeoHookean Potential

$$\begin{aligned}\sigma_{12}^{Ch}(t) = 2\gamma_0 t C_{10} + \frac{G_0}{2}\gamma_0 \int_0^t g_1(t-s)ds \\ + G_0\gamma_0^3 t \int_0^t g_1(t-s)sds\end{aligned} \tag{3.23a}$$

$$\sigma_{12}^{FY}(t) = 2\gamma_0 t C_{10} + \frac{G_0}{2}\gamma_0 \int_0^t g_1(t-s)ds \tag{3.23b}$$

$$\sigma_{12}^{BKZ}(t) = 2\gamma_0 t C_{10} + 2G_0\gamma_0 \int_0^t g_1(t-s)ds \tag{3.23c}$$

$$\sigma_{12}^{Si}(t) = \frac{2}{g_\infty}\gamma_0 t C_{10} + \frac{2}{g_\infty}\gamma_0 t C_{10} \int_0^t \frac{\partial g_1(s)}{\partial s} ds \tag{3.23d}$$

Mooney Rivlin Potential

$$\begin{aligned}\sigma_{12}^{Ch}(t) = 2\gamma_0 t\left(C_{10}+C_{01}\right) + \frac{G_0}{2}\gamma_0 \int_0^t g_1(t-s)ds \\ + G_0\gamma_0^3 t \int_0^t g_1(t-s)sds\end{aligned} \tag{3.24a}$$

$$\sigma_{12}^{FY}(t) = 2\gamma_0 t\left(C_{10}+C_{01}\right) + \frac{G_0}{2}\gamma_0 \int_0^t g_1(t-s)ds \tag{3.24b}$$

$$\sigma_{12}^{BKZ}(t) = 2\gamma_0 t\left(C_{10}+C_{01}\right) + 2G_0\gamma_0 \int_0^t g_1(t-s)ds \tag{3.24c}$$

$$\begin{aligned}\sigma_{12}^{Si}(t) = \frac{2}{g_\infty}\gamma_0 t\left(C_{10}+C_{01}\right) - \frac{2}{g_\infty}\gamma_0 C_{01}\int_0^t \frac{\partial g_1(s)}{\partial s}\left(t-s\right)ds \\ + \frac{2}{g_\infty}\gamma_0 t\left(C_{10}+2C_{01}\right)\int_0^t \frac{\partial g_1(s)}{\partial s} ds\end{aligned} \tag{3.24d}$$

2^{nd} Order Polynomial Potential

$$\begin{aligned}\sigma_{12}^{Ch}(t) &= 2\gamma_0 t\left(C_{10}+2C_{20}\gamma(t)^2+C_{01}+2C_{02}\gamma(t)^2+2C_{11}\gamma(t)^2\right)\\ &+\frac{G_0}{2}\gamma_0\int_0^t g_1(t-s)ds\\ &+G_0\gamma_0^3 t\int_0^t g_1(t-s)sds\end{aligned} \tag{3.25a}$$

$$\begin{aligned}\sigma_{12}^{FY}(t) &= 2\gamma_0 t\left(C_{10}+2C_{20}\gamma(t)^2+C_{01}+2C_{02}\gamma(t)^2+2C_{11}\gamma(t)^2\right)\\ &+\frac{G_0}{2}\gamma_0\int_0^t g_1(t-s)ds\end{aligned} \tag{3.25b}$$

$$\begin{aligned}\sigma_{12}^{BKZ}(t) &= 2\gamma_0 t\left(C_{10}+2C_{20}\gamma(t)^2+C_{01}+2C_{02}\gamma(t)^2+2C_{11}\gamma(t)^2\right)\\ &+2G_0\gamma_0\int_0^t g_1(t-s)ds\end{aligned} \tag{3.25c}$$

$$\begin{aligned}\sigma_{12}^{Si}(t) &= \frac{2}{g_\infty}\gamma_0 t\left(C_{10}+2C_{20}\gamma(t)^2+C_{01}+2C_{02}\gamma(t)^2+2C_{11}\gamma(t)^2\right)\\ &-\frac{2}{g_\infty}\int_0^t\frac{\partial g_1(s)}{\partial s}\left(C_{01}+2C_{02}\gamma^2(t-s)+C_{11}\gamma^2(t-s)\right)\gamma(t-s)ds\\ &+\frac{2}{g_\infty}\gamma_0 t\int_0^t\frac{\partial g_1(s)}{\partial s}\left(C_{10}+2C_{20}\gamma(t-s)^2+2C01\right.\\ &\left.+4C_{02}\gamma(t-s)^2+3C_{11}\gamma(t-s)^2\right)ds\end{aligned} \tag{3.25d}$$

Models response results at differents strain rates have been compared to the experimental data. Results for each material are reported in figs. 3.8 to 3.10. All models shear response is quasi-linear as observed by Rivlin [36]. Considering the NR material, and for both presented strain rates 5% min and 20% min, the experimental data are well approximated only for low strain levels, not to exceed 50% of deformation by Neo-Hookean and Mooney-Rivlin potentials. Exceeding this range, the response of the different models overestimates the experimental data. The 2^{nd} Order Polynomial hyperelastic potential is seen to underestimate the stress level along loading, and reaches the stress level at end of loading. Considering the BIIR and NR/BIIR materials, the prediction is of a less quality than for the NR material. Increasing the hyperelastic potential order leads to a softening of the material response. Fosdick & Yu model shows a good estimation of the material data with a NeoHookean potential for deformation level less than 50%. The response is overestimated over this limit. Christensen model has the ability to stiffen and approximate the stress level at 100% of deformation, but the error is of a great value. BKZ and Simo models

show close responses, at each strain rate. The stress level is underestimated, and the maximum error is of about $0.4MPa$.

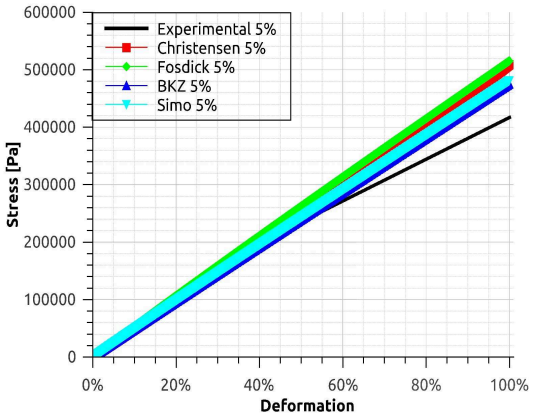

(a) NR 5% min NeoHookean

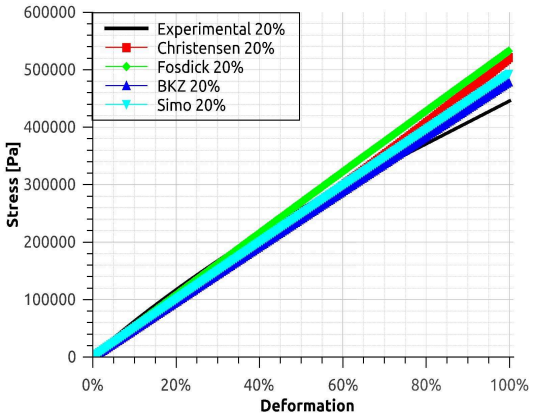

(b) NR 20% min NeoHookean

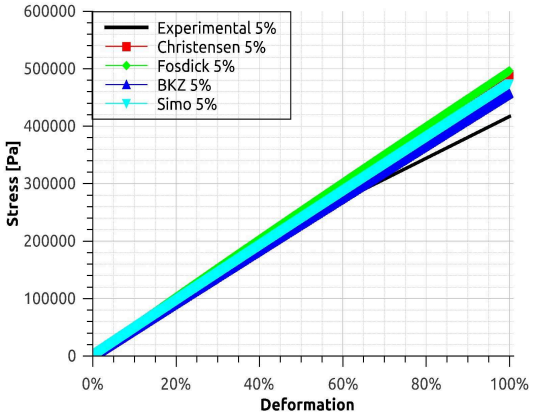

(c) NR 5% min Mooney

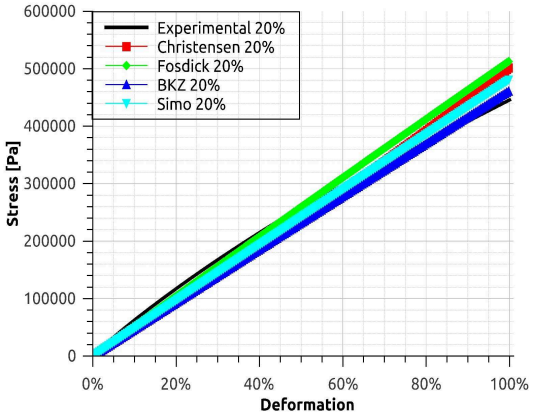

(d) NR 20% min Mooney

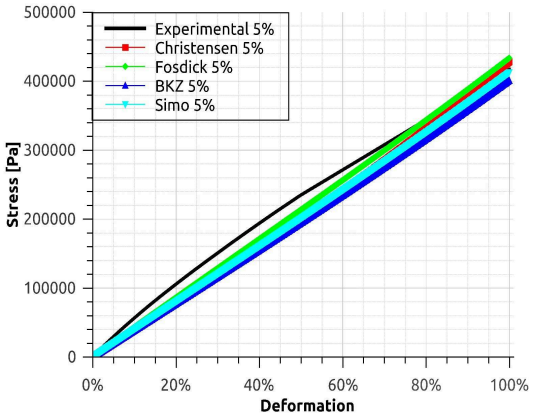

(e) NR 5% min Poly

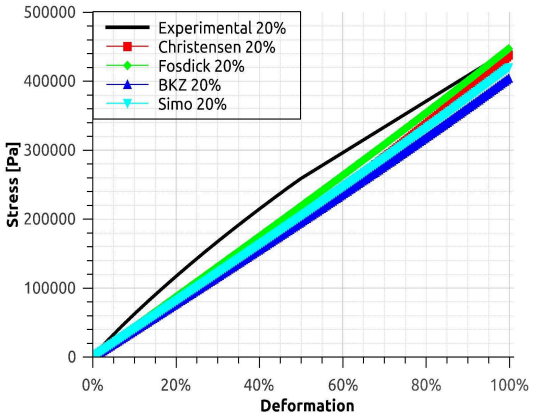

(f) NR 20% min Poly

Figure 3.8: NR monotonic shear models response, for NeoHookean, Mooney-Rivlin and Polynomial Hyperelastic Potentials

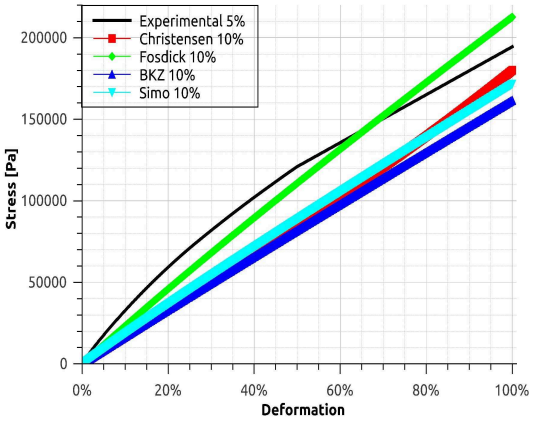

(a) BIIR 5% min NeoHookean

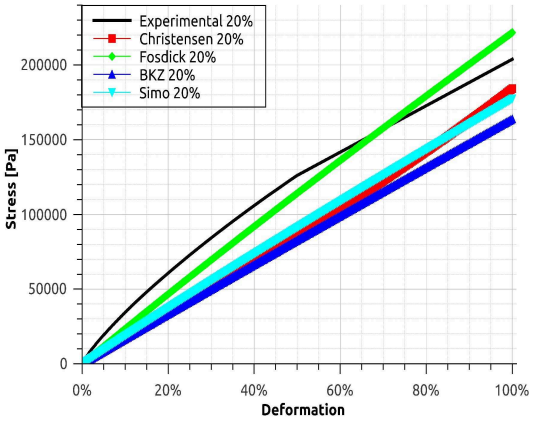

(b) BIIR 20% min NeoHookean

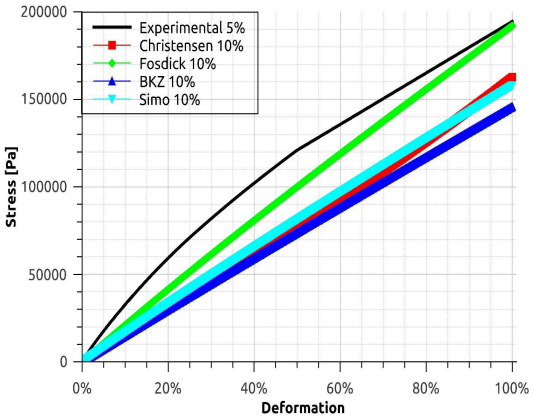

(c) BIIR 5% min Mooney

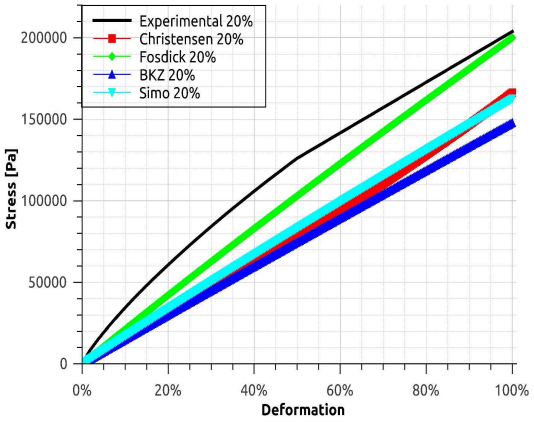

(d) BIIR 20% min Mooney

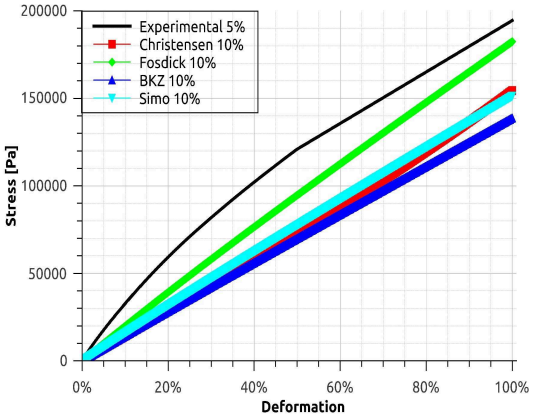

(e) BIIR 5% min Poly

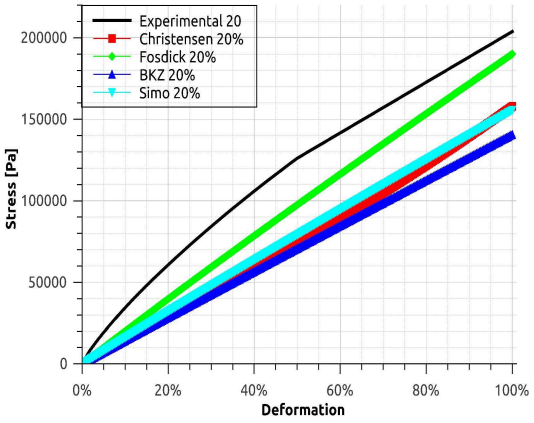

(f) BIIR 20% min Poly

Figure 3.9: BIIR monotonic shear models response, for NeoHookean, Mooney-Rivlin and Polynomial Hyperelastic Potentials

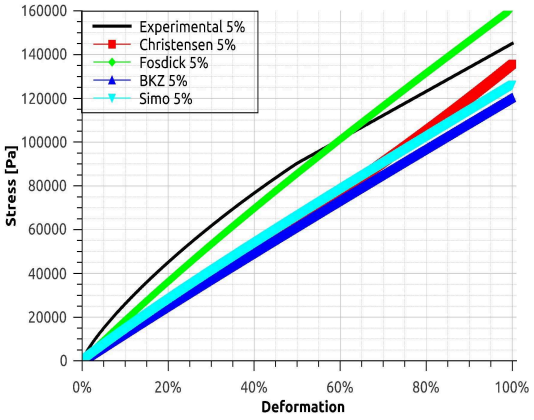

(a) NR/BIIR 5% min NeoHookean

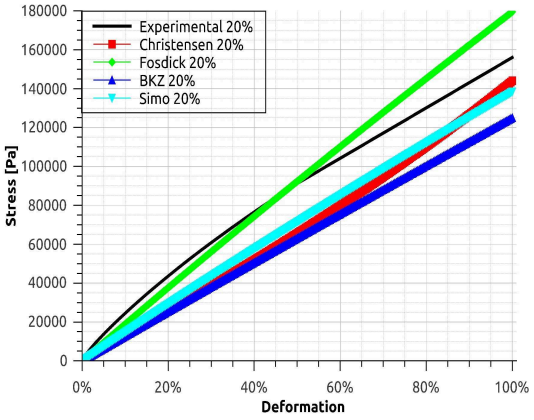

(b) NR/BIIR 20% min NeoHookean

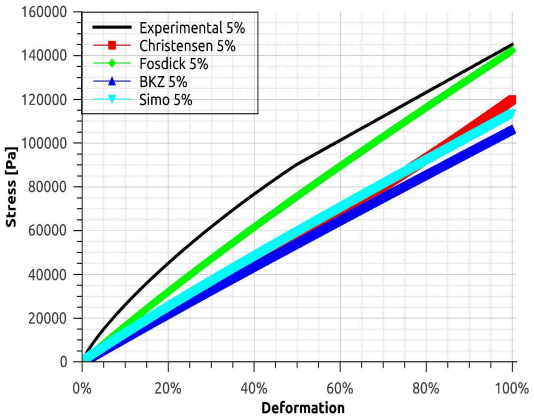

(c) NR/BIIR 5% min Mooney

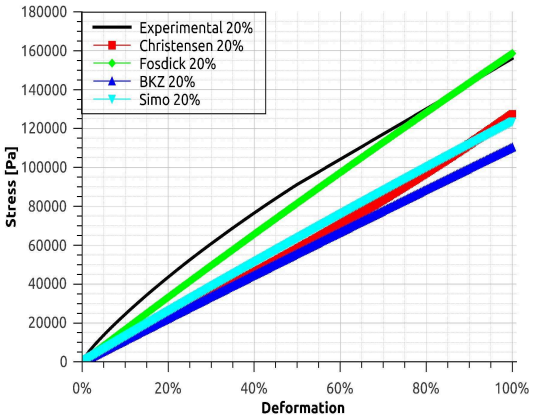

(d) NR/BIIR 20% min Mooney

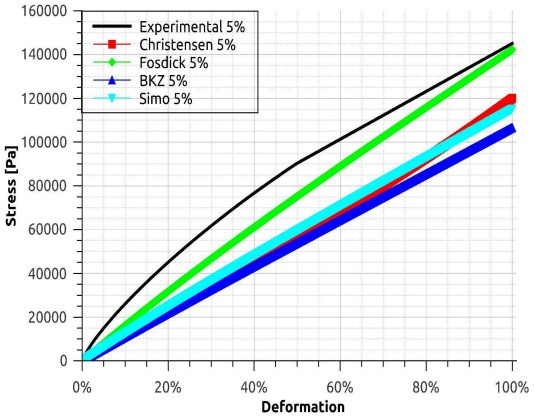

(e) NR/BIIR 5% min Poly

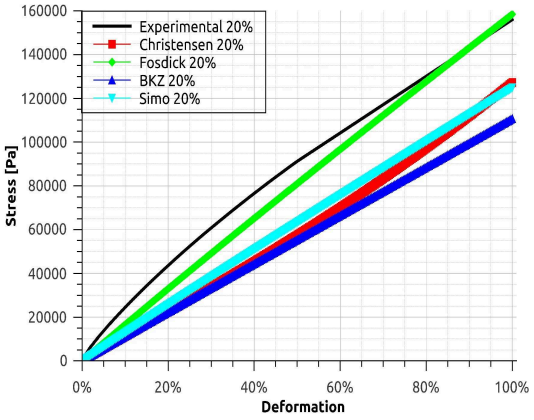

(f) NR/BIIR 20% min Poly

Figure 3.10: NR/BIIR monotonic shear models response, for NeoHookean, Mooney-Rivlin and Polynomial Hyperelastic Potentials

3.6 Predictive capabilities of dynamic properties

3.6.1 Determination of the complex shear modulus

The determination of the complex shear modulus was introduced by [64] and is a Fourrier transform of the governing equations. The frequency domain viscoelasticity is defined for a kinematically small perturbation about a predeformed state. The procedure consists on a linearized vibration solution associated with a long-term hyperelastic material behavior. This assumes that the linear expression for the shear stress still governs the system. Since the available experimental data in the frequency domain are limited to moderate strains, not to exceed 30%, and the procedure is linearized for high order strains, a simple Mooney-Rivlin hyperelastic potential leads to sufficient results. Therefore, we used the following state of loading:

$$\begin{array}{cc} \gamma(s) = 0 & s < 0 \\ \gamma(s) = \gamma_0 & 0 \leqslant s \leqslant t_0 \\ \gamma(s) = \gamma_0 + \gamma_a e^{(i\omega t)} & t_0 \leqslant s \leqslant t \end{array} \tag{3.26}$$

with
We assume that $|\gamma_a| << 1$ and that the specimen has been oscillating for a very long time so that a steady-state solution is obtained and the dynamic stress has the form:

$$\sigma^*(\omega) = G^*(\omega, \gamma_0)\gamma(\omega) \tag{3.27a}$$

$$G^*(\omega, \gamma_0) = G_s(\omega, \gamma_0) + iG_l(\omega, \gamma_0) \tag{3.27b}$$

where $G_s = \Re\left[G^*(\omega, \gamma_0)\right]$ and $G_l = \Im\left[G^*(\omega, \gamma_0)\right]$ are respectively the shear storage and loss modulus expressed in term of the Fourrier transform of the time-dependent shear relaxation modulus.

Taking into account only first order terms of $\gamma(\omega)$, calculations leads to:

$$\begin{aligned} \sigma_{12}^{*,Ch}(\omega, \gamma_0) = {} & 2(C_{10} + C_{01})\gamma^*(\omega) \\ & + G_0\left(\frac{1}{2} + \gamma_0^2\right)\left[i\omega\int_0^\infty g_1(s)e^{(-i\omega s)}ds\right]\gamma^*(\omega) \end{aligned} \tag{3.28a}$$

$$\sigma_{12}^{*,FY}(\omega,\gamma_0) = 2(C_{10}+C_{01})\gamma^*(\omega) + \frac{G_0}{2}\left[i\omega\int_0^\infty g_1(s)e^{(-i\omega s)}ds\right]\gamma^*(\omega) \tag{3.28b}$$

$$\sigma_{12}^{*,BKZ}(\omega,\gamma_0) = 2(C_{10}+C_{01})\gamma^*(\omega) + 2G_0\left[i\omega\int_0^\infty g_1(s)e^{(-i\omega s)}ds\right]\gamma^*(\omega) \tag{3.28c}$$

$$\sigma_{12}^{*,Si}(\omega,\gamma_0) = \left(\frac{2}{g_\infty}(C_{10}+C_{01}) - 2C_{01}\frac{(1-g_\infty)}{g_\infty}\right)\gamma^*(\omega) - \frac{2C_{01}}{g_\infty}\left[i\omega\int_0^\infty g_1(s)e^{(-i\omega s)}ds\right]\gamma^*(\omega) \tag{3.28d}$$

$\sigma_{12}^*(\omega,\gamma_0)$ is the dynamic stress component that should be additioned to the equilibrium static stress $\sigma_{12}^{Equilibrium} = 2(C_{10}+C_{01})\gamma_0$ component to obtain the total stress quantity.
The determinated complex shear modulus for the considered models is then:

$$G^{*,Ch}(\omega,\gamma_0) = 2(C_{10}+C_{01}) + G_0\left(\frac{1}{2}+\gamma_0^2\right)\left[i\omega\int_0^\infty g_1(s)e^{(-i\omega s)}ds\right] \tag{3.29a}$$

$$G^{*,FY}(\omega,\gamma_0) = 2(C_{10}+C_{01}) + \frac{G_0}{2}\left[i\omega\int_0^\infty g_1(s)e^{(-i\omega s)}ds\right] \tag{3.29b}$$

$$G^{*,BKZ}(\omega,\gamma_0) = 2(C_{10}+C_{01}) + 2G_0\left[i\omega\int_0^\infty g_1(s)e^{(-i\omega s)}ds\right] \tag{3.29c}$$

$$G^{*,Si}(\omega,\gamma_0) = \left(\frac{2}{g_\infty}(C_{10}+C_{01}) - 2C_{01}\frac{(1-g_\infty)}{g_\infty}\right) - \frac{2C_{01}}{g_\infty}\left[i\omega\int_0^\infty g_1(s)e^{(-i\omega s)}ds\right] \tag{3.29d}$$

3.6.2 Complex modulus comparison results

We firstly report on the results concerning the shear storage modulus, which are shown in figs. 3.11 to 3.13. The considered materials have shown a frequency dependent dynamic behavior. Increasing frequency leads to increasing the shear storage modulus in the frequency range. At each considered predeformation level, following observations have been made:

- Simo model have shown an excellent approximation of the dynamic shear storage modulus with respect to frequency and predeformation. At lowest frequencies, the experimental data are seen to be slightly overestimated.
- Christensen model underestimates the shear modulus at 10% of deformations and overestimate the properties at higher predeformation: this model was not able to predict the softening of the material occuring with increasing predeformation level.
- Fosdick and Yu model's response underestimates the materials response. Even though increasing predeformation leads to a stiffening of the model response, the predicted data are slightly lower than the experimental data.
- The BKZ model's response is not in an acceptable range. The predicted shear storage modulus shows the ability to take into account the frequency effect and the predeformation level but not the moduli level.

Interested in the shear loss factor, the frequency dependence of the compared models is pronounced, and all models are seen to offer a good approximation of this factor as shows figs. 3.11 to 3.13. The Simo model slightly underestimate the response, and the maximum deviation is of about 10%. One can observe that although the BKZ model could not predict the storage modulus, is have shown the ability to well approximate the damping of the materials.

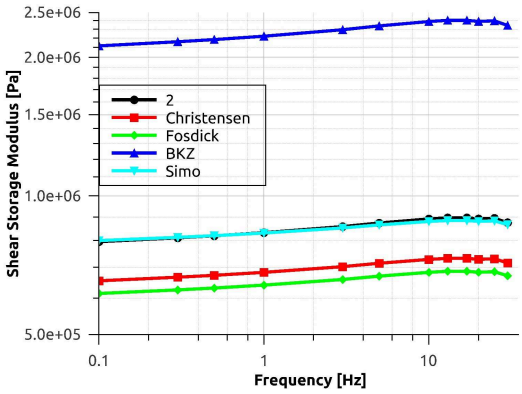

(a) NR shear storage Modulus 10% predeformation

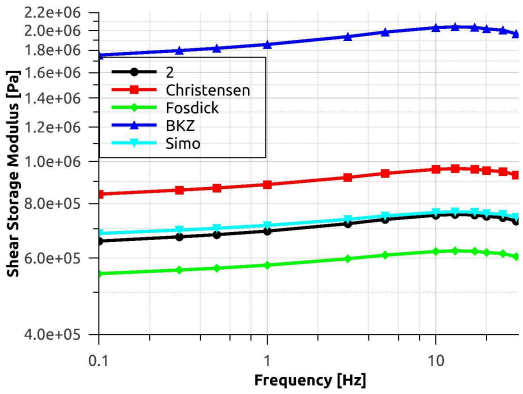

(b) NR shear storage Modulus 30% predeformation

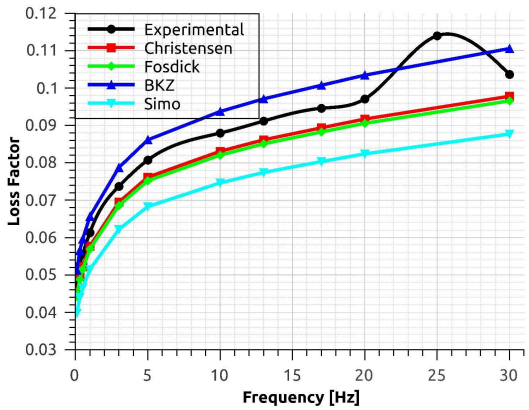

(c) NR loss factor 10% predeformation

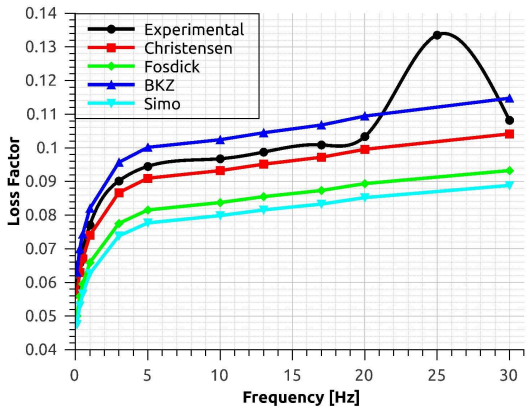

(d) NR loss factor 30% predeformation

Figure 3.11: NR dynamic properties models response, for Mooney-Rivlin Hyperelastic Potentials

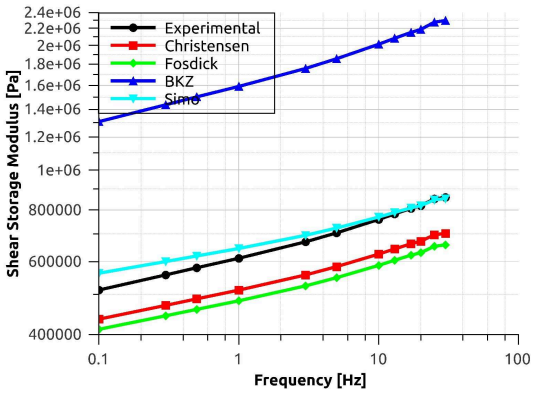

(a) BIIR shear storage Modulus 10% predeformation

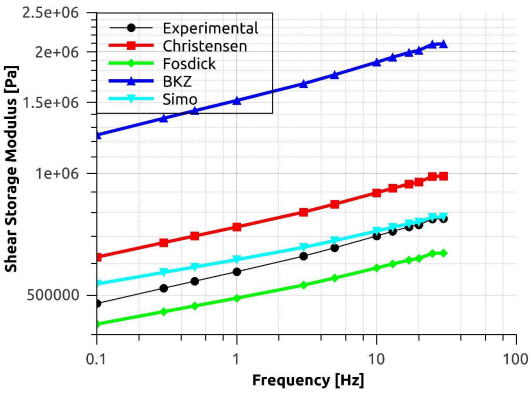

(b) BIIR shear storage Modulus 30% predeformation

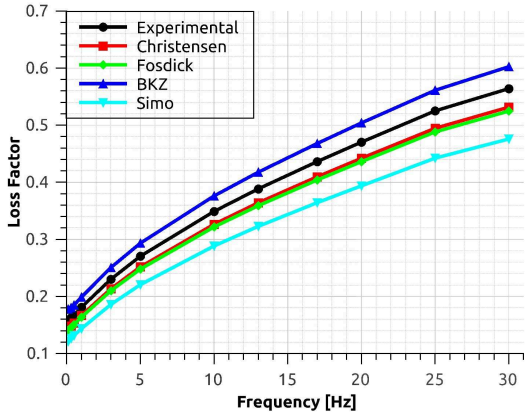

(c) BIIR loss factor 10% predeformation

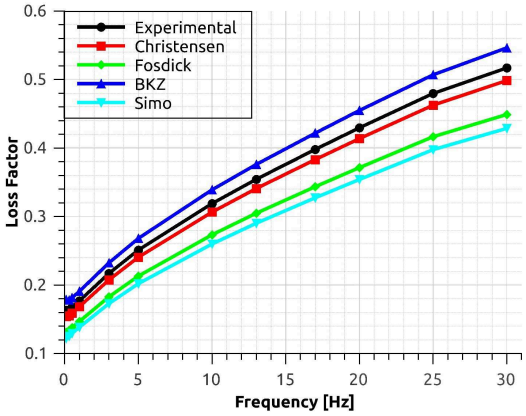

(d) BIIR loss factor 30% predeformation

Figure 3.12: BIIR dynamic properties models response, for Mooney-Rivlin Hyperelastic Potentials

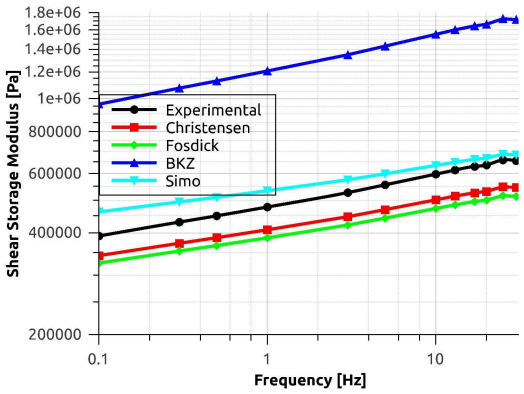

(a) NR/BIIR shear storage Modulus 10% predeformation

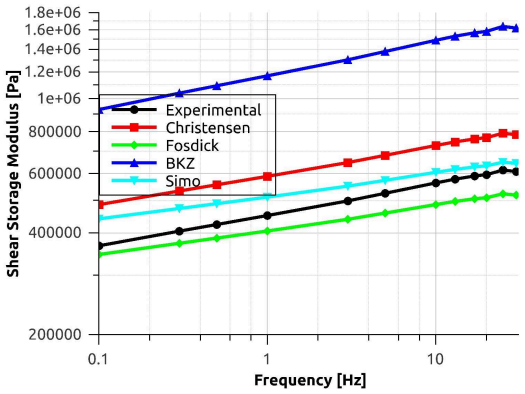

(b) NR/BIIR shear storage Modulus 30% predeformation

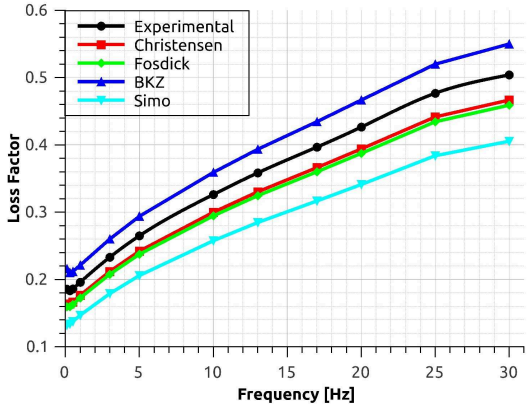

(c) NR/BIIR loss factor 10% predeformation

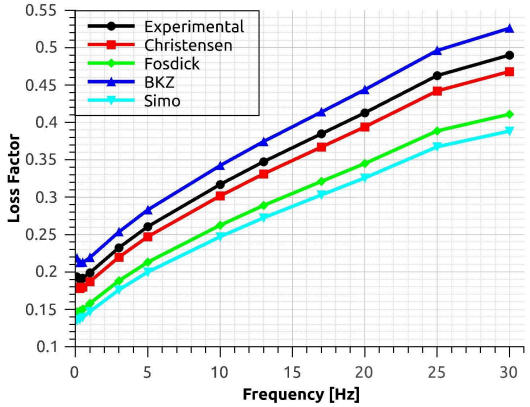

(d) NR/BIIR loss factor 30% predeformation

Figure 3.13: NR/BIIR dynamic properties models response, for Mooney-Rivlin Hyperelastic Potentials

3.7 Conclusions

Within this chapter, we propose an analysis of the predictive capabilities of some finite strain viscoelastic models under time-strain seperability assumption, based on experimental observations. We determined the response of four models, well adapted for engineering applications, for monotonic uniaxial tension/simple shear motions, shear relaxation and shear dynamic response. We have found that the choice of the hyperelastic potential is of a major importance, since this choice defines the equilibrium point commonly called the service point for vibration problems in industrial context. We determined the strain-rate dependent response of the considered mod-

els, and the major difference have been found on the transient response. For the Christensen model, we have seen that it is more suitable to be used for mid range deformations while, whith a good choice of hyperelastic potential, all other models could predict the response over a wider range of deformations. In frequency domain, models have shown the capability to take into account frequency and predeformation effects. For shear storage modulus, except BKZ model, all predicted data could be in an acceptable range. For the damping capability governed by the estimation of the loss factor, all models could estimate this faculty in an acceptable range. As prospect, this analysis can be conducted with consideration to the temperature effect which highly influences the phenomenological behavior of elastomerers in frequency domain specially and could lead to brittle damage of the materials.
With these findings concerning the set of the hyperelastic potential and material parameters and the fidelity observed for the Simo model reproducing to the best the experimental data, the following chapter will be dedicated to the application on the industrial component.

Chapter 4

Elastomeric device: Numerical simulations

Contents

4.1 Introduction

The dimensioning of structures integrating a constrained hyper-viscoelastic layer requires a predictive model capable of quantifying the reduction of the vibration level [130][131][132]. The difficulty of analyzing such structures arises from the frequency dependence of the viscoelastic material, as well as the need to carefully model forces transmitted to the viscoelastic layer [132][133]. There are various approaches, analytical or numerical, to estimate the damping induced by the application of the passive treatment [11][134]. In the framework of this thesis, the finite element calculation code ABAQUS 6.14 was used to investigate the dynamic properties of such structure.

In that sens, this chapter is devoted to the concretization of the work explained in the previous chapters of this report on the real model part. While in the second chapter we conducted an experimental investigation, through monotonic tests, relaxation and dynamic tests, on three candidate rubber materials for the industrial application, chapter 3 was dedicated to the finite strain viscoelastic models aiming to carefully reproduce the experimental data with good fidelity and analyse the predictive capabilities of those models.

This chapter is organized as follows: in the first section, we present the technical specifications and details for the Ariane 6 Launcher interstage. We develop in the following section the strong and weak formulations of the problem, using the finite element method and handling the previous explained constitutive models and behavior laws. A description of the implemented model will be aim of the section 4.3, with the definition of the boundary conditions and the different computational steps with respects to the industrial requirements. This will be followed by numerical simulation results as a parametric dynamic study calibrate the choice of the damping material and the geometrical parameters.

4.2 Technical Specifications

4.2.1 Overview

The overarching aim of Ariane 6 is to provide guaranteed access to space to Europe without requiring public sector support to exploitation. The target date for the first flight of Ariane 6 is 2021, followed by a transition period with a progressive phasing in of Ariane 6 and phasing out of the launch systems it will replace, so as

to demonstrate Ariane 6 reliability to customers.
Ariane 5, which is actually the world reference for heavy-lift launchers have faced several vibratory problems mainly for the demonstration flights [135][136]. For Ariane 6, intended to be the new reference for heavy-lift launchers, the prediction and the control of the structure vibration levels is a primary feature to be considered. For this prospect, the new design as well as the ignition system and the different components are under investigation for more controllability of the system. To respond to this requirement, many leading groups are participating in this project, as shows fig. 4.1.

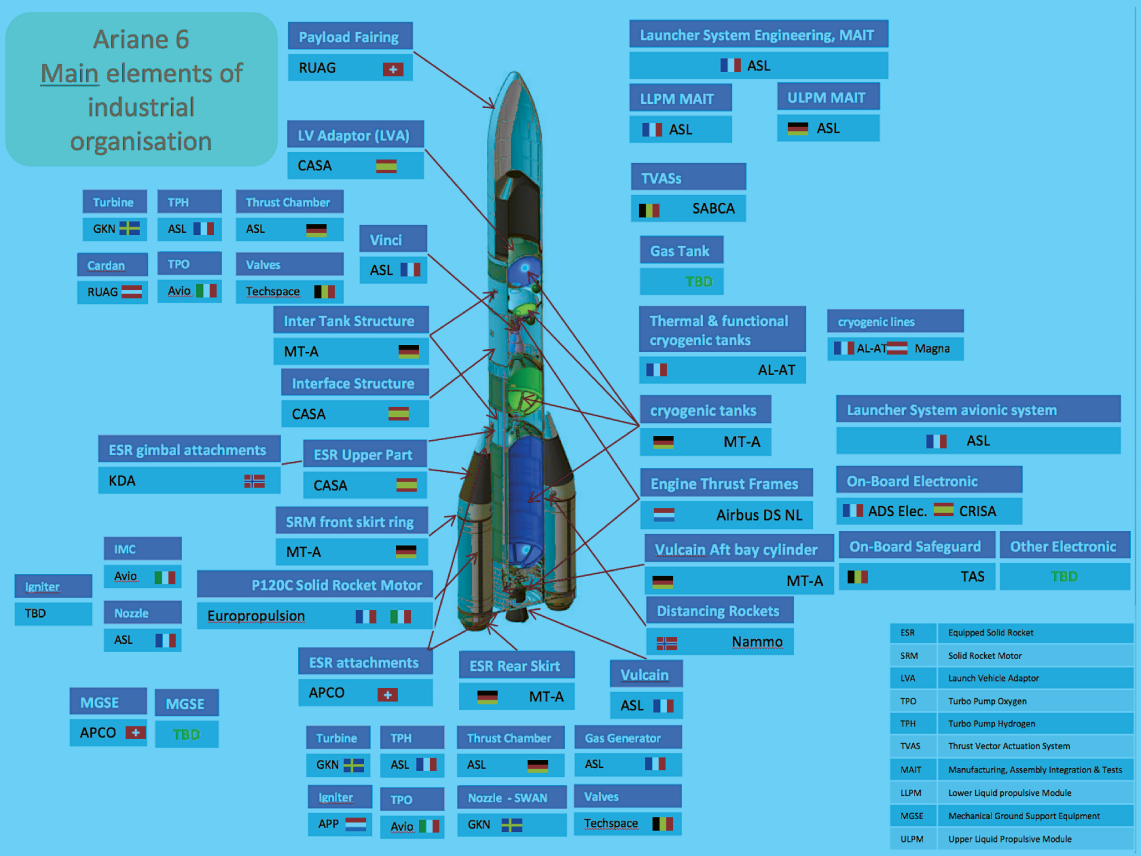

Figure 4.1: Ariane 6 project industrial organisation

4.2.2 Different Configurations

Many configurations of Ariane 6 Launcher have been revealed to public. The configuration of interest for our study concerns the A62 shown in fig. 4.2.
Within this configuration of 60 meters height and mainly 5.4 meters of diameter,

the main purpose of this study is the interstage 2-3 as shown in fig. 4.2.
This Inter-Stage is of conic shape with 5.4m diameter on base, 4.4m diameter on top and 5m height. We admit this configuration for the rest of the document. This device is chosen to be a rubber-metal laminate used as a transmission organ between the two stages, as well as a dynamic softener. The physical problem consists on a dynamic oscillatory phase after a predeformation phase installed within assembly of the parts.

4.2.3 Technical requirements

Some technical requirements are available within the public document A6 NT - 0 - X - 11001 –ESA [137].
The inter-stage is described as a structure in interface with the 2^{nd} stage assembly and with the 3^{rd} stage. The structure shall include a separation ring (to be cut by a pyrotechnic system during the flight).
The main function of this device are:

- To transmit mechanical loads from the 2^{nd} stage SRM to the 3rd stage of the Launch Vehicle, during its integration and transportation to the launch pad, before and during flight.
- To allow the correct separation between the 3^{rd} and the 2^{nd} stages/assemblies through a correct behaviour of the separation system and of the involved parts of the assembly.
- To guarantee global structure stiffness.
- To provide the necessary accessibility in order to allow pre lift-off functional checks and operations.
- To accommodate the necessary equipment and protect them against environment
- To support the Launch Vehicle during its integration and transportation to the launch pad, as well as during its operational life phase.
- The structure shall present interfaces able to allow the integration on the 2^{nd} stage once the supported equipment are integrated on the Inter-Stage.

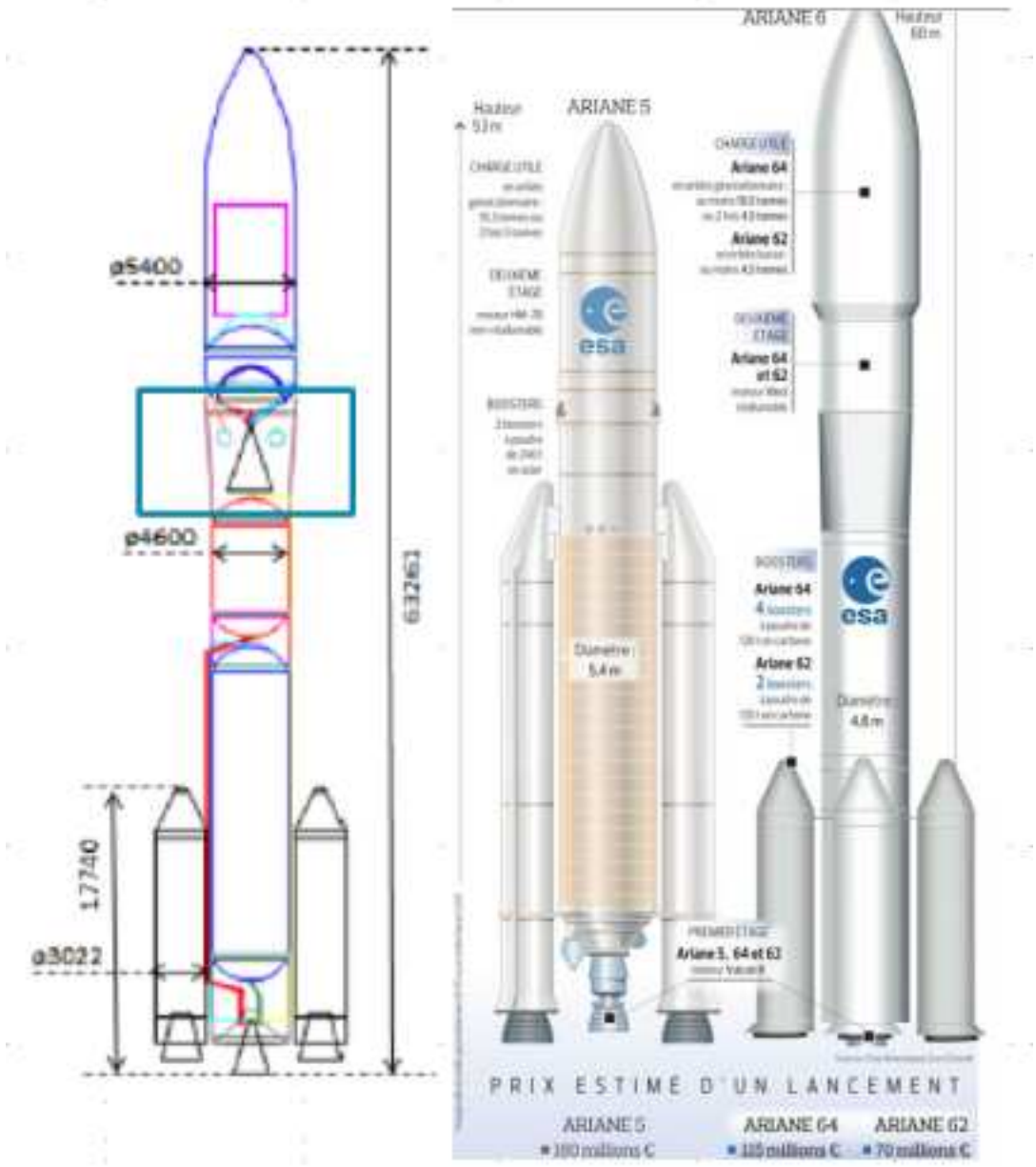

Figure 4.2: Ariane 6 Configurations

Within this work, we intentionally neglect the separation system as well as the thermal protective shield.

The physical requirements are:

- Main dimensions and envelope: rear frame diameter 4.4 m, front frame diameter 5 m to 5.4 m. Skirt height 5 m to 10 m depending on the upper stage architecture

- Mass $<$ 2000 kg (for 5 m height skirt) 2/3 shall be assured.

- Structure primarily sized vs. mechanical fluxes of 1000 N/mm (maximal operational flux) at the lower flange, but additional stiffness requirement should become the dimensioning driver.

Environment

Based on Ariane 5 data [138], and during flight, the spacecraft is subjected to static and dynamic loads. Such excitations may be of aerodynamic origin (e.g. wind, gusts or buffeting at transonic velocity) or due to the propulsion systems (e.g. longitudinal acceleration, thrust buildup or tail-off transients, or structure-propulsion coupling, etc.). Figure 4.3 shows a typical static longitudinal acceleration-time history [139] for the Launch Vehicle during its ascent flight. The highest longitudinal acceleration occurs at the end of the solid rocket boost phase and does not exceed 4.55 g for Ariane 5. The highest static lateral acceleration may be up to 0.25 g.
For Ariane 6, we consider the highest longitudinal acceleration of about 10 g. The Inter-Stage 2/3 have an application time of about 700s. With these considerations, the dynamic load is converted to an equivalent quasi-static load QSL integrating inertial effects and the dynamic magnification of the structure [140][141][142].

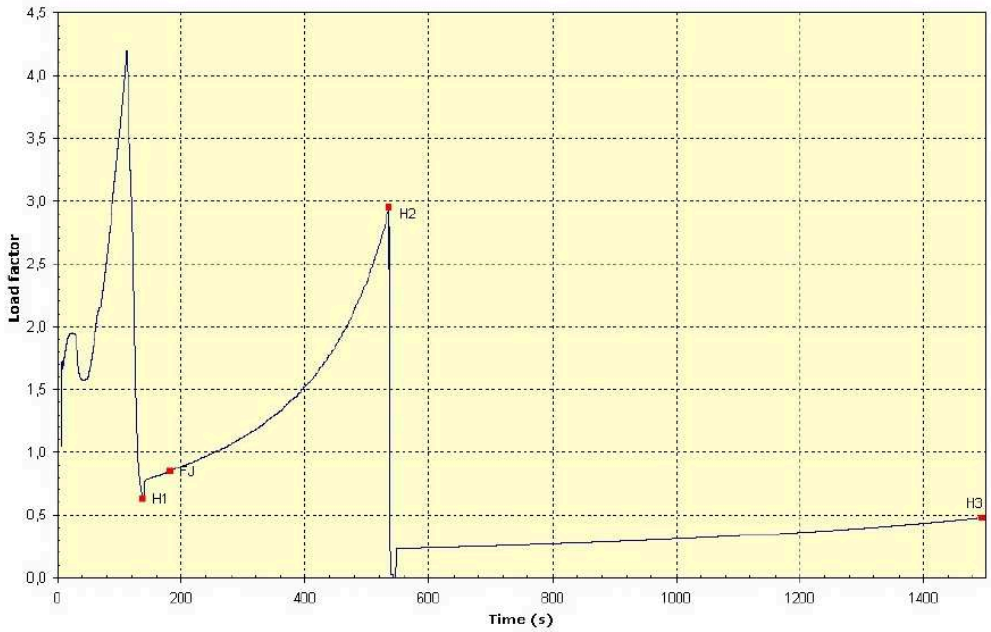

Figure 4.3: Typical longitudinal static acceleration

Frequency Requirements

The operating frequency range of this device is in low-frequencies domain, of $[0-50]$ Hz. To prevent dynamic coupling between the low-frequency launch vehicle and spacecraft modes, the spacecraft should be designed with a structural stiffness which ensures that

- The 1^{st} fundamental lateral frequency $\geq$ 10 Hz
- The fundamental frequency in the longitudinal axis of a spacecraft cantilevered at the interface must be $\geq$ 27 Hz
- No secondary mode should be lower than the first primary mode
- With the integration of the rubber within the structure, and for stiffness requirements, the decrease of the 1^{st} fundamental frequency value should not exceed 20%

with "primary" defines modes associated with large effective masses.

Summary

The previous paragraphs details the technical requirements for the Inter-Stage 2/3 of Ariane 6 launcher. The main specifications to take into account are hence:

- Main dimensions and envelope: 5m height, 5.4m rear frame, 4.4m front frame
- Mass specification: $\leq$ 2000 Kg
- Stiffness specification: decrease of the 1^{st} fundamental frequency value $\leq$ 20%

Within these specifications, in the following section we present the modeling procedure and methodology, aiming to choose the adequate rubber mixture, from those experimentally investigated in chapter 2, which offers the best damping capabilities. We denote that all the dynamic loads specification are converted to QSL (Quasi-Static loads).

4.3 Numerical Model

4.3.1 Finite Elements modeling

Modeling by finite element method is often used in design of industrial parts. This step can determine the critical areas of a complex structure and also predict its dynamic behavior [143][144][145][146].
The finite element method consists in discretizing a solid in elements of simple geometries attached to nodes to which kinematic quantities are associated [147]. At each node are associated variables or degrees of freedom (dof). The fields are then approximated at all points of the elements by an interpolation based on the values associated with the different nodes. The functions chosen must satisfy the conditions of continuity between the various elements. In the same way, the geometry of the real component is discretized into subdomains. This method is based on variational formulations such that the equations of the strong formulation, valid in all points, are verified on average over the set of elements.

4.3.2 Geometry

The proposed geometry for the assembly is shown in fig. 4.4, as a conic assembly between up and down skirts with variable elastomer thickness and fixed metalic thickness of 5mm.

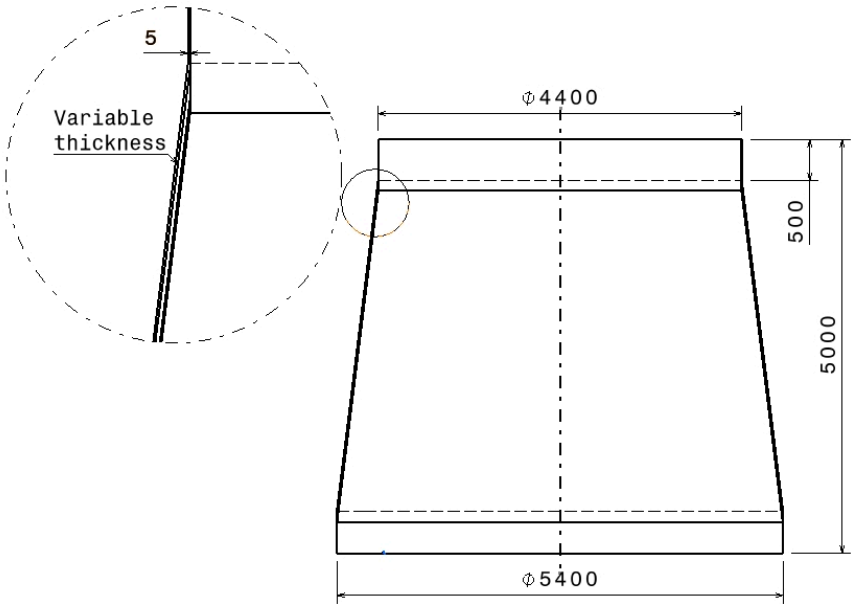

Figure 4.4: Proposed Inter-Stage 2/3 geometry

4.3.3 Methodology

The physical problem consists on a dynamic oscillatory phase after a predeformation phase as illustrated in fig. 4.5.

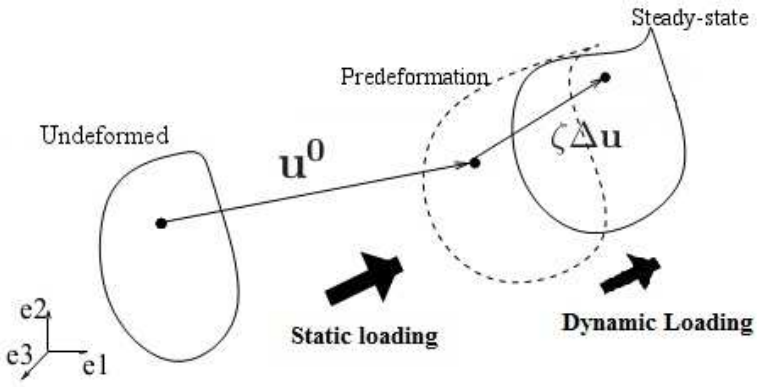

Figure 4.5: Dynamic predeformed problem

The key element of the proposed geometry is the elastomer thickness since the aluminium thickness is fixed to be of 5mm. This parametric study face mainly the following constraints:

- increasing the rubber insert thickness leads to a stiffness loss
- decreasing the rubber insert thickness leads to less damping capabilities

Hence, a compromise between these properties must be found.
Moreover, we supposed that the rubber-aluminum interaction is of perfect bonding. No interaction properties have been set [2].
To satisfy the previously mentionned requirements (in term of mass, stiffness and dynamic damping), we have organized our calculation steps as shown in fig. 4.6:

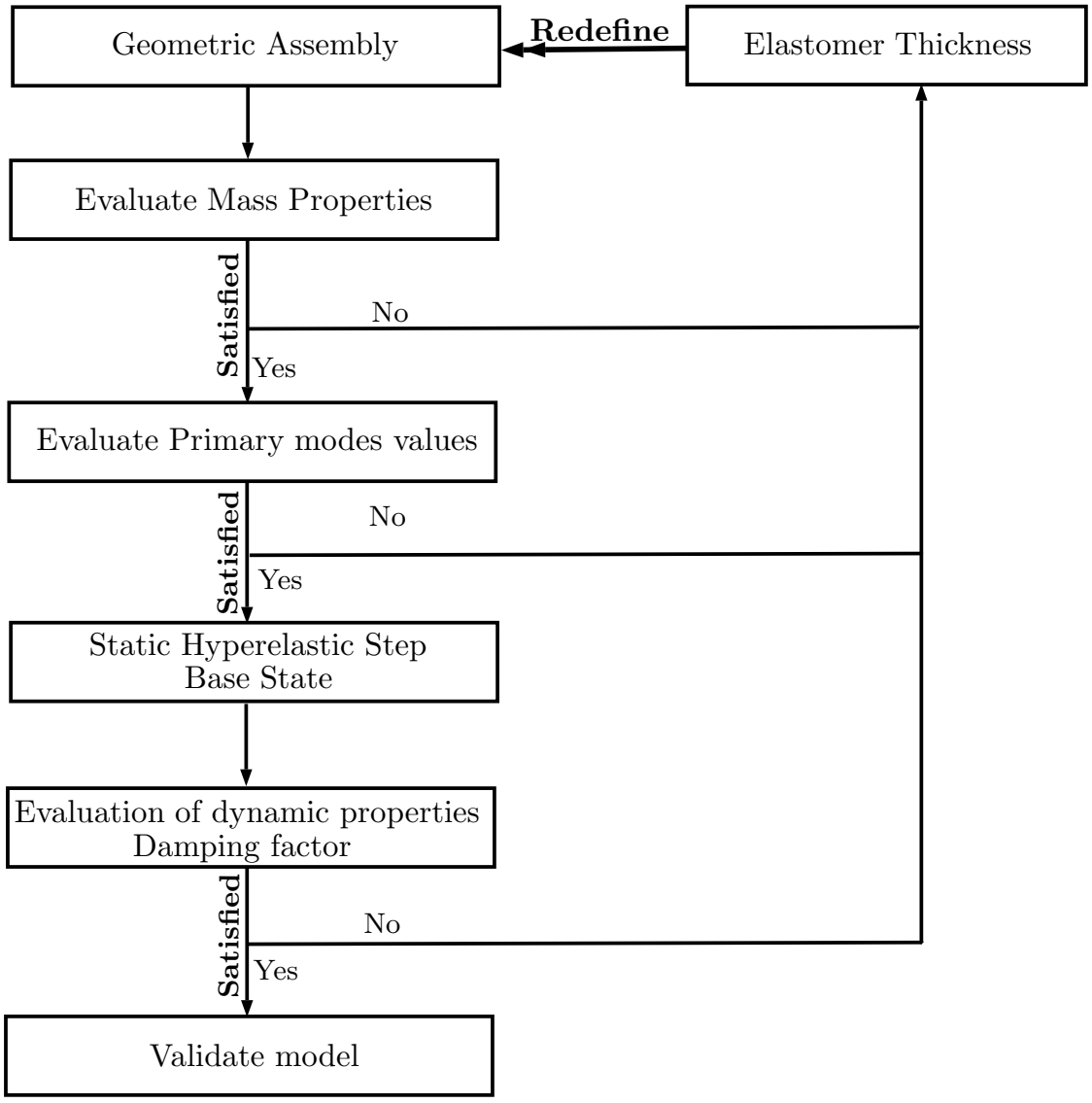

Figure 4.6: Followed methodology

4.3.4 Problem Formulation and procedures

We firstly denote $\Omega \subset R^3$ the domain occupied by our system subject to a static/dynamic load. We consider two types of boundary conditions:

- imposed displacement on S_1, where $\mathbf{u} = \mathbf{0}$
- imposed load on S_2, where $\boldsymbol{\sigma} \,.\, \mathbf{n} = \mathbf{f}$

where $\mathbf{n}$ denotes the external normal to the surface.
All other borders are load-free.
The basis geometry to model the physical problem is proposed on fig. 4.7.

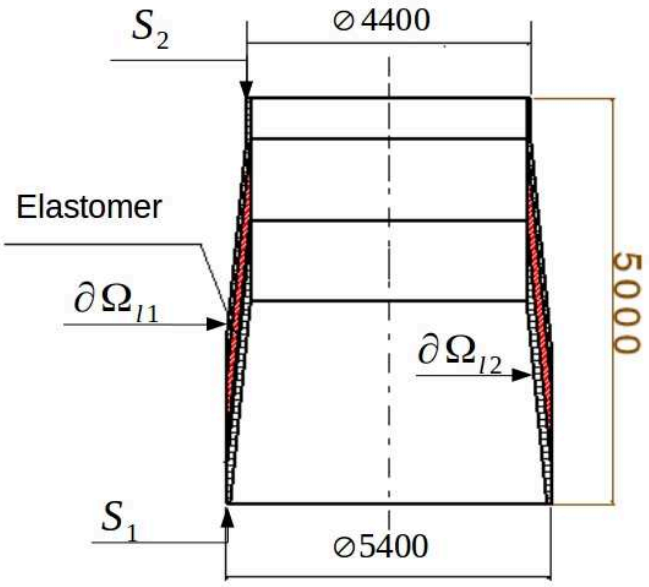

Figure 4.7: Inter-Stage 2/3 geometry

4.3.4.1 Natural frequencies extraction: undeformed state

For this step, we consider only the encastre boundary condition, i.e:

- imposed displacement on S_1, where $\mathbf{u}_d = 0$

All other borders are load-free.
The mathematical eigenvalue problem is a classical field of study, and much work has been devoted to providing eigenvalue extraction methods [148], and authors provide

an excellent compendium on the problem [149]. The eigenvalue problems arising out of finite element models are a particular case: they involve large but usually narrowly banded matrices, and only a small number of eigenpairs are usually required. For many important cases the matrices are symmetric [150].
In the absence of static load, the frequency dynamics of the structure is governed by the system of equations:

$$\begin{cases} div\,\boldsymbol{\sigma} - \rho\,\omega^2\,\mathbf{u} = 0 & on \quad \Omega \\ \mathbf{u} = \mathbf{u}_d = 0 & on \quad S_1 \\ \boldsymbol{\sigma}\,.\,\mathbf{n} = 0 & on \quad S_2 \cup \partial\Omega_{l1} \cup \partial\Omega_{l2} \end{cases} \tag{4.1}$$

We define C_u a sufficiently regular set of functions and $C_u^* = \{\delta u \in C_u \setminus \delta u = 0 \quad on\ S_1\}$ the space of the kinematically admissible test functions.
The weak (variational) formulation is obtained by multiplying eq. (4.1) with $\delta\mathbf{u} \in C_u^*$. After some algebric manupilations, we obtain:

$$\int_\Omega \boldsymbol{\sigma} : grad(\delta\mathbf{u})\, d\Omega - \rho\,\omega^2 \int_\Omega \delta\mathbf{u}\,.\,\mathbf{u}\, d\Omega = 0 \quad \forall \quad \delta\mathbf{u} \in C_u^* \tag{4.2}$$

The eigenvalue problem for natural modes of small vibration of a finite element model is

$$\left(\omega^2[M] + \omega[C] + [K]\right)\{\phi\} = 0 \tag{4.3}$$

where $[M]$ is the mass matrix, which is symmetric and positive definite; $[C]$ is the damping matrix; $[K]$ is the stiffness matrix and ϕ is the eigenvector—the mode of vibration.
Since the structure contains viscoelastic materials, some authors use a decomposition of the stiffness matrix to become complex and frequency-dependent [151] and this eigensystem will have complex eigenvalues and eigenvectors:

$$[K^*(\omega)] = [K_e] + [K_v(\omega)] \tag{4.4}$$

where $[K_e]$ references to the elastic part of the structure and $[K_v(\omega)]$ references to the viscoelastic part.

In ABAQUS, this decomposition is not being used [125], and the stiffness matrix is evaluated at each frequency. Moreover, this system is symmetrized by assuming that $[K]$ is symmetric and by neglecting $[C]$ during eigenvalue extraction. The symmetrized system has real squared eigenvalues, ω^2 , and real eigenvectors only.

In this case ω becomes an imaginary eigenvalue where ω is the circular frequency, and the eigenvalue problem can be written as

$$\left(-\omega^2 [M] + [K]\right) \{\phi\} = 0 \tag{4.5}$$

For numerical extraction, we will make use of the subspace iteration method [152], a classical method that was introduced into finite element applications by [150]

4.3.4.2 General Static Step: static load application

This step is used to generate the base predeformed state for the steady-state dynamic analysis. During this step, we only consider the time-independent elastic properties, i.e the purely hyperelastic response. This choice is made since within the industrial application, this softener device is subjected to static deformation before being put into service and dynamically excited. Hence, we assume that the system take sufficient time to relax and that the response is only of the equilibrium hyperelastic response.
Combining the local equilibrium equations and the boundary conditions, the problem is set as:

$$\begin{cases} div(\boldsymbol{\sigma}) = 0 & & \\ \boldsymbol{\sigma} = -p\,\mathbf{I} + 2\,\mathbf{B}\,\frac{\partial W}{\partial \mathbf{B}} & & \\ \mathbf{u} = \mathbf{0} & on & S_1 \\ \boldsymbol{\sigma}.\mathbf{n} = \mathbf{f}_s & on & S_2 \\ \boldsymbol{\sigma}.\mathbf{n} = 0 & on & \partial\Omega_{l,1} \\ \boldsymbol{\sigma}.\mathbf{n} = 0 & on & \partial\Omega_{l,2} \end{cases} \tag{4.6}$$

where $\mathbf{f}_s$ is the applied static load.

4.3.4.3 Natural frequencies extraction around predeformed state

We have hitherto studied the free vibration of the structure with no predeformation effect. We shall now show that in the case of a structure subjected to a strong field of stress at its equilibrium, the vibratory characteristics are modified [153][154][149]. The knowledge of the vibratory state and natural frequencies around the predeformed state is a primary feature to judge the stability of the structure, and to identify the critical load for buckling problems [155].

For this step, we consider the encastre boundary condition and the predeformation

induced by application of the quasi-static load, i.e:

- imposed displacement on S_1, where $\mathbf{u}_d = 0$
- imposed load on on S_2, where $\mathbf{f} = \mathbf{f}_s$

The stiffness matrix is function of the permanent stresses field applied on the equilibrium structure, and is hence written:

$$[K] = [K_{undeformed}] + [K_\sigma] \tag{4.7}$$

where $[K_\sigma]$ is the contribution of the static load to the stiffness matrix [156]. The problem formulation is hence modified as:

$$\left(-\omega^2 [M] + ([K_{undeformed}] + [K_\sigma])\right) \{\phi\} = 0 \tag{4.8}$$

4.3.4.4 Steady-State Dynamics step: oscillation around predeformed state

Subspace-based method

Steady-state dynamic analysis provides the steady-state amplitude and phase of the response of a system subjected to harmonic excitation at a given frequency [125]. Usually such analysis is done as a frequency sweep, by applying the loading at a series of different frequencies and recording the response. In Abaqus the subspace-based steady-state dynamic analysis procedure is used to conduct the frequency sweep.

In a subspace-based steady-state dynamic analysis the response is based on direct solution of the steady-state dynamic equations projected onto a subspace of modes. The modes of the undamped, symmetric system must first be extracted using the eigenfrequency extraction procedure. The modes will include eigenmodes and, if activated in the eigenfrequency extraction step, residual modes. The procedure is based on the assumption that the forced steady-state vibration can be represented accurately by a number of modes of the undamped system that are in the range of the excitation frequencies of interest. The number of modes extracted must be sufficient to model the dynamic response of the system adequately. The projection of the dynamic equilibrium equations onto a subspace of selected modes leads to a small system of complex equations that is solved for modal amplitudes, which are

then used to compute nodal displacements, stresses, etc...

When defining a subspace-based steady-state dynamic step, we specify the frequency ranges of interest and the number of frequencies at which results are required in each range (including the bounding frequencies of the range). In addition, we can specify the type of frequency spacing (linear or logarithmic) to be used.
The subspace-based steady-state dynamic analysis procedure can be used:

- for nonsymmetric stiffness;
- when any form of damping (except modal damping) is included;
- when viscoelastic material properties must be taken into account.

While the response in this procedure is for linear vibrations, the prior response can be nonlinear. Initial stress effects (stress stiffening) will be included in the steady-state dynamic response if nonlinear geometric effects were included in any general analysis step prior to the eigenfrequency extraction step preceding the subspace-based steady-state dynamic procedure.

To summarize this, a subspace-based steady-state dynamic analysis:

1. is used to calculate the steady-state dynamic linearized response of a system to harmonic excitation;
2. is based on projection of the steady-state dynamic equations on a subspace of selected modes of the undamped system;
3. is a linear perturbation procedure;
4. provides a cost-effective way to include frequency-dependent effects (such as frequency-dependent damping and viscoelastic effects) in the model;
5. allows for nonsymmetric stiffness;
6. requires that an eigenfrequency extraction procedure be performed prior to the steady-state dynamic analysis;
7. is an alternative to direct-solution steady-state dynamic analysis, in which the system's response is calculated in terms of the physical degrees of freedom of the model;

8. is computationally cheaper than direct-solution steady-state dynamics but more expensive than mode-based steady-state dynamics;

9. is less accurate than direct-solution steady-state analysis, in particular if significant material damping or viscoelasticity with a high loss modulus is present;

10. is able to bias the excitation frequencies toward the values that generate a response peak.

Steady-state dynamics problem formulation

This procedure is a perturbation procedure, where the perturbed solution is obtained by linearization about the current base state. Structural and viscous damping are included in the procedure using the structural damping and the viscoelastic parameters coefficients specified under the material definition.
The strong formulation of the problem is written:

$$\begin{cases} div(\boldsymbol{\sigma}) - \rho\,\ddot{\mathbf{u}} = \mathbf{f} \\ \boldsymbol{\sigma} = -p\,\mathbf{I} + 2\,\mathbf{B}\,\dfrac{\partial W}{\partial \mathbf{B}}\,\dfrac{1}{g_\infty} + \\ \qquad dev\left[\displaystyle\int_0^t \frac{\partial g_1(s)}{\partial s}\mathbf{F}_t^{-1}(t-s)\frac{2}{g_\infty}\mathbf{B}(t-s)\frac{\partial W}{\partial \mathbf{B}}\mathbf{F}_t^{-T}(t-s)\,ds\right] \\ \mathbf{u} = 0 \quad on \quad S_1 \\ \boldsymbol{\sigma}.\mathbf{n} = \mathbf{f}_d \quad on \quad S_2 \\ \boldsymbol{\sigma}.\mathbf{n} = 0 \quad on \quad \partial\Omega_{l,1} \\ \boldsymbol{\sigma}.\mathbf{n} = 0 \quad on \quad \partial\Omega_{l,2} \end{cases} \tag{4.9}$$

where $\mathbf{f}_d$ is the applied dynamic load.

The weak formulation based on the dynamic virtual work equation as written in Abaqus is hence:

$$\int_\Omega \rho\,\delta\mathbf{u}\,.\,\ddot{\mathbf{u}}\,d\Omega + \int_\Omega \rho\,\alpha\,\delta\mathbf{u}\,.\,\dot{\mathbf{u}}\,d\Omega + \int_\Omega \delta\boldsymbol{\epsilon} : \boldsymbol{\sigma}\,d\Omega = \int_{\partial\Omega} \delta\mathbf{u}\,.\,\mathbf{f}_d\,d\partial\Omega \tag{4.10}$$

where $\dot{\mathbf{u}}$ and $\ddot{\mathbf{u}}$ are the velocity and the acceleration, ρ is the density of the material. α is a generalized damping factor of the system evaluated in ABAQUS at each frequency step. This factor enclose damping options proposed in the solver, as structural, Rayleigh coefficient or material internal damping.
$\mathbf{f}$ is the applied dynamic load.

The discretized form of this equation is

$$\delta u^N \{[M]\ddot{u} + [C]\dot{u} + [I] - [F]\} = 0 \tag{4.11}$$

where $[I]$ defines the internal load vector enclosing the stiffness matrix, while $[F]$ is the external load vector.
The discretization of such problem and the used procedure are detailed in [143][147][152].

4.3.5 Model parameters

4.3.5.1 Materials Parameters

For the assembly, two materials are used:

- Aluminium alloy for the fittings, used as linear elastic material with a structural damping of 0.002
- Rubber material to be chosen from the previously investigated materials: NR, BIIR and NR/BIIR, as hyper-visco-elastic material.

All materials parameters are furnished in Appendix A.

4.3.5.2 Mesh controls

The geometric model have been meshed with hex-dominated elements. The mesh elements are C3D8 (fig. 4.8a) for the aluminium and C3D8H for the elastomeric insert; i.e Continumm 3D element, 8 nodes linear brick, and Hybrid formulation to deal with the incompressibility constraint. These elements are general purpose linear brick element and fully integrated (2x2x2 integration points). The structure of the element is straightforward.
C3D8R (fig. 4.8b) are also general purpose linear brick elements with reduced integration (1 integration point),which exhibits some shortcomings:

1. The element tends to be not stiff enough
2. Stresses, strains... are most accurate in the integration points. The integration point of the C3D8R element is located in the middle of the element. Thus, small elements are required to capture a stress concentration at the boundary of a structure

3. There are 12 spurious zero energy modes leading to massive hourglassing: this means that the correct solution is superposed by arbitrarily large displacements corresponding to the zero energy modes. Thus, the displacements are completely wrong. Since the zero energy modes do no lead to any stresses, the stress field is still correct. In practice, the C3D8R element is not very useful without hourglass control.

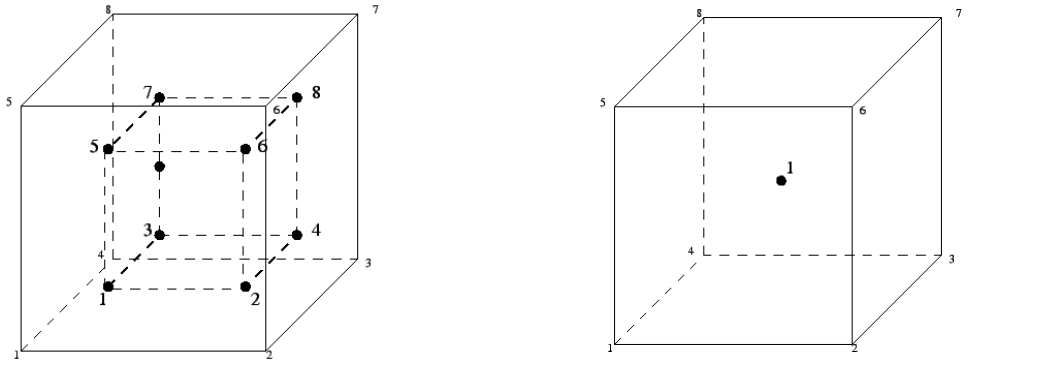

(a) C3D8 2x2x2 integration points

(b) C3D8R 1 integration point

Figure 4.8: Mesh elements: C3D8 vs C3D8R

As well as several elements types, mesh quality is tested by varying the characteristic length l_c of the finite elements, as shows table 4.1. As shows fig. 4.8, increasing the tested mesh characteristic length leads to a higher number of elements. Based on the static response of the structure, we tested these mesh lenghts to decide on the global seed of the structure. Figure 4.9b demonstrates that increasing the number of elements leads to the mesh convergence, which occurs with a characteristic length $l_c = 10\,mm$.
Hence, the retained global seed is of 10 mm, and according to the rubber insert thickness, about 2.10^6 to 3.10^6 elements are generated.

Finally, the structure is meshed with these elements using a sweep technique, and advancing front algorithm. The classical advancing front method, which is one of the techniques of automatic triangulation, was first described by [157] and [158]. Numerous improvements in this technique have been proposed over the years, and a variants of this technique have been proposed to generate quadrilaterals or hexahedra in two and three dimensions [159][160].

mesh	l_c	Number of elements
1	100	37544
2	80	54645
3	50	119592
4	20	666750
5	15	891909
6	10	2011950

Table 4.1: Tested meshes characteristic lengths

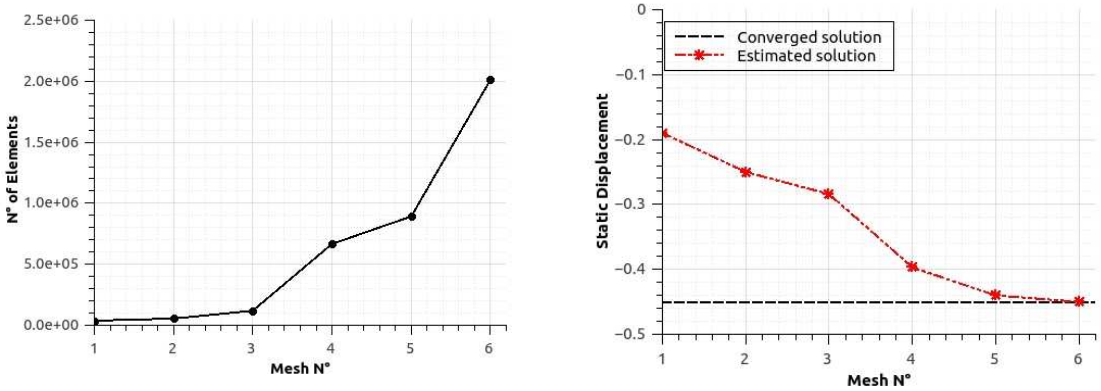

(a) Mesh characteristics

(b) Mesh convergence

Figure 4.9: Mesh Properties

4.3.5.3 Elastomer thickness

In order to satisfy the technical requirements detailed above, the key element or parameter is the elastomer thickness as shown in fig. 4.6. The conducted study is a parametric study where this thickness is variated for the three materials and results are compared to highlight the rubber mixture offering the desired damping factor. Thickness have been chosen to be varied from 2 to 10 mm, and this choice is explained in section 4.4.

All mechanical systems composed of mass, stiffness and damping elements exhibit vibratory response when subject to time-varying disturbances. The prediction and control of these disturbances is fundamental to the design and operation of mechanical equipment.

To evaluate the structure response, we determinate the frequency response of the system or in the Laplace domain the transfer functions $H(\omega)$ [161][162].

4.4 Simulation results

4.4.1 Mass requirement

The mass properties of the considered model are the first criterion which indicates the thickness range to be taken into account.
Table 4.2 resumes the obtaines mass properties with thickness of inserts from 2 to 10 mm. This first requirement leads to a first idea about the thickness range. Comparing damped/undamped models, the rubber inserts offer a primary feature for the modern aerospatial structures: lightness. We observed that including rubber inserts lead to a gain of mass of about 20 to 30%.
From this table, we observe that models with 10 mm rubber thickness slightly exceed the requirement of 2000 Kg. Nevertheless, we will hold these models within the validation of the next requirement.

Insert Thickness	2mm	4mm	6mm	8mm	10mm
Undamped (Full Alu)	1820 Kg	2160 Kg	2500 Kg	2840 Kg	3180 Kg
Damped NR	1610 Kg	1740 Kg	1870 Kg	2000 Kg	2150 Kg
Damped BIIR	1590 Kg	1710 Kg	1830 Kg	1950 Kg	2070 Kg
Damped NR/BIIR	1600 Kg	1720 Kg	1848 Kg	1970 Kg	2090 Kg

Table 4.2: Models mass with/without rubber inserts

4.4.2 Stiffness requirement

As mentionned in section 4.2.3, the natural frequencies are primary features to be evaluated to ensure the system stiffness.
We found that this requirement is satisfied for all models and all inserts thicknesses:

- ✓ All 1^{st} fundamental lateral frequencies are $\geq$ 10 Hz for the retained geometry
- ✓ The fundamental frequency in the longitudinal axis is $\geq$ 27 Hz
- ✓ All first fundamental longitudinal modes are situated in the range $[45-50]$ Hz.

As shows figs. 4.10 and 4.11, the first lateral mode of the undamped or damped system are of same shape. This is due to the symmetry of the problem. Moreover, the introduction of rubber materials as inserts and the conicity of the structure leads to a combination of compression and shear deformations modes.

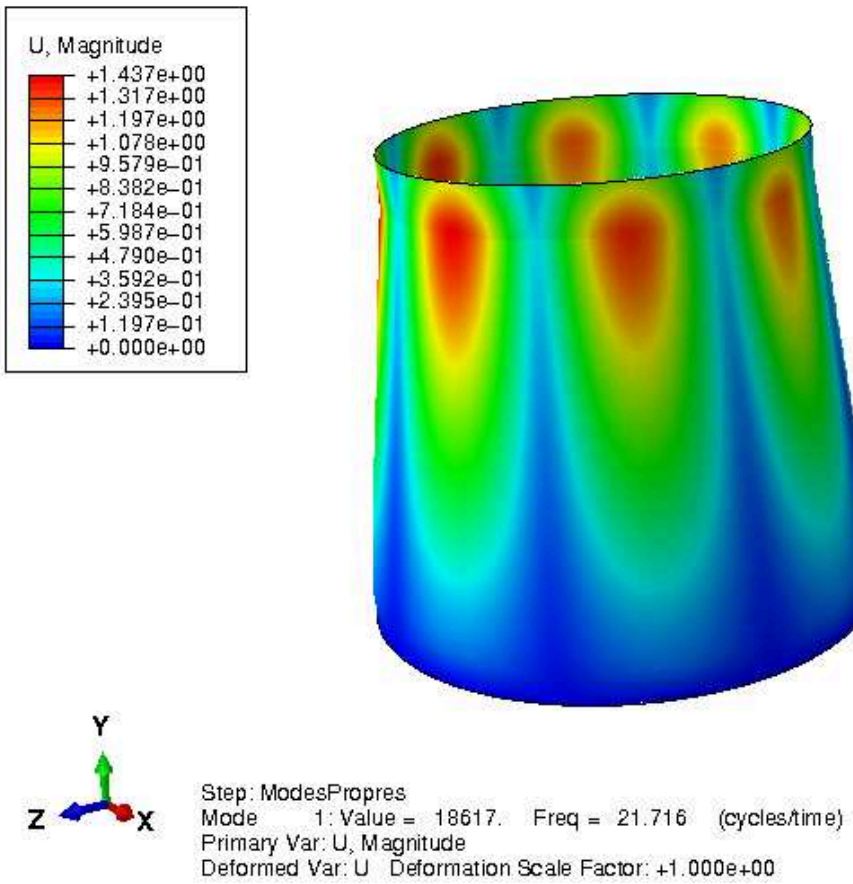

Figure 4.10: 1^{st} fundamental lateral mode shape: Undamped Alu

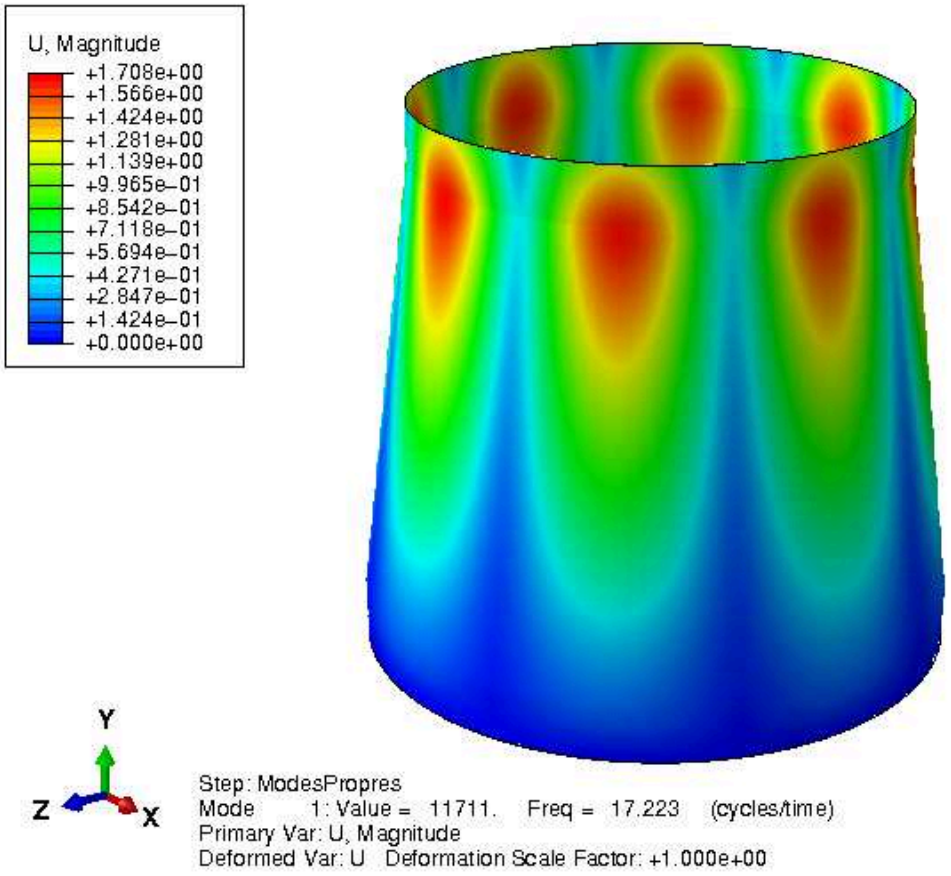

Figure 4.11: 1^{st} fundamental lateral mode shape: Damped BIIR

The second requirement for natural modes concerns the value of the first fundamental lateral mode and the deviation tolerance from the undamped system. Table 4.3 summarizes the obtained values for the first lateral natural frequencies.
The decrease of the 1^{st} fundamental frequency value is set to not exceed 20%. The deviation values are summarized in table 4.4. We can notice that for the NR material, all thicknesses except 10 mm satifies this requirement while for the BIIR and NR/BIIR mixtures, the thickness range is limited to 8 mm.
For the following step, the rubber inserts thicknesses are set to 2, 4 and 6 mm for all mixtures.

4.4.3 Frequency extraction at predeformed state

As mentionned in section 4.3.4.4, the subspace procedure require an eigenfrequency extraction procedure be performed prior to the steady-state dynamic analysis and

Insert Thickness	2mm	4mm	6mm	8mm	10mm
Undamped (Full Alu)	21.47 Hz	21.3 Hz	21.4 Hz	21.71 Hz	21.56 Hz
Damped NR	19.51 Hz	18.66 Hz	18.01 Hz	17.44 Hz	16.94 Hz
Damped BIIR	19.02 Hz	18.31 Hz	17.74 Hz	17.22 Hz	16.75 Hz
Damped NR/BIIR	19.18 Hz	18.37 Hz	17.75 Hz	17.18 Hz	16.68 Hz

Table 4.3: Models fundamental lateral modes with/without rubber inserts at initial state

Insert Thickness	2mm	4mm	6mm	8mm	10mm
Damped NR	9 %	12 %	15 %	19.66 %	**21.4 %**
Damped BIIR	10.6 %	14 %	17.1 %	**20.68 %**	**22.3 %**
Damped NR/BIIR	10.6 %	13.57 %	17.05 %	**20.86 %**	**22.63 %**

Table 4.4: Fundamental frequency requirement criterion

take into account the initial stress effects due to the quasi-static load application. In the case of a structure subjected to a strong field of stress at its equilibrium, the vibratory characteristics are modified and natural frequencies around the predeformed state are the criterion to judge the stability of the structure, and to identify the critical load for buckling problem.
Increasing the static load value leads to a modification in term of values of natural frequencies. This decrease must be not significant to ensure the stability of the assembly [155][154] and it is known that if the first natural frequency value tends to zero, then buckling occurs.

Table 4.5 summarize the values of the fundamental lateral modes with/without rubber inserts at predeformed state. All obtained results around the predeformed state are far away from the zero value, and this ensure no risk of buckling. This observation secure that the applied load is sufficiently distant from the critical value of the static load. In comparison with table 4.3, the values of fundamental lateral

modes are observed to increase for the predeformed state. This is observed due to the inclusion of the nonlinear geometric effects in the previous static general step.

Insert Thickness	2mm	4mm	6mm
Undamped (Full Alu)	28.46 Hz	27.96 Hz	27.42 Hz
Damped NR	26.25 Hz	25.115 Hz	24.12 Hz
Damped BIIR	25.4 Hz	24.5 Hz	23.7 Hz
Damped NR/BIIR	25.74 Hz	24.68 Hz	23.75 Hz

Table 4.5: Models fundamental lateral modes with/without rubber inserts at predeformed state

4.4.4 Damping requirement

4.4.4.1 Evaluation of the damping capacity

Evaluation of the damping capacity is the main objective of this study. Many methods can be used to evaluate the damping capacity of a structure [163][161][153]. There are two general ways by which damping measurements can be made:

- Time-Response Method
- Frequency-response methods

Within this study, we restrict our choice to the second method; i.e Frequency-response methods.

Magnification Factor method

Consider the single degree of freedom oscillatory system with viscous damping , the magnification factor is

$$|H(\omega)| = \frac{\omega_n^2}{\left[(\omega_n^2 - \omega^2)^2 + 4\zeta^2\omega_n^2\omega^2\right]^{\frac{1}{2}}} \tag{4.12}$$

where ω_n is the undamped natural frequency of this single degree of freedom system. The peak value of magnitude occurs in the denominator as:

$$\frac{d}{d\omega}\left[(\omega_n^2 - \omega^2)^2 + 4\zeta^2\omega_n^2\omega^2\right] = 0 \tag{4.13}$$

Resulting solution of resonant frequency is

$$\omega_r = \sqrt{1 - 2\zeta^2}\ \omega_n \tag{4.14}$$

The damping factor ζ is then:

$$\zeta = \frac{1}{\sqrt{2}}\sqrt{1 - \left(\frac{\omega_r}{\omega_n}\right)^2} \tag{4.15}$$

Multi degree freedom system model damping can be estimated by bode plots, as shows fig. 4.12.

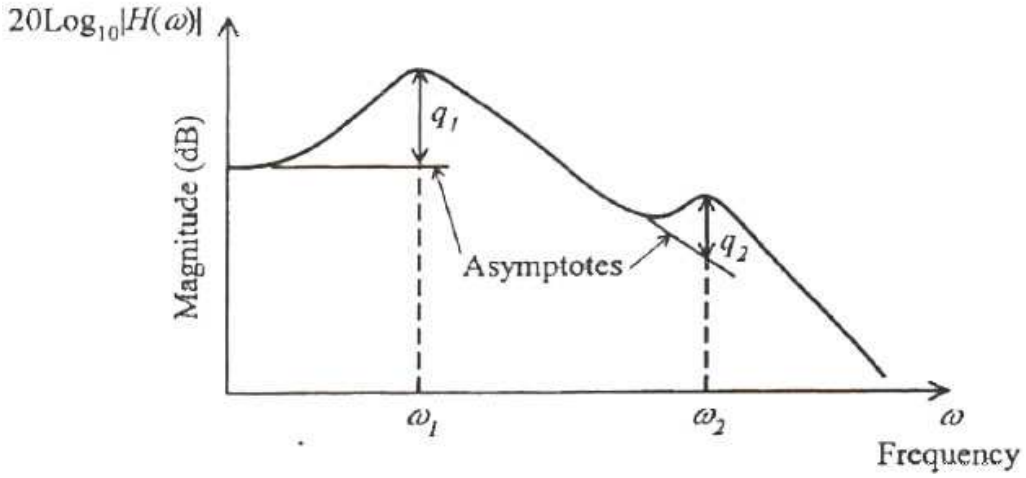

Figure 4.12: Magnification Factor method applied to a multi dof system

Bandwidth method

The bandwidth method of damping measurement is based on frequency response. The peak magnitude is given by equation for low damping. Bandwidth (half-power) is defined as the width of the frequency-response magnitude curve when the magnitude is $1/\sqrt{2}$ times the peak value

$$\frac{\omega_n^2}{[(\omega_n^2 - \omega^2)^2 + 4\zeta^2\omega_n^2\omega^2]^{\frac{1}{2}}} = \frac{1}{2\sqrt{2}\,\zeta} \tag{4.16}$$

The damping ratio can be estimated, for a single degree of freedom as shows fig. 4.13,by using bandwidth in the relation

$$\omega_1^2\,\omega_2^2 = 2(1 - 2\zeta^2)\,\omega_n^2 \tag{4.17}$$

The term $Q = 1/2\zeta$ is often called the quality factor.
A common assumption for small values of ζ is commonly introduced:

$$(\omega_2 - \omega_1)^2 \cong 4\zeta^2\omega_n^2 \tag{4.18}$$

and this assumption leads to

$$\zeta = \frac{1}{2}\frac{\Delta\omega}{\omega_r} \tag{4.19}$$

This assumption is held for higher values of ζ, as mentionned in [161].
For a multi degrees of freedom system, for the i^{th} mode as shows fig. 4.14, the

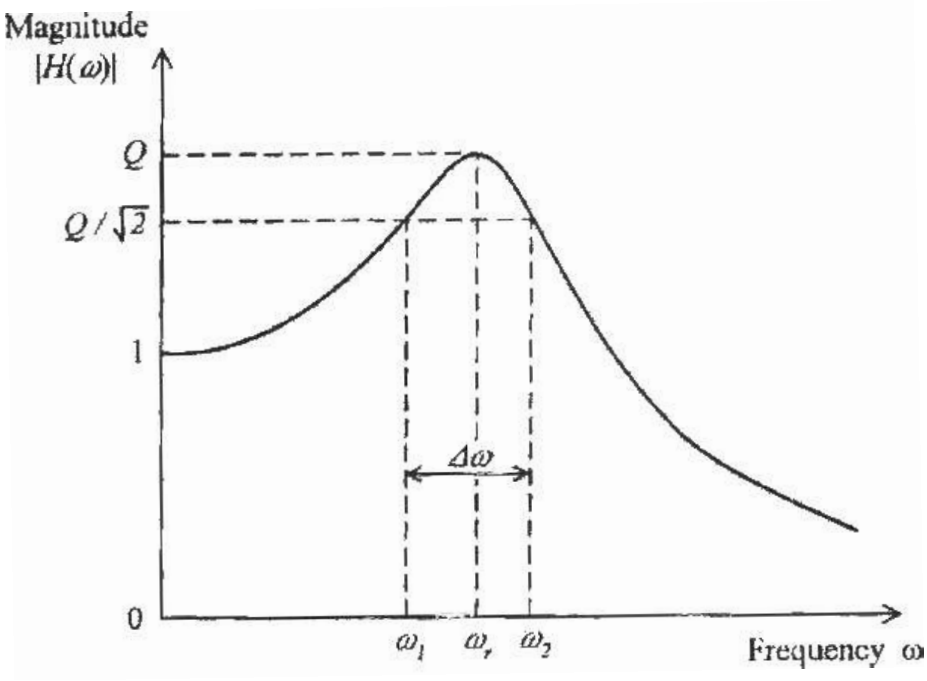

Figure 4.13: Bandwidth method of damping measurement applied to a single dof system

damping ratio is given by:

$$\zeta_i = \frac{1}{2}\frac{\Delta\omega_i}{\omega_i} \tag{4.20}$$

Energy evaluated damping

The damping capacity of a device is energy dissipated in a complete cycle.

$$\Delta\Psi = \oint \frac{d\epsilon}{dt}\, d\epsilon \tag{4.21}$$

The specific damping capacity D is given by ratio of

$$D = \frac{\Delta\Psi}{\Psi_{max}} \tag{4.22}$$

The loss factor is hence defined as:

$$\eta = \frac{\Delta\Psi}{2\pi\Psi_{max}} \tag{4.23}$$

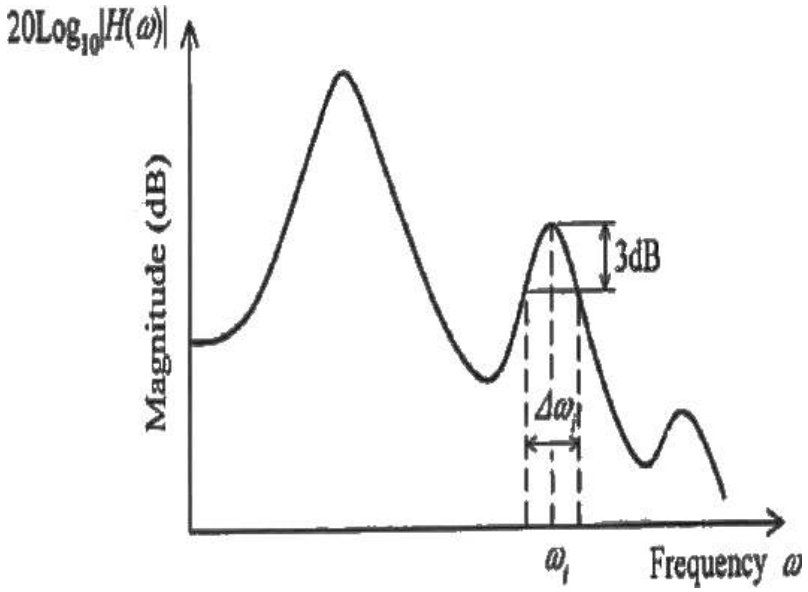

Figure 4.14: Bandwidth method of damping measurement applied to a multi dof system

and this loss factor is approximately given as

$$\eta = 2\zeta \tag{4.24}$$

4.4.4.2 Steady-state dynamic response

The dynamic response of the structure is estimated for the three considered materials as well as for the three retained thicknesses: 2, 4 and 6 mm.
These results were evaluated in term of normalized transfer functions $H(\omega)$ vs normalized frequency (by value of first natural frequency ω_r) as well as acceleration quantities at top of the structure, indicating the inertance of the system $I(\omega)$.

Thickness 2 mm

The normalized transfer function of the damped system is illustrated in fig. 4.15. The analysis of this curve demonstrates that all elastomeric materials exhibit slightly the same damping properties. Moreover, we conclude that damping occurs with a good factor of about $\zeta = 0.3$ which is considered of a high value.
With concern to the magnitude of the acceleration quantities on top of structure, which is plotted in fig. 4.16, the NR mixture offers the lowest values of these quan-

tities, while the BIIR shows the highest. Nevertheless, the acceleration quantities of damped models are of high values of about 150 g while those of the undamped structure are 3 to 5 times higher depending on frequency of interest.

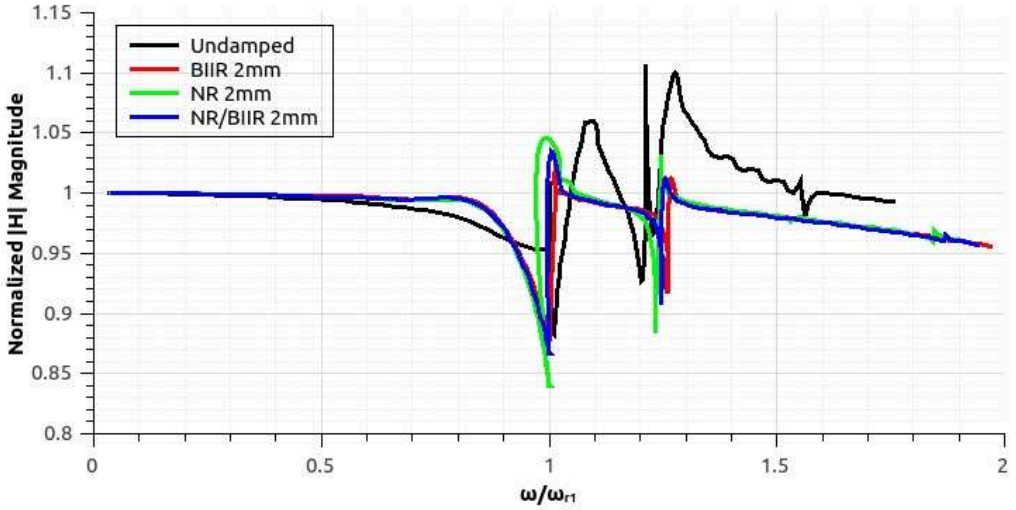

Figure 4.15: Transfert function with 2 mm thickness of rubber insert

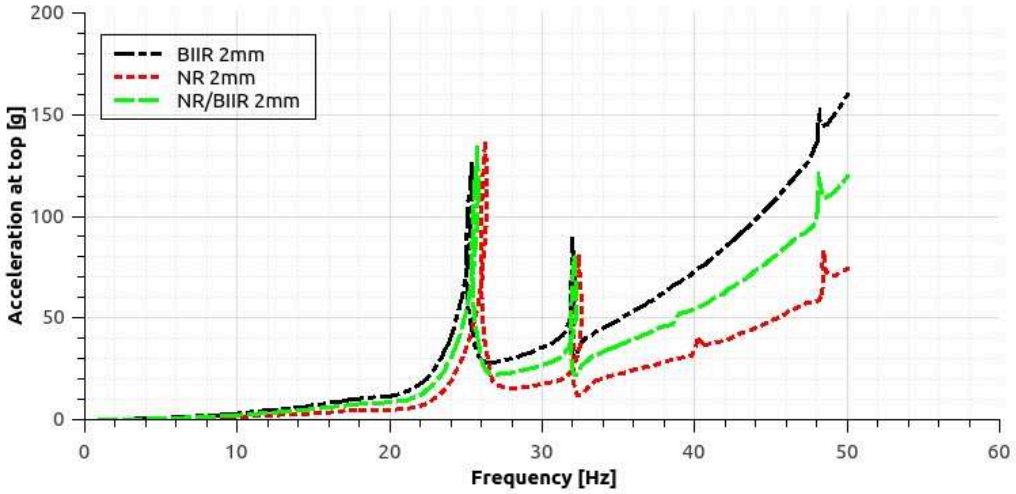

Figure 4.16: Acceleration quantity with 2 mm thickness of rubber insert at node 2465

Thickness 4 mm

The normalized transfer function of the damped system is illustrated in fig. 4.17. Since the frequency is normalized by the 1^{st} resonance frequency value, peaks of the first vibration mode are in the same region. The analysis of this curve demonstrates that the NR mixture offers the best attenuation of the peak of the curve, as well as the best enlargement of the vibration bell. The NR/BIIR mixture offers an almost similar response. The BIIR mixture, although experimentally exhibit the highest loss factor in the sample scale, offer a slightly lower value of damping according to this curve. Meanwhile, the damping factor obtained within this elastomer thickness is of about $\zeta = 0.7$ which is the highest value obtained within this analysis.
With concern to the magnitude of the acceleration quantities at top plotted in fig. 4.18, the three materials exhibit slightly the same response over the frequency range, with peaks at the resonance frequencies. Meanwhile, this thickness offers the lowest acceleration quantities, from 5 to 13 g at first resonance frequency, with comparison to the other models.

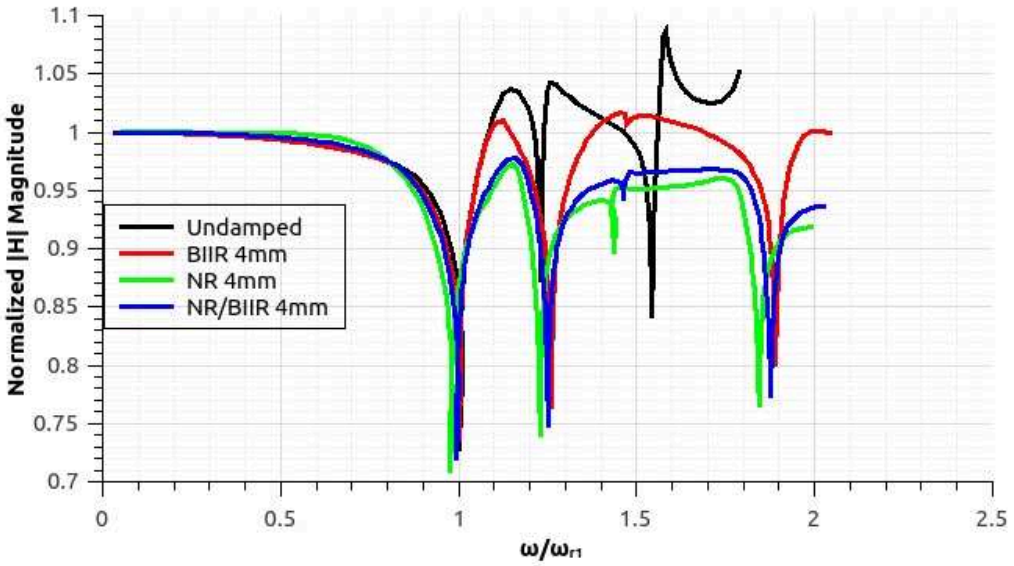

Figure 4.17: Transfert function with 4 mm thickness of rubber insert

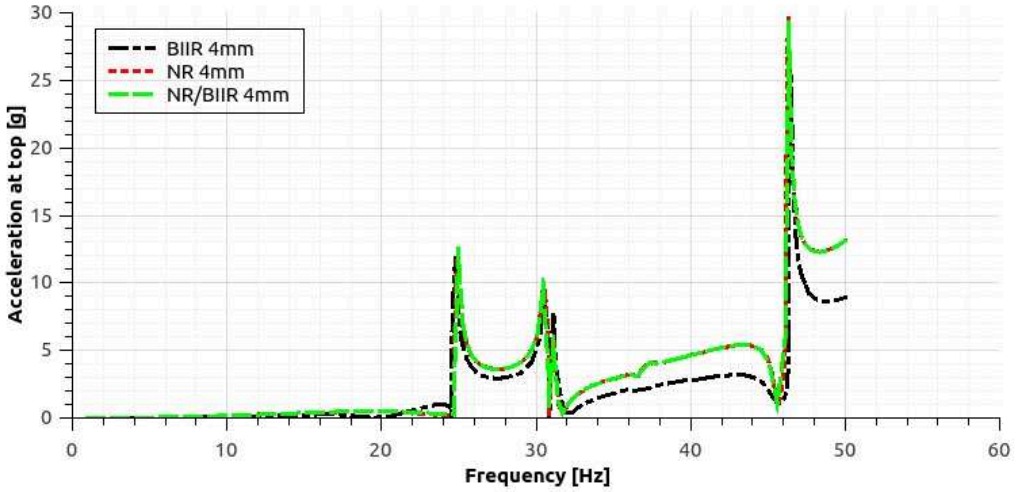

Figure 4.18: Acceleration quantity with 4 mm thickness of rubber insert at node 2465

Thickness 6 mm

The normalized transfer function of the damped system is illustrated in fig. 4.19. The analysis of this curve demonstrates that the NR and NR/BIIR mixtures offer a good attenuation of the peak of the undamped curve, playing the well know role of isolators. The BIIR mixture exhibit a good damping capability with a large mode bell. The obtained factor is of about $\zeta = 0.5$.

With concern to the magnitude of the acceleration quantities plotted in fig. 4.20, both NR and NR/BIIR exhibit highly monotonic accelerations with increasing frequencies while BIIR preserves the same response as for 4 mm thick with an acceleration value of 10 g for the first longitudinal natural frequency.

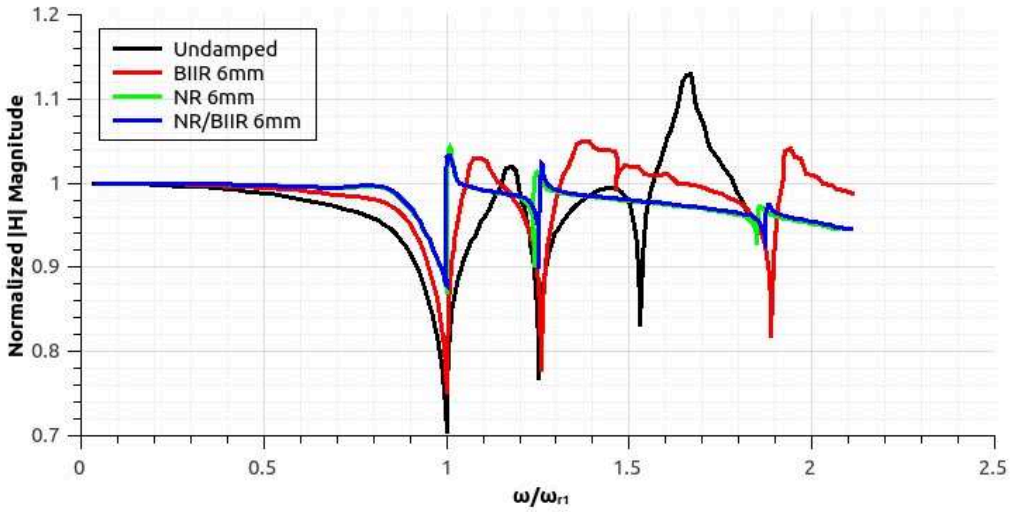

Figure 4.19: Transfert function with 6 mm thickness of rubber insert

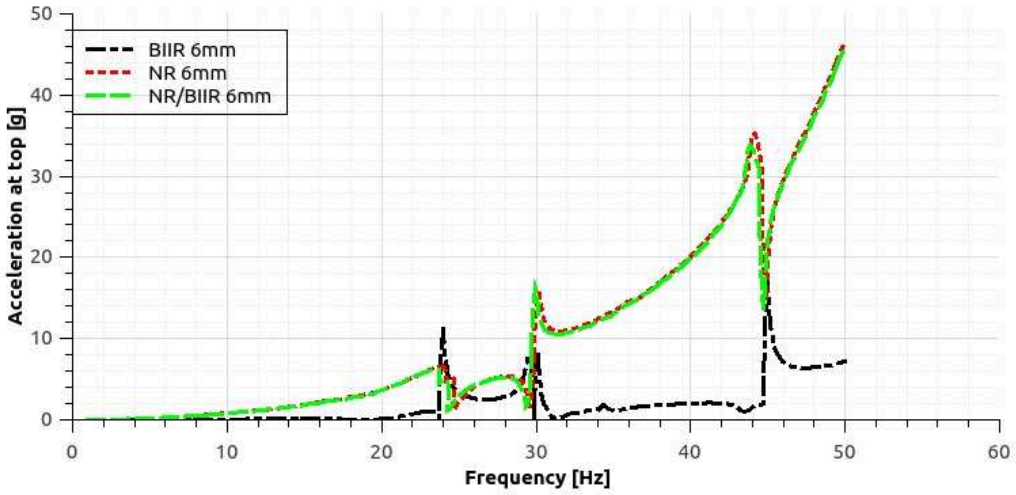

Figure 4.20: Acceleration quantity with 6 mm thickness of rubber insert at node 2465

Choice of thickness

According to the analysis made within the previous paragraph mainly with interest to the acceleration quantities, we can retain the thickness of 4 mm. The acceleration quantities are of acceptable values and respect a fundamental criterion of design: to not exceed 10 g far from resonance frequencies of structure at low frequencies.

This focus made on acceleration quantities is related to the great interest to this parameter within aerospatial structures, being sollicitated dynamically for short times at different conditions and cycles [138].
To conclude on the choice of rubber mixture to be retained for the industrial application, we graphically illustrate the acceleration quantities of the damped/undamped models with a 4 mm thickness, along path from top (application load side) to bottom (encastre side). This illustration is made at a fixed frequency corresponding to the fundamental frequency of each model. Figure 4.21 shows that at fixed frequency, NR and NR/BIIR mixtures offers a low damping in term of acceleration in comparison with undamped structure. These mixtures offers best damping capabilities within higher thicknesses. Meanwhile, the BIIR mixture shows very low acceleration quantities, valued of about half of those with concern to undamped model, from top to bottom of the system. The first part of the curve being with concern to the metallic part, we notice an increase of acceleration quantities till a value of 8 g and a rapid decrease along path, crossing the viscoelastic layer. The BIIR plays the key role in this phenomenon and offers the best damping capabilities.

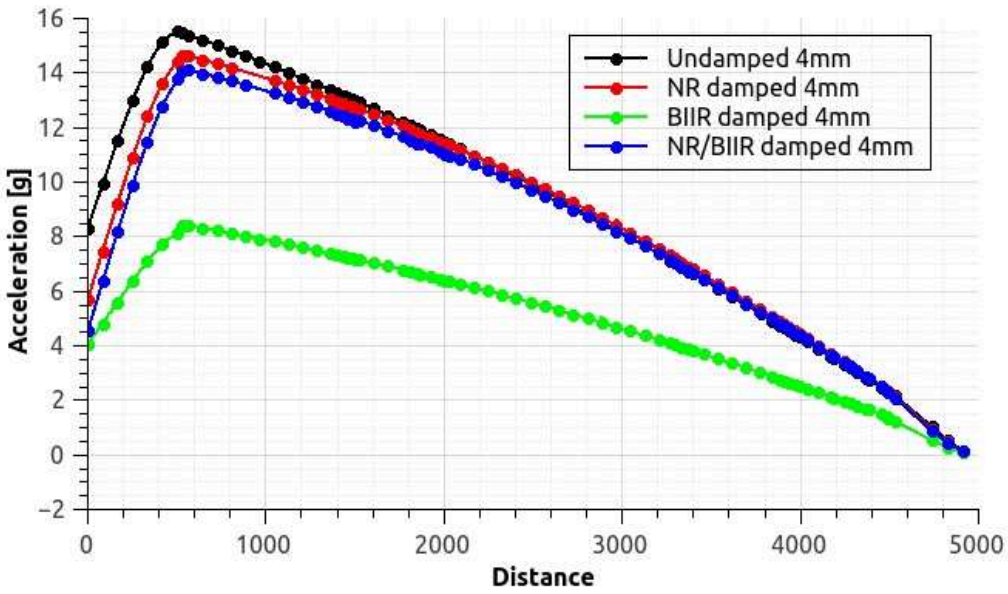

Figure 4.21: Acceleration quantity along path with 4 mm thickness of rubber insert

4.5 Conclusion

This chapter describes the modeling methodology adopted in the finite element code ABAQUS aiming to dimension an industrial component which integrate a constrained hyper-viscoelastic layer. To this end, we conducted a parametric study in order to satisfy some industrial criterions and requirements.

- The methodlogy adopted for this parametric study and the satisfaction of the two first requirements of mass and stiffness, has bounded the elastomer thickness to only three values.
- The elastic structure as well as the viscoelastic inserts are modeled by linear solid elements with no locking or hourglass problems. The mesh parameters are well suited for this analysis.
- Elastomeric inserts offers an acceptable stiffness to the system with a highly light structure
- The damping capabilities from a sample point of view highly differ from those of structure point.
- Not as intuitively predicted, increasing rubber insert thickness does not leed to a more damping capability

A compromise solution have been found leading to the satisfaction of all technical requirements. This solution is not really the expected one. BIIR and NR/BIIR mixtures are seen to offer the highest material loss factor level while the NR offers the lowers angle. Neverthelless, this last mixture have shown the best damping capabilities with the median thickness of 4 mm.

Conclusions and future work

This manuscript addresses two types of difficulty classically encountered for the design of elastomeric devices:

- On the one hand, a behavioral problem (i.e. we are only interested in the material) to select the adapted materials for the application, with the choice of efficient testing procedures in order to characterize the behavior of an elastomeric material
- On the other hand, a difficulty which can be described as numerical, in the sense that it resides more in the organization of calculations than in the behavior of materials
- Finally, a compromise is given in the case of a problem presenting both these difficulties simultaneously, under technical requirements and industrial constraints

In that sense, an experimental database have been built in first place to understand the behavior of the rubber-like materials used for the intended industrial application. The selected elastomeric materials are widely used in industry either for their stiffness like natural rubber or for their isolator behavior as bromobutyl and the mixture of bromobutyl/natural rubber. This database have been constructed through quasi-static and dynamic tests. Quasi-static experiments englobe uniaxial tension and quad-shear tests, at different strain rates. Aiming to determine the long-term hyperlastic response, multistep tests have been adopted with sufficient relaxation times so time-dependent quantities vanish. A common phenomena observed during monotonic tests is the Mullins Effect, known to be a softening effect occuring for first cycles of cyclic tests. This phenomena is irrelevant for our investigation since for the industrial application, it is recommanded to sufficiently load-unload material so the stable loop is reached. Relaxation tests were conducted in order

to identify the viscoelastic parameters of the tested materials. This behavior have been observed to be time dependent none deformation dependent i.e time-strain separable. This experimental observation is of great interest since it is frequently introduced in the formulation of finite strain viscoelasticity constitutive models and affords a large theoretical simplicity. The dynamic experiments were conducted to evaluate the frequecy dependent materials parameters, primary variables to be considered for the dynamic response. We have intentionally avoided the Payne Effect and this is justified by the constant dynamic loading amplitude for the industrial application. Moreover, frequency and temperature dependence were evaluated and discussed within the second chapter and a coupled temperature-frequency dependence is highlighted leading to estimate the dynamic behavior over a wide range of frequency. In addition, a great interest have been devoted to the influence of static predeformation on the dynamic response, focusing on the mounting point of the system. This work leads us to draw conclusions about materials properties and a comparison of the different response is naturally fonded.

In second place, we made interest in modeling the mechanical behavior of rubber-like materials. In order to be as predictive as possible, the behavior laws must best approximate the results observed experimentally. To this end, the third chapter is dedicated to the analysis of the predictive capabilities of the hyper-viscoelastic models. Although in litterature models are issued following different frameworks, the focus herein have been bevoted to single integral-based models under the previously justified separability assumption and four models have been considered within these criterions. Moreover, the chosen models do not require a special identification procedure and all parameters have been identified using Abaqus Evaluate Module. In first place, we made interest to the purely hyperelastic behavior of these materials. The choice of the hyperelastic potential is of great importance to reproduce the experimental data with good fidelity. This leads us to consider three hyperelastic potentials of polynomial construction: NeoHookean, Mooney-Rivlin and a $2^n d$ order polynomial commonly known as generalize Mooney potential. Within this choice, we could draw conclusions in the following part concerning the rate dependent behavior of elastomeric materials. This investigation leads to draw conclusions for time domain and frequency domain, with focus on the capability of the considered models to predict dynamic properties in term of storage modulus and loss factor with respect to the predeformation levels. This analysis made us justify the use of ABAQUS for the numerical simulations conducted in the following part since the Simo model, implemented in this finite element software have given the most

suitable predictive capabilities for our application.

The second difficulty addressed in this manuscript concerns the numerical simulation and the work on a geometrical launcher configuration. This work started by the definition of the technical requirements and the different industrial constraints. The analysis of these dependencies leads us to define a parameteric study following a specific requirements algorithm describing the modeling methodology adopted in the finite element code ABAQUS for the study of structures with viscoelastic materials inserts. This modeling approach introduces a coupling between the predeformation effects and the viscoelastic dissipative effects. This study revealed that the thickness of the elastomeric insert is the primary feature on which the dynamic response of the structure hold on. The idea which come naturally to mind that increasing the thickness increases the damping capability does not stand for our case. Paradoxically, at the material level, we have found that the bromobutyl mixture offers the highest damping capability while at system level, the natural rubber offers the best filtering of the acceleration quantities. The compromised solution found to lead to the satisfaction of all technical requirements is hence to consider a mid-thick natural rubber mixture, offering a good stiffness as well as damping capabilities.

Following these findings, and as a prospect to this difficulty is added the requirement to develop simplified numerical models: in fact, given the number of elastomeric devices in a launcher configuration, one can not afford to finely model each of these elements to simulate the vibratory behavior during launch. Moreover, the finite element model of an industrial structure can reach millions of degrees of freedom. Reduced or simplified structure model have the advantage of being a model with few degrees of freedom that can be integrated, without excessively increasing the number of degrees of freedom, into a finite element model of an industrial structure. An interesting future work imposes that this reduced or simplified structure modeling methodology must be analytical or semi-analytical so that it is sufficiently handy for a parametric analysis. Analytical or semi-analytical methods are related to the Ritz method, with some kinematic hypotheses, which involve projecting the state matrices of the model into a subspace defined from a reduced number of basic vector.

Appendix A

Identified Hyperelastic Parameters

This appendix summerizes hyperelastic parameters identified with the Abaqus 6.14 "Evaluate" module.

Model	Parameters	Equation
Mooney-Rivlin	$C_{10} = 0.224434819$ $C_{01} = -7.175494879E-02$	1.33
Poly N=2	$C_{10} = 0.308734742$ $C_{01} = 7.092035111E-02$ $C_{20} = 5.655083805E-03$ $C_{11} = -1.641920286E-02$ $C_{02} = -3.081416959E-03$	1.32
R-Poly N=6	$C_{10} = 0.204778110$ $C_{20} = -9.635936917E-03$ $C_{30} = 9.191905207E-04$ $C_{40} = -4.348677257E-05$ $C_{50} = 1.107154360E-06$ $C_{60} = -1.106589992E-08$	1.34
NeoHookean	$C_{10} = 0.186320587$	1.36
Yeoh	$C_{10} = 0.187319431$ $C_{20} = -2.239423283E-03$ $C_{30} = 8.132003494E-05$	1.35
Ogden N=3	$\mu_1 = 0.121208583$ $\alpha_1 = 2.49438466$ $\mu_2 = 1.721434390E-03$ $\alpha_2 = 5.44782947$ $\mu_3 = 0.309994144$ $\alpha_3 = -7.130978464E-02$	1.37
Arruda Boyce	$\mu = 0.318671316$ $\mu_0 = 0.328168844$ $\lambda_m = 4.59117146$	1.39
Van der Walls	$\mu = 0.431171188$ $\lambda_m = 7.73158389$ $a = 0.293830246$ $\beta = 0.338485094$	1.40

Table A.1: Identified Parameters of the NR Material

Model	Parameters	Equation
Mooney-Rivlin	$C_{10} = 7.911448022E-02$ $C_{01} = 8.734172589E-03$	1.33
Poly N=2	$C_{10} = 6.801980842E-02$ $C_{01} = 3.874614985E-02$ $C_{20} = 1.554222984E-03$ $C_{11} = -3.086784051E-03$ $C_{02} = -9.069058754E-03$	1.32
R-Poly N=6	$C_{10} = 0.101004182$ $C_{20} = -7.883413601E-03$ $C_{30} = 8.108056492E-04$ $C_{40} = -4.026437366E-05$ $C_{50} = 9.754164863E-07$ $C_{60} = -9.022385489E-09$	1.34
NeoHookean	$C_{10} = 8.239229043E-02$	1.36
Yeoh	$C_{10} = 9.060825199E-02$ $C_{20} = -1.651455576E-03$ $C_{30} = 4.045174346E-05$	1.35
Ogden N=3	$\mu_1 = 0.202742001$ $\alpha_1 = -0.498379489$ $\mu_2 = 2.461782680E-02$ $\alpha_2 = 3.56596575$ $\mu_3 = -1.057016458E-02$ $\alpha_3 = -7.12655115$	1.37
Arruda Boyce	$\mu = 0.163655756$ $\mu_0 = 0.163959700$ $\lambda_m = 18.0002016$	1.39
Van der Walls	$\mu = 0.203731542$ $\lambda_m = 8.27155661$ $a = 0.339657433$ $\beta = 0.314264338$	1.40

Table A.2: Identified Parameters of the BIIR Material

Model	Parameters	Equation
Mooney-Rivlin	$C_{10} = 5.366176089E-02$ $C_{01} = 3.440673261E-03$	1.33
Poly N=2	$C_{10} = 4.092754545E-02$ $C_{01} = 3.616489797E-02$ $C_{20} = 1.494335510E-03$ $C_{11} = -4.778964862E-03$ $C_{02} = -1.401512780E-03$	1.32
R-Poly N=6	$C_{10} = 7.165792981E-02$ $C_{20} = -5.730427873E-03$ $C_{30} = 5.737951042E-04$ $C_{40} = -2.869417701E-05$ $C_{50} = 7.067761409E-07$ $C_{60} = -6.647049591E-09$	1.34
NeoHookean	$C_{10} = 5.330246889E-02$	1.36
Yeoh	$C_{10} = 6.071222868E-02$ $C_{20} = -1.136220127E-03$ $C_{30} = 2.804902539E-05$	1.35
Ogden N=3	$\mu_1 = 1.963491606E-02$ $\alpha_1 = 3.12942804$ $\mu_2 = 7.709297579E-07$ $\alpha_2 = 8.81373439$ $\mu_3 = 0.132665521$ $\alpha_3 = -0.548874927$	1.37
Arruda Boyce	$\mu = 9.887982287E-02$ $\mu_0 = 0.100302014$ $\lambda_m = 6.53152085$	1.39
Van der Walls	$\mu = 0.155913420$ $\lambda_m = 7.29873228$ $a = 0.370971033$ $\beta = 0.500779936$	1.40

Table A.3: Identified Parameters of the NR/BIIR Material

Appendix B

Identified Prony series

g_i	τ_i [s]
7.54942E-03	1.74110E-02
3.51810E-02	598.66
4.72695E-02	6835.5

Table B.1: Prony Series Parameters: NR

g_i	τ_i [s]
8.57115E-03	2.82821E-02
7.44958E-02	233.23
6.93801E-02	1376.9
9.77678E-02	7517.2

Table B.2: Prony Series Parameters: BIIR

g_i	τ_i [s]
2.41146E-02	1.63421E-02
0.13609	490.45
0.13980	6124.5

Table B.3: Prony Series Parameters: NR/BIIR

Bibliography

[1] L. H. Sperling, "Sound and vibration damping with polymers," ACS Publications, 1990.

[2] D. Boast and V. A. Coveney, *Finite element analysis of elastomers*. Professional Engineering Publishing, 1999.

[3] L. R. G. Treloar, *The physics of rubber elasticity*. Oxford university press, 1975.

[4] N. W. Tschoegl, *The phenomenological theory of linear viscoelastic behavior: an introduction*. Springer Science & Business Media, 2012.

[5] P. Lindley, *Le calcul des elements en caoutchouc naturel dans l'art de l'ingenieur*. Malaysian Rubber Producers' Research Assoc., 1983.

[6] J. D. Ferry, *Viscoelastic properties of polymers*. John Wiley & Sons, 1980.

[7] A. Zdunek, "Determination of material response functions for prestrained rubbers," *Rheologica acta*, vol. 31, no. 6, pp. 575–591, 1992.

[8] V. A. Coveney, *Elastomers and Components: Service Life Prediction-Progress and Challenges*. Woodhead Publishing, 2006.

[9] P. Combette and I. Ernoult, *Physique des polymères,Tome 1 - Structure, fabrication, emploi*. Physique des polymères, Presse internationales Polytechnique, 2005.

[10] K. N. Morman Jr and T. Y. Pan, "Application of finite-element analysis in the design of automotive elastomeric components," *Rubber chemistry and technology*, vol. 61, no. 3, pp. 503–533, 1988.

[11] C. LEWITZKE and L. PING, "Application of elastomeric components for noise and vibration isolation in the automotive industry," *SAE transactions*, vol. 110, no. 6, pp. 1649–1669, 2001.

[12] R. Rivlin, "Large elastic deformations of isotropic materials. iv. further developments of the general theory," *Philosophical Transactions of the Royal Society of London A: Mathematical, Physical and Engineering Sciences*, vol. 241, no. 835, pp. 379–397, 1948.

[13] R. Ogden, "Large deformation isotropic elasticity-on the correlation of theory and experiment for incompressible rubberlike solids," in *Proceedings of the Royal Society of London A: Mathematical, Physical and Engineering Sciences*, vol. 326, pp. 565–584, The Royal Society, 1972.

[14] A. D. Drozdov, *Finite elasticity and viscoelasticity: a course in the nonlinear mechanics of solids*. World Scientific, 1996.

[15] W. Reichert, M. Hopfenmüller, and D. Göritz, "Volume change and gas transport at uniaxial deformation of filled natural rubber," *Journal of materials science*, vol. 22, no. 10, pp. 3470–3476, 1987.

[16] W. N. Findley and F. A. Davis, *Creep and relaxation of nonlinear viscoelastic materials*. Courier Corporation, 2013.

[17] F. J. Lockett, "Creep and stress-relaxation experiments for non-linear materials," *International Journal of Engineering Science*, vol. 3, no. 1, pp. 59–75, 1965.

[18] J.-H. Lee and K.-J. Kim, "Characterization of complex modulus of viscoelastic materials subject to static compression," *Mechanics of Time-Dependent Materials*, vol. 5, no. 3, pp. 255–271, 2001.

[19] C. A. Harper, "Handbook of plastics, elastomers and composites, 1996," *McGraw-Hill Inc*, vol. 2, pp. 2–41, 1996.

[20] *TA Instruments Training Courses*. Woodlands, Texas, 2010.

[21] F. Bueche, "Mullins effect and rubber–filler interaction," *Journal of applied polymer Science*, vol. 5, no. 15, pp. 271–281, 1961.

[22] L. Mullins, "Softening of rubber by deformation," *Rubber chemistry and technology*, vol. 42, no. 1, pp. 339–362, 1969.

[23] A. Lion, "A constitutive model for carbon black filled rubber: experimental investigations and mathematical representation," *Continuum Mechanics and Thermodynamics*, vol. 8, no. 3, pp. 153–169, 1996.

[24] G. Marckmann, *Contribution à l'étude des élastomères et des membranes soufflées*. PhD thesis, Ecole Centrale de Nantes; Université de Nantes, 2004.

[25] A. R. Payne and R. E. Whittaker, "Dynamic properties of materials," *Rheologica Acta*, vol. 9, no. 1, pp. 97–102, 1970.

[26] A. Lion and C. Kardelky, "The Payne effect in finite viscoelasticity: constitutive modelling based on fractional derivatives and intrinsic time scales," *International Journal of Plasticity*, vol. 20, no. 7, pp. 1313–1345, 2004.

[27] P. Saad, *Mod{é}lisation et identification du comportement non lin{é}aire des cales en caoutchouc*. PhD thesis, 2003.

[28] F. J. Lockett, *Nonlinear viscoelastic solids*. Academic Press, 1972.

[29] P. Haupt, *Continuum mechanics and theory of materials*. Springer Science & Business Media, 2013.

[30] G. A. Holzapfel, "Nonlinear solid mechanics: a continuum approach for engineering science," *Meccanica*, vol. 37, no. 4, pp. 489–490, 2002.

[31] J. Bonet and R. D. Wood, *Nonlinear continuum mechanics for finite element analysis*. Cambridge university press, 1997.

[32] R. W. Ogden, *Non-linear elastic deformations*. Courier Corporation, 1997.

[33] Y. B. Fu and R. W. Ogden, *Nonlinear elasticity: theory and applications*, vol. 283. Cambridge University Press, 2001.

[34] M. F. Beatty, "Topics in finite elasticity: hyperelasticity of rubber, elastomers, and biological tissues—with examples," *Applied Mechanics Reviews*, vol. 40, no. 12, pp. 1699–1734, 1987.

[35] J. Salençon, *Elasticité, Milieux curvilignes*. 1988.

[36] R. S. Rivlin and D. Saunders, "Large elastic deformations of isotropic materials. vii. experiments on the deformation of rubber," *Philosophical Transactions of the Royal Society of London A: Mathematical, Physical and Engineering Sciences*, vol. 243, no. 865, pp. 251–288, 1951.

[37] M. Mooney, "A theory of large elastic deformation," *Journal of applied physics*, vol. 11, no. 9, pp. 582–592, 1940.

[38] G. Marckmann and E. Verron, "Comparison of hyperelastic models for rubber-like materials," *Rubber chemistry and technology*, vol. 79, no. 5, pp. 835–858, 2006.

[39] S. Kawabata, Y. Yamashita, H. Ooyama, and S. Yoshida, "Mechanism of carbon-black reinforcement of rubber vulcanizate," *Rubber Chemistry and Technology*, vol. 68, no. 2, pp. 311–329, 1995.

[40] O. Yeoh, "Some forms of the strain energy function for rubber," *Rubber Chemistry and technology*, vol. 66, no. 5, pp. 754–771, 1993.

[41] L. Treloar, "The elasticity of a network of long-chain molecules—II," *Transactions of the Faraday Society*, vol. 39, pp. 241–246, 1943.

[42] E. M. Arruda and M. C. Boyce, "A three-dimensional constitutive model for the large stretch behavior of rubber elastic materials," *Journal of the Mechanics and Physics of Solids*, vol. 41, no. 2, pp. 389–412, 1993.

[43] M. C. Wang and E. Guth, "Statistical theory of networks of non-gaussian flexible chains," *The Journal of Chemical Physics*, vol. 20, no. 7, pp. 1144–1157, 1952.

[44] H.-G. Kilian, H. Enderle, and K. Unseld, "The use of the van der waals model to elucidate universal aspects of structure-property relationships in simply extended dry and swollen rubbers," *Colloid and Polymer Science*, vol. 264, no. 10, pp. 866–876, 1986.

[45] H. Enderle and H.-G. Kilian, "General deformation modes of a van der waals network," in *Permanent and Transient Networks*, pp. 55–61, Springer, 1987.

[46] S. Lejeunes, *Modélisation de structures lamifiées élastomère-métal à l'aide d'une méthode de réduction de modèles.* PhD thesis, Université de la Méditerranée-Aix-Marseille II, 2006.

[47] E. Wiechert, "Gesetze der elastischen nachwirkung für constante temperatur," *Annalen der Physik*, vol. 286, no. 11, pp. 546–570, 1893.

[48] S. Hong, R. Fedors, F. Schwarzl, J. Moacanin, and R. Landel, "Analysis of the tensile stress-strain behavior of elastomers at constant strain rates. i. criteria for separability of the time and strain effects," *Polymer Engineering & Science*, vol. 21, no. 11, pp. 688–695, 1981.

[49] J. L. Sullivan, "Viscoelastic properties of a gum vulcanizate at large static deformations," *Journal of Applied Polymer Science*, vol. 28, no. 6, pp. 1993–2003, 1983.

[50] A. Green and R. Rivlin, "The mechanics of non-linear materials with memory," *Archive for Rational Mechanics and Analysis*, vol. 1, no. 1, pp. 1–21, 1957.

[51] A. E. Green and R. S. Rivlin, "The mechanics of non-linear materials with memory," *Archive for rational mechanics and analysis*, vol. 4, no. 1, pp. 387–404, 1959.

[52] K. Onaran and W. N. Findley, "Combined stress-creep experiments on a non-linear viscoelastic material to determine the kernel functions for a multiple integral representation of creep," *Transactions of The Society of Rheology (1957-1977)*, vol. 9, no. 2, pp. 299–327, 1965.

[53] W. N. Findley and J. Lai, "A modified superposition principle applied to creep of nonlinear viscoelastic material under abrupt changes in state of combined stress," *Transactions of The Society of Rheology (1957-1977)*, vol. 11, no. 3, pp. 361–380, 1967.

[54] A. Pipkin and T. Rogers, "A non-linear integral representation for viscoelastic behaviour," *Journal of the Mechanics and Physics of Solids*, vol. 16, no. 1, pp. 59–72, 1968.

[55] H. J. Lockett and R. O. Stafford, "On special constitutive relations in nonlinear viscoelasticity," *International Journal of Engineering Science*, vol. 7, no. 9, pp. 917–930, 1969.

[56] A. Ravasoo, "Modified constitutive equation for quasi-linear theory of viscoelasticity," *Journal of Engineering Mathematics*, vol. 78, no. 1, pp. 111–118, 2013.

[57] J. Sullivan and K. Mazich, "Nonseparable behavior in rubber viscoelasticity," *Rubber chemistry and technology*, vol. 62, no. 1, pp. 68–81, 1989.

[58] B. D. Coleman and W. Noll, "Foundations of linear viscoelasticity," *Reviews of modern physics*, vol. 33, no. 2, p. 239, 1961.

[59] R. C. Batra and J. H. Yu, "Linear constitutive relations in isotropic finite viscoelasticity," *Journal of Elasticity*, vol. 55, no. 1, pp. 73–77, 1999.

[60] P. Haupt and a. Lion, "On finite linear viscoelasticity of incompressible isotropic materials," *Acta Mechanica*, vol. 159, no. 1-4, pp. 87–124, 2002.

[61] A. Wineman, "Nonlinear viscoelastic solids: a review," *Mathematics and Mechanics of Solids*, vol. 14, no. 3, pp. 300–366, 2009.

[62] J. Ciambella, A. Paolone, and S. Vidoli, "A comparison of nonlinear integral-based viscoelastic models through compression tests on filled rubber," *Mechanics of Materials*, vol. 42, no. 10, pp. 932–944, 2010.

[63] B. Bernstein, E. Kearsley, and L. Zapas, "A study of stress relaxation with finite strain," *Transactions of The Society of Rheology (1957-1977)*, vol. 7, no. 1, pp. 391–410, 1963.

[64] R. M. Christensen, "A nonlinear theory of viscoelasticity for application to elastomers," *Journal of Applied Mechanics*, vol. 47, no. 4, pp. 762–768, 1980.

[65] R. Fosdick and J.-H. Yu, "Thermodynamics, stability and non-linear oscillations of viscoelastic solids—II. History type solids," *International journal of non-linear mechanics*, vol. 33, no. 1, pp. 165–188, 1998.

[66] R. De Pascalis, I. D. Abrahams, and W. J. Parnell, "On nonlinear viscoelastic deformations: a reappraisal of fung's quasi-linear viscoelastic model," in *Proc. R. Soc. A*, vol. 470, p. 20140058, The Royal Society, 2014.

[67] R. M. Christensen and L. Freund, "Theory of viscoelasticity," *Journal of Applied Mechanics*, vol. 38, p. 720, 1971.

[68] Y.-C. Fung *et al.*, "Stress-strain-history relations of soft tissues in simple elongation," *Biomechanics: Its foundations and objectives*, vol. 7, pp. 181–208, 1972.

[69] J. O. Hallquist, "Ls-dyna3d theoretical manual," *Livermore software technology corporation*, 1993.

[70] L. M. Yang, V. P. W. Shim, and C. T. Lim, "A visco-hyperelastic approach to modelling the constitutive behaviour of rubber," *International Journal of Impact Engineering*, vol. 24, no. 6–7, pp. 545–560, 2000.

[71] M. S. H. Fatt and X. Ouyang, "Integral-based constitutive equation for rubber at high strain rates," *International Journal of Solids and structures*, vol. 44, no. 20, pp. 6491–6506, 2007.

[72] A. Muliana, K. Rajagopal, and A. Wineman, "A new class of quasi-linear models for describing the nonlinear viscoelastic response of materials," *Acta Mechanica*, vol. 224, no. 9, pp. 2169–2183, 2013.

[73] A. Muliana, K. Rajagopal, and D. Tscharnuter, "A nonlinear integral model for describing responses of viscoelastic solids," *International Journal of Solids and Structures*, vol. 58, pp. 146–156, 2015.

[74] J. Sullivan, "A nonlinear viscoelastic model for representing nonfactorizable time-dependent behavior in cured rubber," *Journal of Rheology (1978-present)*, vol. 31, no. 3, pp. 271–295, 1987.

[75] P. Höfer and A. Lion, "Modelling of frequency- and amplitude-dependent material properties of filler-reinforced rubber," *Journal of the Mechanics and Physics of Solids*, vol. 57, no. 3, pp. 500–520, 2009.

[76] H. Khajehsaeid, J. Arghavani, R. Naghdabadi, and S. Sohrabpour, "A visco-hyperelastic constitutive model for rubber-like materials: A rate-dependent relaxation time scheme," *International Journal of Engineering Science*, vol. 79, pp. 44–58, 2014.

[77] E. Pucci and G. Saccomandi, "Some remarks about a simple history dependent nonlinear viscoelastic model," *Mechanics Research Communications*, vol. 68, pp. 70–76, 2015.

[78] F. Sidoroff, "Variables internes en viscoélasticité 1. variables internes scalaires et tensorielles," *J. de Mécanique*, vol. 14, no. 3, pp. 545–566, 1975.

[79] F. Sidoroff, "Variables internes en viscoélasticité 2. milieux avec configuration intermédiaire," *J. de Mécanique*, vol. 14, no. 4, pp. 571–595, 1975.

[80] L. Filograna, M. Racioppi, G. Saccomandi, and I. Sgura, "A simple model of nonlinear viscoelasticity taking into account stress relaxation," *Acta mechanica*, vol. 204, no. 1-2, pp. 21–36, 2009.

[81] S. Bouzidi, H. Bechir, and F. Brémand, "Phenomenological isotropic visco-hyperelasticity: a differential model based on fractional derivatives," *Journal of Engineering Mathematics*, pp. 1–28, 2015.

[82] H. Pouriayevali, Y. Guo, and V. Shim, "A constitutive description of elastomer behaviour at high strain rates–a strain-dependent relaxation time approach," *International Journal of Impact Engineering*, vol. 47, pp. 71–78, 2012.

[83] K. Hasanpour, S. Ziaei-Rad, and M. Mahzoon, "A large deformation framework for compressible viscoelastic materials: Constitutive equations and finite element implementation," *International Journal of Plasticity*, vol. 25, no. 6, pp. 1154–1176, 2009.

[84] R. A. Schapery, "An engineering theory of nonlinear viscoelasticity with applications," *International Journal of Solids and Structures*, vol. 2, no. 3, pp. 407–425, 1966.

[85] K. Valanis and T. Peng, *Irreversible Thermodynamics and Constitutive Equations of Viscoelastic Materials with Couple Stress*. Engineering Research Institute, Iowa State University, 1968.

[86] M. Biot, "Theory of stress-strain relations in anisotropic viscoelasticity and relaxation phenomena," *Journal of Applied Physics*, vol. 25, no. 11, pp. 1385–1391, 1954.

[87] E. H. Lee, "Elastic-plastic deformation at finite strains," *Journal of Applied Mechanics*, vol. 36, no. 1, pp. 1–6, 1969.

[88] J. C. Simo, "On a fully three-dimensional finite-strain viscoelastic damage model: formulation and computational aspects," *Computer methods in applied mechanics and engineering*, vol. 60, no. 2, pp. 153–173, 1987.

[89] G. A. Holzapfel and J. C. Simo, "A new viscoelastic constitutive model for continuous media at finite thermomechanical changes," *International Journal of Solids and Structures*, vol. 33, no. 20, pp. 3019–3034, 1996.

[90] S. Peng, K. Valanis, and R. Landel, "Nonlinear viscoelasticity and relaxation phenomena of polymer solids," *Acta Mechanica*, vol. 25, no. 3-4, pp. 229–240, 1977.

[91] J. Lubliner, "A model of rubber viscoelasticity," *Mechanics Research Communications*, vol. 12, no. 2, pp. 93–99, 1985.

[92] S. Reese and S. Govindjee, "A theory of finite viscoelasticity and numerical aspects," *International journal of solids and structures*, vol. 35, no. 26, pp. 3455–3482, 1998.

[93] S. Reese, "A micromechanically motivated material model for the thermo-viscoelastic material behaviour of rubber-like polymers," *International Journal of Plasticity*, vol. 19, no. 7, pp. 909–940, 2003.

[94] A. Amin, A. Lion, S. Sekita, and Y. Okui, "Nonlinear dependence of viscosity in modeling the rate-dependent response of natural and high damping rubbers in compression and shear: Experimental identification and numerical verification," *International Journal of Plasticity*, vol. 22, no. 9, pp. 1610–1657, 2006.

[95] P. Camarasa, "Elastomer-based modular multi-axis vibration/shock isolation device," Aug. 14 2012. US Patent 8,240,614.

[96] R. K. Luo, "Impact simulation and experiment on rubber anti-vibration systems," *Polymer Testing*, vol. 50, pp. 335–342, 2016.

[97] S. Govindjee and J. C. Simo, "Mullins effect and the strain amplitude dependence of the storage modulus," *International journal of solids and structures*, vol. 29, no. 14, pp. 1737–1751, 1992.

[98] J. S. Bergström and M. C. Boyce, "Constitutive modeling of the large strain time-dependent behavior of elastomers," *Journal of the Mechanics and Physics of Solids*, vol. 46, no. 5, pp. 931–954, 1998.

[99] R. Martin and S. Malguarnera, "Strain dependence of the dynamic properties of filled elastomers," *Journal of Elastomers and Plastics*, vol. 13, no. 3, pp. 139–148, 1981.

[100] N. W. Tschoegl, W. G. Knauss, and I. Emri, "Poisson's ratio in linear viscoelasticity–a critical review," *Mechanics of Time-Dependent Materials*, vol. 6, no. 1, pp. 3–51, 2002.

[101] O. J and W. S, "Differential microcalorimeter," Aug. 2 1966. US Patent 3,263,484.

[102] D. J. Charlton, J. Yang, and K. K. Teh, "A review of methods to characterize rubber elastic behavior for use in finite element analysis," *Rubber chemistry and technology*, vol. 67, no. 3, pp. 481–503, 1994.

[103] S. Cantournet, R. Desmorat, and J. Besson, "Mullins effect and cyclic stress softening of filled elastomers by internal sliding and friction thermodynamics model," *International Journal of Solids and Structures*, vol. 46, no. 11, pp. 2255–2264, 2009.

[104] N. Suphadon and J. Busfield, "The dynamic properties of fumed silica filled sbr as function of pre-strain," *Polymer Testing*, vol. 30, no. 7, pp. 779–783, 2011.

[105] M. Klüppel, "Evaluation of viscoelastic master curves of filled elastomers and applications to fracture mechanics," *Journal of Physics: Condensed Matter*, vol. 21, no. 3, p. 35104, 2009.

[106] L. Guo, Y. Lv, Z. Deng, Y. Wang, and X. Zan, "Tension testing of silicone rubber at high strain rates," *Polymer Testing*, vol. 50, pp. 270–275, 2016.

[107] J. Yi, M. C. Boyce, G. F. Lee, and E. Balizer, "Large deformation rate-dependent stress–strain behavior of polyurea and polyurethanes," *Polymer*, vol. 47, no. 1, pp. 319–329, 2006.

[108] V. Coveney and D. Johnson, "Rate-dependent modeling of a highly filled vulcanizate," *Rubber Chemistry and technology*, vol. 73, no. 4, pp. 565–577, 2000.

[109] J. D. Ferry, E. R. Fitzgerald, L. D. Grandine Jr, and M. L. Williams, "Temperature dependence of dynamic properties of elastomers. relaxation distributions," *Rubber Chemistry and Technology*, vol. 25, no. 4, pp. 720–729, 1952.

[110] Y. Kwon and K. S. Cho, "Time-strain nonseparability in viscoelastic constitutive equations," *Journal of Rheology (1978-present)*, vol. 45, no. 6, pp. 1441–1452, 2001.

[111] T. Rey, G. Chagnon, J.-B. Le Cam, and D. Favier, "Influence of the temperature on the mechanical behaviour of filled and unfilled silicone rubbers," *Polymer Testing*, vol. 32, no. 3, pp. 492–501, 2013.

[112] D. I. G. Jones, "Temperature-frequency dependence of dynamic properties of dampiamin ng materials," *Journal of Sound and Vibration*, vol. 33, no. 4, pp. 451–470, 1974.

[113] R. J. Seyler, *Assignment of the glass transition*, vol. 1249. ASTM International, 1994.

[114] C. Gracia-Fernández, S. Gómez-Barreiro, J. López-Beceiro, J. T. Saavedra, S. Naya, and R. Artiaga, "Comparative study of the dynamic glass transition temperature by dma and tmdsc," *Polymer Testing*, vol. 29, no. 8, pp. 1002–1006, 2010.

[115] A. Thorin, A. Azoug, and A. Constantinescu, "Influence of prestrain on mechanical properties of highly-filled elastomers: measurements and modeling," *Polymer Testing*, vol. 31, no. 8, pp. 978–986, 2012.

[116] D. Wollscheid and A. Lion, "Predeformation-and frequency-dependent material behaviour of filler-reinforced rubber: Experiments, constitutive modelling and parameter identification," *International Journal of Solids and Structures*, vol. 50, no. 9, pp. 1217–1225, 2013.

[117] M. L. Williams, R. F. Landel, and J. D. Ferry, "The temperature dependence of relaxation mechanisms in amorphous polymers and other glass-forming liquids," *Journal of the American Chemical society*, vol. 77, no. 14, pp. 3701–3707, 1955.

[118] D. Fesko and N. Tschoegl, "Time-temperature superposition in thermorheologically complex materials," in *Journal of Polymer Science: Polymer Symposia*, vol. 35, pp. 51–69, Wiley Online Library, 1971.

[119] A. F. M. S. Amin, A. Lion, S. Sekita, and Y. Okui, "Nonlinear dependence of viscosity in modeling the rate-dependent response of natural and high damping rubbers in compression and shear: Experimental identification and numerical verification," *International Journal of Plasticity*, vol. 22, no. 9, pp. 1610–1657, 2006.

[120] C. J. Quigley, J. Mead, and A. R. Johnson, "Large strain viscoelastic constitutive models for rubber, part ii: Determination of material constants," *Rubber Chemistry and Technology*, vol. 68, no. 2, pp. 230–247, 1995.

[121] M. Green and A. Tobolsky, "A new approach to the theory of relaxing polymeric media," *The Journal of Chemical Physics*, vol. 14, no. 2, pp. 80–92, 1946.

[122] F. a. Sidoroff, "Un modèle viscoélastique non linéaire avec configuration intermédiaire," *Journal de Mécanique*, vol. 13, no. 4, pp. 679–713, 1974.

[123] H. Bechir and A. Kaci, "Comparaison du module complexe d'Young résultant de deux différents modèles visco-hyper-élastiques," *Rhéologie*, vol. 6, pp. 25–30, 2004.

[124] J. C. Petiteau, E. Verron, R. Othman, H. Le Sourne, J. F. Sigrist, and G. Barras, "Large strain rate-dependent response of elastomers at different strain rates: Convolution integral vs. internal variable formulations," *Mechanics of Time-Dependent Materials*, vol. 17, no. 3, pp. 349–367, 2013.

[125] *Abaqus Analysis User's Guide, version 6.14-5.* 2015.

[126] *Abaqus Theory Guide, version 6.14-5.* 2015.

[127] D. C. Drucker, "A definition of stable inelastic material," tech. rep., DTIC Document, 1957.

[128] *Abaqus Theory Manual v6.14-5 section 4.6.1.* 2015.

[129] J. C. Simo and T. J. Hughes, *Computational inelasticity*, vol. 7. Springer Science & Business Media, 2006.

[130] Q. YUAN, Z. XU, and Z. ZHANG, "Stiffness analysis of rubber bushing based on constructive models," *World Sci-tech R & D*, vol. 5, p. 001, 2014.

[131] S. Gelke and J. Ihlemann, "Simulation of a chassis bushing with regard to strain induced softening of filled rubber," *PAMM*, vol. 16, no. 1, pp. 339–340, 2016.

[132] J. Nakahara, K. Yamazaki, and Y. Otaki, "Rubber bushing model for vehicle dynamics performance development that considers amplitude and frequency dependency," *SAE International Journal of Commercial Vehicles*, vol. 8, no. 2015-01-1579, pp. 117–125, 2015.

[133] D. Koblar and M. Boltežar, "Evaluation of the frequency-dependent young's modulus and damping factor of rubber from experiment and their implementation in a finite-element analysis," *Experimental Techniques*, 2013.

[134] P. E. Austrell, "Modeling of elasticity and damping for filled elastomers," *Report TVSM*, vol. 1009, 1997.

[135] J. Lions *et al.*, "Ariane 5 failure-full report," *Paris: ESA*, 1996.

[136] B. Chemoul, E. Louaas, P. Roux, D. Schmitt, and M. Pourcher, "Ariane 5 flight environments," *Acta Astronautica*, vol. 48, no. 5, pp. 275–285, 2001.

[137] ARIANE 6 Project Team, "Ariane 6 Project Request For Consultation for Ariane 6 Key Launcher Elements. ATTACHMENT II : Technical Conditions ," 2013.

[138] ARIANE 5 Project Team, "Ariane 5 User's Manual Issue 5 Revision 1 ," 2011.

[139] D. A. Caughey, "Introduction to aircraft stability and control course notes for m&ae 5070," *Sibley School of Mechanical & Aerospace Engineering, Cornell University, Ithaca, New York*, pp. 14853–7501, 2011.

[140] W. Johnson *et al.*, "Impact strength of materials," 1972.

[141] D. S. Steinberg, *Vibration analysis for electronic equipment*. John Wiley & Sons, 2000.

[142] A. S. Khan, Y. S. Suh, and R. Kazmi, "Quasi-static and dynamic loading responses and constitutive modeling of titanium alloys," *International Journal of Plasticity*, vol. 20, no. 12, pp. 2233–2248, 2004.

[143] T. J. Hughes, *The finite element method: linear static and dynamic finite element analysis*. Courier Corporation, 2012.

[144] J. Ziobro, "Analysis of suspension element of car body on the example silentblock," *Advances in Science and Technology Research Journal*, vol. 9, no. 28, pp. 125–129, 2015.

[145] A. Carrella, S. Manzato, and L. Gielen, "An approach to identification and simulation of the nonlinear dynamics of anti-vibration mounts," in *Dynamics of Coupled Structures, Volume 1*, pp. 219–227, Springer, 2014.

[146] M. Friswell and J. E. Mottershead, *Finite element model updating in structural dynamics*, vol. 38. Springer Science & Business Media, 2013.

[147] K.-J. Bathe, *Finite element method*. Wiley Online Library, 2008.

[148] J. Wilkinson, "The algebraic eigenvalue problem," *Oxford: Clarendon Press, 1965*, 1965.

[149] M. Géradin and D. Rixen, *Théorie des vibrations: application à la dynamique des structures*, vol. 2. Masson Paris, 1993.

[150] K.-J. Bathe and E. L. Wilson, "Large eigenvalue problems in dynamic analysis," *Journal of the Engineering Mechanics Division*, vol. 98, no. 6, pp. 1471–1485, 1972.

[151] L. Rouleau, *Modélisation vibro-acoustique de structures sandwich munies de matériaux visco-élastiques*. PhD thesis, 2013.

[152] B. P. Baillargeon, S. S. Vel, and J. S. Koplik, "Utilizing ABAQUS to Analyze the Active Vibration Suppression of Structural Systems," pp. 81–94.

[153] R.-J. Gibert, *Vibrations des structures: interactions avec les fluides: sources d'excitation aléatoires*. Eyrolles, 1988.

[154] C. Beards, *Structural vibration: analysis and damping*. Butterworth-Heinemann, 1996.

[155] G. J. Simitses and D. H. Hodges, *Fundamentals of structural stability*. Butterworth-Heinemann, 2006.

[156] S. S. Harak, S. C. Sharma, and S. P. Harsha, "Modal analysis of prestressed draft pad of freight wagons using finite element method," *Journal of Modern Transportation*, vol. 23, no. 1, pp. 43–49, 2015.

[157] S. Lo, "A new mesh generation scheme for arbitrary planar domains," *International Journal for Numerical Methods in Engineering*, vol. 21, no. 8, pp. 1403–1426, 1985.

[158] J. Peraire, M. Vahdati, K. Morgan, and O. C. Zienkiewicz, "Adaptive remeshing for compressible flow computations," *Journal of computational physics*, vol. 72, no. 2, pp. 449–466, 1987.

[159] T. D. Blacker and M. B. Stephenson, "Paving: A new approach to automated quadrilateral mesh generation," *International Journal for Numerical Methods in Engineering*, vol. 32, no. 4, pp. 811–847, 1991.

[160] T. D. Blacker and R. J. Meyers, "Seams and wedges in plastering: a 3-d hexahedral mesh generation algorithm," *Engineering with computers*, vol. 9, no. 2, pp. 83–93, 1993.

[161] G. Genta, *Vibration dynamics and control*. Springer, 2009.

[162] D. Sylvain, *Dynamique des Solides et des Structures*. École Nationale Supérieure des Mines de Saint-Étienne, 2011.

[163] L. Gaul and J. Lenz, "Nonlinear dynamics of structures assembled by bolted joints," *Acta Mechanica*, vol. 125, no. 1, pp. 169–181, 1997.

AUTORISATION DE SOUTENANCE

Vu les dispositions de l'arrêté du 25 mai 2016,

Vu la demande des directeurs de thèse

Messieurs M. ICHCHOU et J. BEN ABDALLAH

et les rapports de

M. W. LARBI
Maître de conférences HDR - Laboratoire de Mécanique des Structures et des Systèmes Couplés (LMSSC) - Conservatoire National des Arts et Métiers (Cnam) Mécanique - case courrier 2D6R10 - 292 rue Saint-Martin - 75141 Paris cedex 03

et de

M. N. BENSEDDIQ
Professeur - Laboratoire de Mécanique de Lille - IUT-A GMP - Université des Sciences et Technologies de Lille - BP 90179 - 59653 Villeneuve d'Ascq

Monsieur JRIDI Nidhal

est autorisé à soutenir une thèse pour l'obtention du grade de **DOCTEUR**

Ecole doctorale MECANIQUE, ENERGETIQUE, GENIE CIVIL ET ACOUSTIQUE

Fait à Ecully, le 11 septembre 2017

P/Le directeur de l'E.C.L
La directrice des Etudes

ECOLE CENTRALE DE LYON
Service
Scolarité
ECULLY

M-A. GALLAND